R. & M. No. 3634

R. & M. No. 3634

MINISTRY OF TECHNOLOGY

AERONAUTICAL RESEARCH COUNCIL
REPORTS AND MEMORANDA

Numerical Appraisal of Multhopp's Low-Frequency Subsonic Lifting-Surface Theory

By H. C. GARNER
Aerodynamics Division N.P.L.

LONDON: HER MAJESTY'S STATIONERY OFFICE
1970
PRICE £2 12s 0d [£2·60] NET

Numerical Appraisal of Multhopp's Low-Frequency Subsonic Lifting-Surface Theory

By H. C. GARNER

Aerodynamics Division N.P.L.

Reports and Memoranda No. 3634*
October, 1968

Summary.

A brief review of oscillatory theories reveals that some of these suffer from a defect that has been corrected in the Algol programme now subject to critical examination. Its features in steady and low-frequency subsonic flow are outlined, and extensive tabulated results are presented for seventeen planforms. The accuracy and convergence of solutions are studied in relation to arbitrary parameters representing chordwise and spanwise collocation positions, spanwise integration points and the essential central rounding of sweptback wings. Rectangular and other wings with streamwise symmetry, untapered and tapered sweptback wings, slender and curved-tipped wings show progressively slower convergence, and they are examined in respect of overall forces, spanwise loading, local aerodynamic centres, central chordwise loading and oscillatory pitching derivatives. Some new general criteria are recommended for selecting the arbitrary parameters.

Serious inaccuracy arising from the original defect is established, and hence the need to examine theories for general frequency. The residual errors in the Algol programme may stem from high or low aspect ratio demanding extra spanwise or chordwise terms, but the most elusive cause of collocation error in the standard solutions is found to be insufficient central rounding of highly sweptback wings. It is demonstrated, however, that the rounding itself often influences the aerodynamics as much as the standard collocation error and in the opposite sense, so that one correction is useless without the other. Approximate results with both effects taken into account provide a few examples of improved comparisons with exact theory and experiment.

*Replaces N.P.L. Aero Report 1278—A.R.C. 30 607.

LIST OF CONTENTS

LIST OF TABLES

LIST OF ILLUSTRATIONS

Figure

Figure

1. *Introduction.*

Consider a planform S in oscillatory vertical motion relative to a free stream of density ρ, subsonic Mach number M and of velocity U parallel to the positive x-axis. Let the real part of $\bar{z}(x, y) \exp(i\omega t)$ denote the upward displacement of the surface at time t, and let the load distribution per unit area over the planform be written as the real part of

$$\tfrac{1}{2}\rho U^2 \bar{l}(x, y) \exp(i\omega t). \qquad (1)$$

Then under the usual linearizing assumptions a double integral equation

$$\iint_S \bar{l}(x', y')\, K(x'-x, y'-y, \omega, M)\, dx'\, dy' = -\frac{\partial \bar{z}}{\partial x} - \frac{i\omega \bar{z}}{U}, \qquad (2)$$

with a complicated kernel function K, relates the complex loading function $\bar{l}$ to the instantaneous flow direction at (x, y) on the planform. Oscillatory lifting-surface theory poses the problem of evaluating $\bar{l}$, when $\bar{z}$ is given. With very few exceptions (*see* Section 3) mathematical solutions are unobtainable and recourse to numerical analysis is essential.

Garrick[1] has described the historical background to the subject from the earliest theoretical methods to those available some twelve years ago. He remarks that the problem of three-dimensional flow about wings must be considered to be in a state of continuing development, and the statement remains true. Williams[2] has contributed a later account of theoretical progress with emphasis on the mathematical formulation. Theoretical methods differ according to whether exponential factors are inserted in the expression (1) or whether the velocity potential over the wing and wake is used in place of $\bar{l}$ in equation (2). The corresponding changes in the kernel function transform the analysis, but of perhaps greater importance are the basic distinctions in the technique of evaluating equation (2) as exemplified in the different classes of solution, *viz.*, strip theory, vortex lattice, box grid, low aspect ratio, high aspect ratio and exact kernel.

The most simple procedure with its powerful empirical capability is strip theory. Van de Vooren and Eckhaus[3] have developed this for tapered swept wings, and their method has been extended by Eckhaus[4] to compressible subsonic flow. Such methods are known to give inaccurate aerodynamic damping forces at low frequencies, and their main application is to cases of high aspect ratio and frequency. Vortex lattice and box grid methods for unsteady flow have been developed since the publication of Ref. 1. These exploit changes in mathematical model involving discrete elements of vorticity to simplify the evaluation of equation (2) or some corresponding double integral. Lehrian's[5] vortex lattice method for incompressible flow and its further development for subsonic and sonic flow by Runyan and Woolston[6] have been widely used. The chief disadvantage of such methods is the uncertainty resulting from the extra parameters that define the lattice, and there is the burden of proof that the results converge as the lattice spacing is reduced. Although a box method, such as that due to Stark[7], is probably more promising from the standpoint of establishing accuracy, the same disadvantages have to be overcome. The whole problem of accuracy stems from the fact that there are no exact mathematical solutions for practical planforms, and the change of mathematical model requires justification by numerical analysis alone.

Other methods involve simplifications to the kernel function. One extreme is slender wing theory, formulated for incompressible flow by Garrick[8] and for compressible flow by Mazelsky[9]. Lawrence and Gerber[10] have treated wings of low aspect ratio in incompressible flow by splitting the downwash integral into a slender wing term and a residual part in which an approximation is made. The counterparts for wings of high aspect ratio are Cicala's[11] lifting line theory and the extension for subsonic compressible flow by Reissner[12] who splits the downwash integral into a two-dimensional term and a residual part with a suitable approximation. Theories such as Refs. 10 and 12 lead to interesting mathematics, but suffer from restricted applicability. Moreover, they stem from the decade before the intensive development of computers and the readjustment of theoretical methods that has ensued.

The use of the exact kernel function is no longer inhibited by computational demands. The basic methods of Watkins *et al*[13] and Richardson[14] differ in that Ref. 13 makes no concessions to expediency of computation, while Ref. 14 implies greater numerical approximation in the pursuit of economy. The latter has been developed by Hsu[15], and both Lashka[16] and Davies[17] have fully mechanized applications of equation (2) with K as formulated in equation (22) of Ref. 13. The procedure is first to evaluate the chordwise integral with respect to x', and then to integrate across the span. This latter spanwise integration turns out to be crucial and represents a considerable threat to accuracy.

All the theoretical methods mentioned above (Refs. 3 to 17) apply to general frequencies of oscillation. The mathematical formulation is of course much simpler when only first order effects of frequency are sought. The low-frequency method of Ref. 18 has been developed with a view to the reduction of numerical errors from spanwise integration. In the present report extensive calculations for a wide range of planforms are analysed in order to demonstrate the errors and how they are reduced. The uncertainties that remain are probably no greater than those due to the initial linearization. The convergence of solutions for the aerodynamic loading has been studied with more success for some planforms than others, but the less amenable ones are of more practical interest. Although the primary purpose of the investigation is the appraisal of Ref. 18 as a numerical technique, perhaps of greater importance is the implication that the methods of Refs. 13 to 17 for general frequency are capable of significant improvement by straightforward modification.

2. *Steady-Flow and Low-Frequency Theories.*

Before the essential features of Ref. 18 are described, a brief account of the historical development of Multhopp's low-frequency subsonic lifting-surface theory is desirable. The original steady-flow theory of Ref. 19 was extended to slow pitching oscillations in Ref. 20. The chordwise integration of equation (2) is carried out first. Although Multhopp recognized the need for care in the subsequent spanwise integration and paid attention to the logarithmic singularity in the integrand, his treatment was promptly improved by Mangler and Spencer[21]; with this refinement Multhopp's theory has been widely used for many years. The same basic technique of spanwise integration is carried over into Refs. 16 and 17. Multhopp's original theory was wisely restricted to $N = 2$ chordwise terms in the load distribution, and subsequent extensions to larger N have been made without due care. These applications entail collocation points at chordwise positions

$$\xi = \frac{x-x_l}{c} = \tfrac{1}{2}\left(1-\cos\frac{2\pi p}{2N+1}\right) \quad \text{with} \quad p = 1, 2, \ldots N\,, \tag{3}$$

which extend closer to the leading edge $x = x_l$ as N increases. Let $\bar{m}$ denote an odd number of spanwise integration points between the wing tips, *viz.*,

$$\eta = \frac{y}{s} = \sin\frac{\pi\bar{n}}{\bar{m}+1} \quad \text{with} \quad \bar{n} = 0, \pm 1, \ldots \pm\tfrac{1}{2}(\bar{m}-1)\,. \tag{4}$$

Then it is shown in Ref. 22 that, to ensure 1 per cent accuracy in the calculated steady downwash at the centre of simply loaded rectangular wings of aspect ratio A, it is necessary to take $(\bar{m}+1) > 4A$. The analysis of Ref. 22 has been extended to downwash points towards the leading edge of the centreline ($\eta = 0$) and reveals inaccuracies greater than 1 per cent if $(\bar{m}+1) < 2A/\xi$. An increase in N with fixed $\bar{m}$ must ultimately lead to divergent results, and it is tentatively recommended in Ref. 18 that

$$\bar{m}+1 \geqslant 2A \sec\Lambda_1 \operatorname{cosec}^2\frac{\pi}{2N+1}\,, \tag{5}$$

where Λ_1 is the angle of trailing-edge sweepback. Thus for $A = 6$, $\Lambda_1 = 30°$ and $N = 4$, say, equation (5) would require that $\bar{m} > 117$.

Ref. 18 meets this demand by an increase in the number of spanwise integration points to

$$\bar{m} = q(m+1)-1\,, \tag{6}$$

where m is the number of collocation sections and q is either unity or an even integer which will need to be increased as N is increased. When $q = 1$, the summation of downwash takes the form of equation (22) of Ref. 18 and the calculation is simply that of Ref. 20. As described in Section 2.4 of Ref. 18, the procedure for spanwise integration for $q \geqslant 2$ is to evaluate the downwash at the same collocation sections

$$\eta_\nu = \cos\theta_\nu = \sin\frac{\pi\nu}{m+1} \quad \text{with} \quad \nu = 0, \pm 1, \ldots \pm \tfrac{1}{2}(m-1) \tag{7}$$

in terms of the loading coefficients at the $\bar{m}$ sections of equation (4). Then Multhopp's interpolation polynomial

$$g(\theta) = (-1)^{\frac{1}{2}(m+1)} \sum_{\nu=-z}^{z} g(\theta_\nu) \frac{(-1)^{\nu-1}\sin\theta_\nu \sin(m+1)\theta}{(m+1)(\cos\theta - \cos\theta_\nu)} \tag{8}$$

with $z = \frac{1}{2}(m-1)$ is applied to each loading coefficient at every value of

$$\theta = \frac{\pi}{2} - \frac{\bar{n}\pi}{\bar{m}+1} \tag{9}$$

that occurs from equation (4) in the summation of downwash. Thus the downwash is expressed more accurately as a linear combination of the coefficients in the load distribution

$$\begin{aligned} \bar{l}(x', y') = \exp\left(\frac{i\omega M^2 x'}{\beta^2 U}\right)\frac{8s}{\pi c_n}\Big[& \gamma_n \cot\tfrac{1}{2}\phi + 4\mu_n(\cot\tfrac{1}{2}\phi - 2\sin\phi) \\ & + \kappa_n(\cot\tfrac{1}{2}\phi - 2\sin\phi - 2\sin 2\phi) \\ & + \lambda_n(\cot\tfrac{1}{2}\phi - 2\sin\phi - 2\sin 2\phi - 2\sin 3\phi)\Big]. \end{aligned} \tag{10}$$

Here the number of functions γ_n, μ_n, etc., is equal to N, $\beta^2 = 1-M^2$, the subscript n denotes that

$$y' = y'_n = s\sin\frac{\pi n}{m+1} \quad \text{with} \quad n = 0, \pm 1, \ldots \pm\tfrac{1}{2}(m-1) \tag{11}$$

and the angular chordwise co-ordinate ϕ is given by

$$x' = x_{ln} + \tfrac{1}{2}c_n(1-\cos\phi)\,. \tag{12}$$

The boundary conditions (2) at the mN collocation points, defined by equations (3) and (7), become ordinary linear simultaneous equations to determine the unknowns γ_n, μ_n, etc.

More recent developments in steady subsonic lifting-surface theory are described in Refs. 23 and 24. Zandbergen *et al*[23] use a parameter such as q in equation (6), but couple this with a refined technique for spanwise integration. Hewitt and Kellaway[24] offer a different approach in which the spanwise integration of equation (2) precedes the chordwise integration. Although both these methods have certain advantages in numerical technique, Ref. 18 is adequate for many purposes and has the additional facility for treating low-frequency oscillations.

The present applications are to wings at a steady uniform incidence α or in oscillatory pitching motion. In steady flow the single solution

$$\alpha = \alpha_1 = 1 \tag{13}$$

is required, and the load distribution $l = l_1$ is obtained in the form of equation (10) without its exponential factor. In most of the oscillatory cases four additional solutions are obtained with

$$\left.\begin{aligned} &\alpha = \alpha_2 = x/\bar{c} \text{ giving } l = l_2 \\ &\alpha = \alpha_3 \quad \text{from equation (23) of Ref. 18 with } l = l_1 \\ &\alpha = \alpha_4 = (x/\bar{c})^2 \text{ giving } l = l_4 \\ &\alpha = \alpha_5 \quad \text{from equation (23) of Ref. 18 with } l = l_2 \end{aligned}\right\}, \tag{14}$$

where $\bar{c}$ is the geometric mean chord and a full derivation of α_3 is given in Ref. 20. To each incidence $\alpha = \alpha_r$ there corresponds a steady wing loading

$$\begin{aligned} l_r = \frac{8s}{\pi c_n}\Big[&\gamma_{nr} \cot \tfrac{1}{2}\phi + 4\mu_{nr} (\cot \tfrac{1}{2}\phi - 2 \sin \phi) \\ &+ \kappa_{nr} (\cot \tfrac{1}{2}\phi - 2 \sin \phi - 2 \sin 2\phi) \\ &+ \lambda_{nr} (\cot \tfrac{1}{2}\phi - 2 \sin \phi - 2 \sin 2\phi - 2 \sin 3\phi) \Big], \end{aligned} \tag{15}$$

from which are calculated the coefficients of lift and pitching moment

$$\left.\begin{aligned} C_{Lr} &= \frac{1}{\beta} I_{Lr} = \frac{\pi A}{m+1} \sum_{n=-z}^{z} \gamma_{nr} \cos \frac{n\pi}{m+1} \qquad \left[z = \tfrac{1}{2}(m-1) \right] \\ -C_{mr} &= -\frac{1}{\beta} I_{mr} = \frac{\pi A}{m+1} \sum_{n=-z}^{z} \frac{1}{\bar{c}} \left\{ \gamma_{nr} \left(x_{ln} + \tfrac{1}{4} c_n \right) - \mu_{nr} c_n \right\} \cos \frac{n\pi}{m+1} \end{aligned}\right\} \tag{16}$$

and also the second moment coefficients

$$\begin{aligned} -I^*_{mr} = \frac{\pi\beta A}{m+1} \sum_{n=-z}^{z} \frac{1}{\bar{c}^2} \Big\{ &\gamma_{nr} \left(x_{ln}^2 + \tfrac{1}{2} x_{ln} c_n + \tfrac{1}{8} c_n^2 \right) \\ &- \mu_{nr} \left(2x_{ln} c_n + \tfrac{3}{4} c_n^2 \right) + \kappa_{nr} \left(\tfrac{1}{16} c_n^2 \right) \Big\} \cos \frac{n\pi}{m+1}. \end{aligned} \tag{17}$$

These coefficients determine the four pitching derivatives as formulated in equations (39) of Ref. 18 and also those for the reversed planform by equations (38) of Ref. 18.

In the treatment of swept wings major uncertainty arises from the central kink in the planform. Although the form of load distribution (10) or (15) is acceptable for smooth planforms, it is known to lead to logarithmically infinite downwash along a section where a kink occurs. The common practice is therefore to smooth the planform by means of artificial rounding. In order to define the planform at the sections (4), the rounding is formulated according to equation (28) of Ref. 18. When both leading and trailing edges have straight portions in the range

$$0 < y < y_1 = s \sin \frac{\pi}{m+1}, \tag{18}$$

the leading edge and chord in the range $|y| \leqslant y_1$ become

$$\left.\begin{aligned} x_l(y) &= x_l(y_1)\left[\frac{|y|}{y_1}+\frac{1}{6}\left(1-\frac{|y|}{y_1}\right)^6\right] \\ c(y) &= c_r+\left[\frac{|y|}{y_1}+\frac{1}{6}\left(1-\frac{|y|}{y_1}\right)^6\right]\quad \{c(y_1)-c_r\} \end{aligned}\right\}. \tag{19}$$

Here c_r is the true central chord and the origin is chosen at the leading apex so that

$$x_l(y_1) = y_1 \tan \Lambda_0\,, \tag{20}$$

where Λ_0 is the angle of leading-edge sweepback. The factor 1/6 in equations (19) is chosen to be consistent with Multhopp's rule in Appendix VI of Ref. 19. Although this standard rounding is controlled by the value of m through equation (18), there is provision for any other desired rounding.

For a given planform, including any artificial rounding and the usual lateral scaling factor β in cases of compressible flow, there are only the three integers m, N and q to specify the matrices that govern the simultaneous equations for γ_n, μ_n, etc. The programme of Ref. 18 limits the number of chordwise terms to $N \leqslant 4$ and there are interdependent restrictions on m, N and q imposed by the capacity (32K) of the N.P.L. KDF9 computer and an arbitrary maximum running time of 45 minutes. The tables in Section 1 of Ref. 18 illustrate the restrictions and typical running times. In the present applications it is possible to study the convergence of the theoretical results with respect to each of the parameters. The extent to which full convergence is frustrated by the restrictions is dependent on the planform and the aerodynamic quantity being considered. To be necessary, the method must show inadequate convergence with respect to N when $q = 1$. To be successful, it must show convergence with respect to q, m and N.

3. *Numerical Results.*

Calculations have been made for the seventeen planforms listed in Table 1. When both leading and trailing edges are straight, the planform is defined by the tabulated values of aspect ratio $A = 2s/\bar{c}$, $c_r/\bar{c}$, $\tan \Lambda_0$ and $\tan \Lambda_1$, themselves related by

$$c_r/\bar{c} = 1+\tfrac{1}{4} A (\tan \Lambda_0 - \tan \Lambda_1)\,. \tag{21}$$

The exceptions are Planforms 4, 6, 15, 16 and 17 for which additional formulae or data are included. The final column of Table 1 gives references to earlier work on some of the planforms. Stark's[25] theory has been applied to the rectangular wing ($A = 2$). The circular planform is one example of an exact solution by Van Spiegel[26], whose theory and corrected results are presented by Benthem and Wouters[27]. Other examples where exact theory is available are the very slender delta and gothic planforms ($A = 0{\cdot}0001$) to which Garrick's[8] theory is applicable. Planforms 10, 11 and 17 are chosen because they have formed the subjects of earlier theoretical and experimental research (Refs. 30, 31 and 35). Although comparison with experimental results forms a very minor part of the present investigation, five of the remaining planforms have been chosen because measured aerodynamic data were available in Refs. 28, 29, 32, 33 and 34. These represent a wide range of shapes and offer the opportunity to examine the difficulties associated with high and low aspect ratio, leading-edge and trailing-edge sweepback and curved tips.

The tabulated theoretical results for each of the planforms are summarized in Table 2. Tables 3 to 34 concerning steady flow ($\alpha = 1$) are sub-divided into complete solutions and total forces (Tables 3 to 22) and into spanwise distributions of lift and aerodynamic centre (Tables 23 to 34). The next sequence involves oscillatory pitching motion, the coefficients being given in Tables 35 to 42 and the pitching derivatives in Tables 43 to 48. As the discussion unfolds, it will become clear that one crucial source of inaccuracy is associated with the need for artificial central rounding of sweptback wings, as defined in equations (18) to (20). Some attempts have been made to reduce these errors and to evaluate the effect of rounding, and Tables 48 to 50 are included primarily for this purpose.

3.1. *Steady Flow.*

In the case of zero frequency Ref. 18 reduces to steady flow, and altogether over 200 solutions have been obtained for the planforms listed in Table 1 at unit incidence. The non-dimensional loading

$$\frac{\Delta p}{\frac{1}{2}\rho U^2} = \Delta C_p = l$$

at the sections $\eta = \sin\dfrac{\pi n}{m+1}$ are given by equation (15) where the subscript $r(=1)$ may be omitted. The solutions in Tables 3 to 22 are N sets of functions $\gamma_n, \mu_n, \ldots$, e.g. when $N = 4$,

$$\gamma_0, \gamma_1, \ldots \gamma_z; \mu_0, \mu_1, \ldots \mu_z; \kappa_0, \kappa_1, \ldots \kappa_z; \lambda_0, \lambda_1, \ldots \lambda_z$$

where $z = \frac{1}{2}(m-1)$. The local lift coefficient and aerodynamic centre are given by

$$C_{LL} = \frac{4s\,\gamma_n}{c_n} \tag{22}$$

and

$$X_{ac} = \frac{1}{4} - \frac{\mu_n}{\gamma_n}. \tag{23}$$

The total lift and moment about the origin at the leading edge of the root chord are evaluated as coefficients $C_L = C_{L1}$ and $C_m = C_{m1}$ from equations (16). The centre of lift or aerodynamic centre acts at a distance x_{ac} downstream of the origin and is readily evaluated as

$$\frac{x_{ac}}{\bar{c}} = -\frac{C_m}{C_L}. \tag{24}$$

The spanwise centre of pressure of the half wing is defined as

$$\bar{\eta} = \int_0^1 \frac{c\,C_{LL}}{\bar{c}\,C_L}\,\eta\,d\eta = \frac{2A}{C_L}\int_0^1 \gamma\eta\,d\eta\,, \tag{25}$$

where $cC_{LL}/\bar{c}\,C_L$ represents the spanwise loading and the distribution of γ satisfies equation (8). For symmetrical spanwise loading we may write

$$\gamma = \sum_{k=0}^{z} a_{2k+1} \sin(2k+1)\theta\,. \tag{26}$$

Thus $C_L = \frac{1}{2}\pi A a_1$, and it follows from equations (8), (25) and (26) that

$$\bar{\eta} = \frac{4}{\pi a_1} \sum_{k=0}^{z} \frac{(-1)^{k+1}\, a_{2k+1}}{(2k-1)(2k+3)}, \tag{27}$$

where

$$a_{2k+1} = \frac{2}{m+1} \sum_{v=-z}^{z} \gamma_v \sin(2k+1)\,\theta_v\,. \tag{28}$$

A typical result, for $m = 11$, is

$$\bar{\eta} = \frac{0{\cdot}02671\,\gamma_0 + 0{\cdot}24372\,\gamma_1 + 0{\cdot}43514\,\gamma_2 + 0{\cdot}49904\,\gamma_3 + 0{\cdot}43349\,\gamma_4 + 0{\cdot}24980\,\gamma_5}{0{\cdot}50000\,\gamma_0 + 0{\cdot}96593\,\gamma_1 + 0{\cdot}86603\,\gamma_2 + 0{\cdot}70711\,\gamma_3 + 0{\cdot}50000\,\gamma_4 + 0{\cdot}25882\,\gamma_5}. \tag{29}$$

Nearly every solution that has been obtained with $\bar{m} = m$ or $q = 1$ is seen to be inadequate. There are examples in Tables 3, 4, 5, 7, 8, 10, 12, 13, 17, 18, 20, 21 and 22, and the behaviour of κ_n or λ_n with increasing q illustrates the point at once. In some cases C_L and C_m prove to be unacceptable, and there is no doubt that the method of Ref. 18 (with $q \geqslant 2$) is necessary. More careful study is required to establish whether the method converges satisfactorily. Fig. 1 shows the behaviour of local aerodynamic centres from equation (23) for simple rectangular planforms. Convergence with respect to m is so perfect that X_{ac} can be plotted against a logarithmic scale of $(\bar{m}+1)$ with insignificant changes as m is increased from 7 to 15. The horizontal lines joining points corresponding to the larger values of $(\bar{m}+1)$ show convergence with respect to $\bar{m}$ or q. The separate results for $N = 2, 3$ and 4 chordwise terms show perfect convergence for the centre section when $A = 2$ and satisfactory, but slower, convergence with respect to N near the tip when $A = 4$. The results for the smaller aspect ratio when $\bar{m} = m = 7$ illustrate, perhaps surprisingly, how the previous method (Ref. 18 with $q = 1$) diverges with respect to N. A less favourable example is the highly swept Planform 16 with curved tips considered in Fig. 2 where, as in Fig. 1, the false zeros and large scale tend to exaggerate the discrepancies. The lift slope $\partial C_L/\partial\alpha$ and the overall centres of pressure $\bar{\eta}$ and $x_{ac}/\bar{c}$ are plotted against $(\bar{m}+1)$. The effect of increasing m from 15 to 31 is now discernible, but not large. Convergence with respect to $\bar{m}$ is slower, but satisfactory. Convergence with respect to N would appear to be fairly good for $q = 1$ and $q = 8$ (respectively $\bar{m}+1 = 16$ and 128 when $m = 15$), but this is illusory in the former case and the resulting lift slope is about 7 per cent too high and the aerodynamic centre nearly $0{\cdot}04\bar{c}$ too far forward.

These examples serve as preliminary illustrations. The different types of planform, in steady and oscillatory flow, will be considered in Section 4 where each sheds new light on the numerical appraisal. An attempt is made in Section 5 to recommend a suitable choice of m, N and $\bar{m}$. A critical study of the use of artificial central rounding is deferred until Section 6.

3.2. *Oscillatory Flow.*

The output from the Algol programme of Ref. 18 can give the coefficients

$$I_{Lr}\,(r = 1, 2, \dots 5), \quad -I_{mr}\,(r = 1, 2, \dots 5) \quad \text{and} \quad -I^*_{mr}\,(r = 1, 2) \tag{30}$$

from equations (16) and (17). The coefficients are listed from various solutions for thirteen of the planforms in Tables 35 to 42, but in the last instance and in a few other solutions not all twelve coefficients are available. But there are always sufficient to determine the pitching derivatives defined by

$$\left.\begin{aligned} \text{Lift} &= \text{Real part of} \quad -\rho U^2 S(z_\theta + i\bar{\nu} z_{\dot\theta})\theta_0\, e^{i\omega t} \\ \text{Moment} &= \text{Real part of} \quad \rho U^2 S\bar{c}(m_\theta + i\bar{\nu} m_{\dot\theta})\theta_0\, e^{i\omega t} \end{aligned}\right\}, \tag{31}$$

where the frequency parameter $\bar{\nu} = \omega\bar{c}/U$, θ_0 is the amplitude of pitching oscillation and the pitching moment is nose-up and about the axis $x = x_0$. In terms of the coefficients (30)

$$\left.\begin{aligned} -z_\theta &= \frac{1}{2\beta} I_{L1} \\ -m_\theta &= \frac{1}{2\beta}\left[-\frac{x_0}{\bar{c}} I_{L1} + (-I_{m1}) \right] \\ -z_{\dot\theta} &= \frac{1}{2\beta}\left[-\frac{x_0}{\bar{c}} I_{L1} + \frac{\beta^2 - M^2}{\beta^2} I_{L2} + \frac{1}{\beta^2} I_{L3} + \frac{M^2}{\beta^2}(-I_{m1}) \right] \\ -m_{\dot\theta} &= \frac{1}{2\beta}\left[\frac{x_0^2}{\bar{c}^2} I_{L1} - \frac{x_0}{\bar{c}}\left\{ \frac{\beta^2 - M^2}{\beta^2} I_{L2} + \frac{1}{\beta^2} I_{L3} + \frac{1}{\beta^2}(-I_{m1}) \right\} \right. \\ &\qquad \left. + \left\{ \frac{\beta^2 - M^2}{\beta^2}(-I_{m2}) + \frac{1}{\beta^2}(-I_{m3}) + \frac{M^2}{\beta^2}(-I^*_{m1}) \right\} \right] \end{aligned}\right\} \tag{32}$$

where $\beta^2 = 1 - M^2$.

Among the various applications of the reverse-flow theorem considered by Lehrian and the present author, Section 5.1 of Ref. 36 gives the formulation for low-frequency pitching oscillations. The derivatives (32) may be expressed in terms of the coefficients (30) for the reversed wing, i.e. the given planform in a stream of reversed direction and unchanged Mach number. These coefficients are denoted by $\bar{I}_{Lr}$, $-\bar{I}_{mr}$ and $-\bar{I}^*_{mr}$. It can be shown that there are precise relationships between the two sets of coefficients, which are conveniently expressed in matrix form as follows.

$$\begin{bmatrix} I_{L1} \\ I_{L2} \\ I_{L4} \\ -I_{m1} \\ -I_{m2} \\ -I_{m4} \\ -I^*_{m1} \\ -I^*_{m2} \end{bmatrix} = \begin{bmatrix} 1 & 0 & 0 & 0 & 0 & 0 & 0 & 0 \\ \lambda & -1 & 0 & 0 & 0 & 0 & 0 & 0 \\ \lambda^2 & -2\lambda & 1 & 0 & 0 & 0 & 0 & 0 \\ \lambda & 0 & 0 & -1 & 0 & 0 & 0 & 0 \\ \lambda^2 & -\lambda & 0 & -\lambda & 1 & 0 & 0 & 0 \\ \lambda^3 & -2\lambda^2 & \lambda & -\lambda^2 & 2\lambda & -1 & 0 & 0 \\ \lambda^2 & 0 & 0 & -2\lambda & 0 & 0 & 1 & 0 \\ \lambda^3 & -\lambda^2 & 0 & -2\lambda^2 & 2\lambda & 0 & \lambda & -1 \end{bmatrix} \begin{bmatrix} \bar{I}_{L1} \\ -\bar{I}_{m1} \\ -\bar{I}^*_{m1} \\ \bar{I}_{L2} \\ -\bar{I}_{m2} \\ -\bar{I}^*_{m2} \\ \bar{I}_{L4} \\ -\bar{I}_{m4} \end{bmatrix} \tag{33}$$

and

$$\begin{bmatrix} I_{L3} \\ I_{L5} \\ -I_{m3} \\ -I_{m5} \end{bmatrix} = \begin{bmatrix} 1 & 0 & 0 & 0 \\ \lambda & -1 & 0 & 0 \\ \lambda & 0 & -1 & 0 \\ \lambda^2 & -\lambda & -\lambda & 1 \end{bmatrix} \begin{bmatrix} \bar{I}_{L3} \\ -\bar{I}_{m3} \\ \bar{I}_{L5} \\ -\bar{I}_{m5} \end{bmatrix}, \tag{34}$$

where $\lambda = c_r/\bar{c}$ and the length c_r enters in as the displacement between the origins of the two co-ordinate systems. Both square matrices have the property of self-inversion, so that the column matrices on the two sides of equation (33) or (34) can be interchanged. The numerical results do not satisfy these equations exactly, and proof of inaccuracy due to inadequate collocation or spanwise integration can often be established.

Woodcock[37] and Dat *et al*[38] have considered the accuracy of collocation solutions to oscillatory problems in subsonic lifting-surface theory. Ref. 37 reveals large discrepancies for the present Planforms 1, 4 and 11 at high frequency parameter, and it is important to resolve any similar discrepancies at low frequency. Ref. 38 suggests that lifting-surface theory can be optimized in aeroelastic applications with the aid of the reverse-flow theorem, and it will be relevant to study the convergence of the pitching derivatives from equations (32), not only with the usual coefficients from direct flow but also by reverse flow with the aid of equations (33) and (34).

The peculiar problems of the various types of planform will be discussed in Sections 4.1 to 4.6. But, as for steady flow, two figures have been prepared to illustrate the convergence of pitching derivatives under favourable and adverse circumstances. In Fig. 3 all four pitching derivatives are plotted against a logarithmic scale of $(\bar{m}+1)$ for Planform 6 having a smooth hyperbolic leading edge and constant chord. The small slopes of the lines joining points corresponding to the larger values of $\bar{m}$ show satisfactory convergence, although the damping derivatives are somewhat slower to settle. The results for $\bar{m} = 95$ indicate satisfactory convergence with respect to m and N. The points (0) for $m = \bar{m} = 15$ show relatively poor convergence with respect to N when $q = 1$, but the discrepancies for $N = 4$ nowhere exceed 0·02. Planform 12 has high aspect ratio $A = 8$ and a central kink typical of sweptback wings, and both these features would be expected to aggravate convergence. Figure 4 shows the direct pitching derivatives for an axis $x_0 = 2\bar{c}$ against a logarithmic scale of $(m+1)$. With $N = 3$ throughout, convergence is sought firstly with $q = 1$ and secondly with $\bar{m} = 95$ up to the limit of m imposed by the KDF9 computer. The two processes show a tendency to approach a common limit, but for neither m_θ nor $m_{\dot{\theta}}$ do the respective curves come within 0·03 of each other. The comparable discrepancies in Fig. 3 for the smooth edges and lower aspect ratio are of order 0·002.

4. *Convergence of Solutions.*

The planforms of Table 1 have been chosen from different standpoints, and it is convenient to group them in the following sub-sections. The rectangular wings (Planforms 1, 2, 3) cover a range of aspect ratio, and the rate of convergence with respect to $\bar{m}$ shows an inverse correlation with A. The wings with streamwise (fore-and-aft) symmetry for which oscillatory calculations have been made (Planforms 2, 4, 5) form a natural group and are used for studying numerical results from direct and reverse flow. The three wings of constant chord with $A = 4$ (Planforms 2, 6, 7) show the separate effects of sweepback and the central kink. Planforms 8 to 12 constitute an assortment of tapered sweptback wings; the effect of Mach number is considered, and the problems posed by Fig. 4 are elaborated. The slender wings (Planforms 13, 14, 15) include one that is not-so-slender with better convergence properties illustrated by the chordwise loading; the results for the really slender wings ($A = 0{\cdot}0001$) are subjected to comparison with exact theory. Wings with curved tips (Planforms 16, 17) show the greatest discrepancies when $q = 1$ and peculiarly slow convergence associated with the tips.

4.1. *Rectangular Wings.*

Selected solutions for the rectangular wings of aspect ratios 2 and 4 at unit incidence are given in

Tables 3, 4 and 5. In Table 3 the subscript n of the four loading functions γ_n, μ_n, κ_n and λ_n relates to equations (10) and (11) with $m = 15$. It is seen that the outermost values κ_6 and λ_6 converge more rapidly with respect to q than κ_0 and λ_0 do; the more central sections of the wing show discrepancies in the fourth decimal place up to $\bar{m} = 127$, while by $\bar{m} = 47$ these have practically disappeared near the tip. The last two columns of Table 3 are in remarkable agreement, showing little change as m is increased from 7 to 15. Furthermore, unpublished solutions for m, N, q = 15, 4, 2 and 31, 4, 1 are identical to six decimal places. An independent check from Table 3 of Ref. 25 gives in the present notation $C_L = 2{\cdot}471$ and $x_{ac} = 0{\cdot}2089\bar{c}$, which are in very satisfactory agreement with values in the present Table 3.

In Table 4 the major part of the error with $q = 1$ is eliminated as q is increased to 2. It will be found that the spanwise integration in Hsu's[15] theory is virtually equivalent to that from Ref. 18 with $q = 2$ and is commended thereby. Solutions for $A = 4$, $N = 4$ and the same value of $\bar{m}$ in Tables 4 and 5 show surprisingly little effect of increasing m from 7 to 15. The first two and last columns of Table 5 demonstrate excellent convergence with respect to N at the centre section and slower convergence near the tip as in Fig. 1.

Table 23 presents material for a fuller analysis of local aerodynamic centres on the two rectangular wings, and Table 24 gives further results for the high aspect ratio $A = 8$. Unless the consequences of Ref. 18 are fully appreciated, a solution for this wing with m, N, q = 23, 3, 1 and 36 collocation points on the half wing might seem to promise good accuracy. Yet Table 24 shows that the lift slope $\partial C_L/\partial\alpha$ is more than 2 per cent low when $q = 1$, while the local X_{ac} at $\eta = 0$ is $0{\cdot}002c$ too far aft when $q = 1$ and nearly $0{\cdot}004c$ too far forward when $q = 2$. These findings are rationalized in Fig. 5, where the errors in the two quantities are plotted convincingly against $(\bar{m}+1)/\beta A$ from the available data for $N = 3$. Similar curves with slower convergence can be drawn for $N = 4$. As foreshadowed in Ref. 22, wings of high aspect ratio pose a major problem, especially when larger numbers of chordwise terms are needed.

Results for oscillatory flow in Tables 35 and 43 will be discussed in Section 4.2.

4.2. *Wings with Streamwise Symmetry.*

The oscillating circular planform in incompressible flow is a notable exception to the intractable methematical problems of lifting-surface theory. The analysis is due to Van Spiegel[26] and a correction to his numerical result for the pitching damping is given by Benthem and Wouters in Table 2 of Ref. 27. We consider first the solutions by the collocation method of Ref. 18 for steady flow in Table 6. Convergence with respect to q is very good, except near the tip as indicated by the values of λ_5 when $m = 11$ and $N = 4$. The solutions with $N = 2$ and 3 show a small effect of reducing m to 5. The results for the largest values of q are tabulated below and show remarkable convergence with respect to N in perfect agreement with exact theory.

Solution	$\partial C_L/\partial\alpha$	$x_{ac}/\bar{c}$
$N = 2$	1·7888	0·3015
$N = 3$	1·7906	0·3052
$N = 4$	1·7903	0·3049
Exact	1·7902	0·3049

The aerodynamic centre is plotted against q at the top of Fig. 6. It must be admitted that the circular planform is a favourable case with smooth edges and low aspect ratio.

Table 25 gives the local aerodynamic centres for circular and symmetrically tapered planforms. The results for the circular planform ($A = 1{\cdot}27$) show excellent convergence with respect to m, N and q except near the tip where in no respect is the convergence quite complete. Unfortunately there are no reliable numerical results from exact theory to form a basis for comparison. The symmetrically tapered wing

($A = 4{\cdot}33$) shows good convergence with respect to q and, except near the centre section, little effect of increasing m from 11 to 23. Although $(m+1) = 2A$ is acceptable for rectangular wings, $(m+1) \geqslant 4A$ seems desirable for both the others.

Wings with streamwise symmetry present a convenient opportunity to use the relationships in direct and reverse flow, since the coefficients $\bar{I}_{Lr} = I_{Lr}$ and $\bar{I}_{mr} = I_{mr}$. Thus by equations (33) the aerodynamic centre may be calculated from reverse flow to be

$$\frac{x_{ac}}{\bar{c}} = \frac{c_r}{\bar{c}} - \frac{I_{L2}}{I_{L1}}. \tag{35}$$

This is compared with equation (24) for direct flow against the logarithmic scale of q in Fig. 6. The results with $N = 3$ are shown to converge to good accuracy within 0·0005 for the rectangular wing ($A = 4$, $m = 15$), but for the symmetrically tapered wing the discrepancies between equations (24) and (35) are 0·004 when $m = 11$ and 0·002 when $m = 23$ and show little sign of disappearing as q is increased. Such uncertainty, though tolerable, is a danger signal.

The coefficients for the three wings in oscillatory flow are given in Table 35 and the derivatives have been calculated for pitching motion about the axes of symmetry from equations (32) with $\beta = 1$. Table 43b shows excellent results for the circular wing, good convergence of $z_{\dot\theta}$ and $m_{\dot\theta}$ with respect to N close to exact theory and reverse-flow checks that only reveal errors in the fifth decimal place. Damping derivatives for the rectangular and symmetrically tapered wings with $N = 3$ from Tables 43a and 43c are plotted against q in Fig. 7 together with the corresponding results when the reverse-flow equations (33) and (34) are used for the coefficients. The upper diagram shows $-z_{\dot\theta}$ for the rectangular wing with good correlation when $q = 4$ and 6, but a substantial error of 8 per cent when $q = 1$. The lower diagram shows $-m_{\dot\theta}$ for the symmetrically tapered wing with a persisting discrepancy of nearly 0·01 between direct and reverse flow for $m = 11$, that is halved when $m = 23$ and is compatible with eventual convergence with respect to m.

4.3. *Wings of Constant Chord.*

Planforms 2, 6 and 7 all have constant chord and aspect ratio 4 and are considered in incompressible flow. The first two have smooth edges and illustrate the effect of sweepback without the complication of a central kink. The last two have 45 deg of sweepback at the tip and illustrate the effect of the kink.

From the solutions for steady flow in Tables 4, 5, 7 and 8 there is found to be no appreciable worsening of the convergence with respect to q due to the sweepback or kink. Neither of the swept wings exhibits the same remarkable convergence with respect to m as is noted for the rectangular wing in Section 4.1: the last two columns of Table 8 show somewhat poorer convergence for the skinked straight-edged planform. Moreover, the larger values of λ_0 suggest that there could be a local problem of convergence with respect to N at the central kink as well as near the tip. The local aerodynamic centres for the three wings are fully listed in Tables 23b, 26a and 26b, and some of the spanwise distributions with $N = 4$ are plotted in Fig. 8. For the rectangular wing there is no effect of m and the small effect of q barely exceeds 0·003. In the case of hyperbolic edges there is a minor effect of m and that of q exceeds 0·01 locally. When there is the central kink, the effect of q is similar near the tip, but near the centre section both m and q produce changes of 0·035 in X_{ac} and its distribution, referred to the planform without artificial rounding, is less well defined.

The coefficients for oscillatory motion are given in Tables 35a, 36 and 37. Convergence with respect to q is evidently less sensitive to sweepback than to aspect ratio (Section 4.1), but the kinked wing introduces a marked deterioration in convergence with respect to m. The four pitching derivatives for the swept wings have been calculated from equations (32), and their convergence for the hyperbolic-edged wing has already been demonstrated in Fig. 3. The results for both wings in Table 44 include sets of derivatives calculated from solutions with $m, N, q = 15, 3, 6$ in reverse flow. The pitching damping derivative $-m_{\dot\theta}$ is plotted against axis position $x_0/\bar{c}$ in Fig. 9. The effect of N is indiscernible, and for each wing the full curve represents $N = 3$ and $N = 4$. But, whereas for the hyperbolic edges the curve from reverse flow is also indiscernible, the broken curve for the kinked wing reveals discrepancies in m_θ of order 10 per cent and exceeding 0·1 for rearward axes. This is an order of magnitude greater than likely residual errors from insufficient q and N and still several times what would be expected from the poorer convergence with respect to m. For conventional sweptback wings this aspect of numerical solutions needs more detailed study.

4.4. *Tapered Sweptback Wings.*

The five planforms in this category were all chosen for comparison with other work beyond the scope of the present report. Planforms 8, 9 and 12 relate to steady measurements of pressure distribution, and Planforms 10 and 11 to particular oscillatory applications (Refs. 28 to 32). It will not be necessary to discuss all the tabulated results, and we shall now concentrate mainly on the effects of m and M.

The solutions for the cropped delta wing at $M = 0{\cdot}8$ in Table 10 include a set of three with $N = 3$, $\bar{m} = 31$ and $m = 7$, 15 and 31. Although the effect of m is quite small, the convergence with respect to m is unconvincing. Tables 11 to 13 give results, all with $m = 15$, for an arrowhead wing of identical leading-edge sweepback at $M = 0$, 0·6 and 0·8. Table 11, comprising solutions for the two lower Mach numbers with $N = 2, 3, 4$ and $q = 2N$, shows excellent convergence with respect to N and no adverse effect of compressibility. Figure 10 is prepared from the more comprehensive results for $M = 0{\cdot}8$. The lift slope and aerodynamic centre are plotted against N for three conditions, $q = 1$ showing errors of about 3 per cent, $q = 2$ showing great improvement, and $q = 2N$ when the convergence is really convincing. For $N = 3$, $x_{ac}/\bar{c}$ is plotted against M in the lower part of Fig. 10; although the correct trend is predicted with $q = 1$, the curve for $q = 6$ shows that the error is of the same order as the effect of compressibility. Tables 27 and 28 give the calculated local aerodynamic centres at $M = 0{\cdot}8$ for these wings and Planform 10 of lower aspect ratio and sweepback. The latter with $N = 4$, fixed $\bar{m} = 95$ and $m = 7$, 11 and 15 shows no alarming effects on spanwise loading or X_{ac}, but it is the use of the parameter m for high aspect ratio and sweepback that needs critical examination.

Planform 12 has aspect ratio $A = 8$ and quarter-chord sweepback of 45 deg. As has already been seen in Fig. 4 (Section 3.2), oscillatory pitching derivatives for this wing at $M = 0$ converge inconsistently with respect to m; no common limit is approached with $q = 1$ and $\bar{m} = 95$ before the capacity of the KDF9 computer is exceeded. Results for steady flow are contained in Tables 15, 29, 30 and 31. The overall forces from eleven solutions with $N = 3$ are plotted against the same logarithmic scale of $(m+1)$ in Fig. 11, where besides the values for $q = 1$ and $\bar{m} = 95$ there are some further results in which the artificial rounding is defined by equations (18) to (20) with $m = 15$, i.e. with $y_1 = s \sin(\pi/16)$, while the number of collocation sections m is increased. Under these conditions both the lift slope and aerodynamic centre lie between the best values obtainable with $q = 1$ and $\bar{m} = 95$ and the uncertainties appear to be reduced to $\pm 1\frac{1}{2}$ per cent in $\partial C_L/\partial\alpha$ and $\pm 0{\cdot}015$ in $x_{ac}/\bar{c}$. The local load grading $cC_{LL}/\bar{c}C_L$ and X_{ac} at $\eta = 0$ are plotted similarly in Fig. 12, where by contrast the uncertainties are broadened when the fixed $m = 15$ rounding is considered and reach respective values 4 per cent and 0·04.

The coefficients and pitching derivatives about the mid-root-chord axis are given for four of the swept-back tapered wings in Tables 38, 39, 40, 45 and 48. The typical effect of m is illustrated in Fig. 13 by curves of the damping derivatives against axis position for Planform 10 at $M = 0{\cdot}8$. The factors such as β^{-2} inside the square brackets of the appropriate equations (32) may not improve convergence, and there is evidence in Table 45b to this effect; nevertheless, with $N = 4$ and $\bar{m} = 95$ the curves in Fig. 13 for $m = 11$ and $m = 15$ are close enough to allay serious doubts. It remains to look more closely at the separate effects of m as collocation parameter and rounding parameter, and the results for Planform 11 in Tables 48 are used for this purpose in Section 6.

4.5. *Slender Wings.*

Let $s(x)$ be the local semi-span of a slender planform. Then, provided that the gradient

$$ds/dx = s'(x) \geqslant 0\,,$$

the trailing edge is unswept and the incidence is uniform, slender-wing theory gives a load distribution

$$\frac{\Delta C_p}{\alpha} = \frac{4\, s(x)\, s'(x)}{[\{s(x)\}^2 - y^2]^{1/2}}. \tag{36}$$

Planforms 13 and 14 are complete delta wings of contrasting aspect ratios 1·5 and 0·0001. In the latter case equation (36) is applicable, but ΔC_p remains non-zero along the trailing edge $x = c_r$. Thus the assumed loading in equation (15), which behaves like $0(c_r - x)^{1/2}$, is incorrect for all η. The slender gothic Planform 15 has been chosen to have

$$\frac{s(x)}{s} = 1 - \left(1 - \frac{x}{c_r}\right)^{3/2}, \tag{37}$$

so that equation (15) is no longer violated at the trailing edge when α is constant. In this case the singularities in chordwise loading at the leading and trailing edges are consistent with Multhopp's theory, except at the leading apex.

Steady-flow solutions for these three wings are found in Tables 16 to 18. In Table 16 the not-so-slender wing shows good convergence with respect to q everywhere and with respect to N away from the tip. Table 17 reveals poorer convergence in both respects when $A = 0{\cdot}0001$. Solutions for the slender gothic planform converge much better with respect to N, as demonstrated by the values of λ_0 in Tables 17 and 18, but no satisfactory solutions could be obtained for $q > 6$, as there appears to be a sudden ill-conditioning of the equations. Fortunately there is exact theory (Ref. 8) with which to compare solutions with $m = 11$ and $q = 6$ in the table below.

Solution	Slender delta wing		Slender gothic wing	
	C_L/A	$x_{ac}/\bar{c}$	C_L/A	$x_{ac}/\bar{c}$
$N = 2$	1·4931	1·2318	1·5755	0·9339
$N = 3$	1·5400	1·3331	1·5681	0·9296
$N = 4$	1·5579	1·3189	1·5728	0·9290
Exact	1·5708	1·3333	1·5708	0·9167

These overall aerodynamic characteristics are inaccurate by comparison with the corresponding table for the circular planform in Section 4.2, but this is perhaps to be expected in view of the sharp central kinks.

The calculated local aerodynamic centres for the delta wing ($A = 1{\cdot}5$) in Table 32a show rather poorer convergence with respect to N than with respect to q, but would meet normal practical requirements. Tables 32b and 32c include the exact values for the slender delta wing

$$X_{ac} = \frac{1}{1-\eta}\left[\tfrac{1}{2} - \eta + \frac{\eta^2 \operatorname{sech}^{-1}\eta}{2(1-\eta^2)^{1/2}}\right] \tag{38}$$

and for the slender gothic wing

$$X_{ac} = \frac{3}{2(1-\xi_1)(1-\eta^2)^{1/2}} \int_{\xi_1}^{1} \frac{(\xi-\xi_1)(1-\xi)^{1/2}[1-(1-\xi)^{3/2}]}{[\{1-(1-\xi)^{3/2}\}^2 - \eta^2]^{1/2}}\, d\xi \tag{39}$$

where $\xi_1 = 1 - (1 - |\eta|)^{2/3}$. These are derived from equation (36) with $s(x) = sx/c_r$ and from equation (37) respectively. The spanwise distributions are drawn in Fig. 14 for $N = 2$, 3 and 4. Although the solutions become unreliable close to the tip, the results for both slender wings in the range $0{\cdot}5 < \eta < 0{\cdot}9$ approach the exact curve as N increases. Near the centre the comparisons are less convincing; the delta wing shows poor convergence, and X_{ac} at $\eta = 0$ for the gothic wing appears to converge to a value 0·424 instead of the exact 0·4.

The central chordwise loadings on the two delta wings are plotted in Fig. 15. The trailing-edge condition is seen to have a dominant effect on the convergence with respect to N. Such detailed aerodynamic characteristics demonstrate the wide gulf between the slender-wing and lifting-surface theories. Since Planform 13 is nearly as slender as planforms are likely to become, the divergence in the upper diagram is academic, but so also may be the slender-wing theory in this context.

Garrick's[8] theory for oscillations of low frequency is formulated for pitching motion in Appendix III of Ref. 20. Under the same conditions as equation (36) it can be shown that

$$\left.\begin{aligned} -z_\theta &= \tfrac{1}{4}\pi A \\ -m_\theta &= \tfrac{1}{4}\pi A\left[\frac{c_r - x_0}{\bar{c}} - \frac{c_r}{\bar{c}}\int_0^1 \left(\frac{s(x)}{s}\right)^2 d\left(\frac{x}{c_r}\right)\right] \\ -z_{\dot\theta} &= \tfrac{1}{4}\pi A\left[\frac{c_r - x_0}{\bar{c}} + \frac{c_r}{\bar{c}}\int_0^1 \left(\frac{s(x)}{s}\right)^2 d\left(\frac{x}{c_r}\right)\right] \\ -m_{\dot\theta} &= \tfrac{1}{4}\pi A\left[\frac{c_r - x_0}{\bar{c}}\right]^2 \end{aligned}\right\} . \tag{40}$$

Although negative damping is never predicted, $-m_{\dot\theta}$ falls to zero when the pitching axis coincides with the trailing edge. Now

$$\frac{c_r}{\bar{c}} = 2 \text{ and } \int_0^1 \left(\frac{s(x)}{s}\right)^2 d\left(\frac{x}{c_r}\right) = \frac{1}{3} \quad \text{for the delta wing,}$$

$$\frac{c_r}{\bar{c}} = \frac{5}{3} \text{ and } \int_0^1 \left(\frac{s(x)}{s}\right)^2 d\left(\frac{x}{c_r}\right) = \frac{9}{20} \quad \text{for the gothic wing,}$$

and hence the picthing derivatives are easily evaluated. Coefficients from the collocation solutions are given for the three wings in Table 41, where the delta wing ($A = 1{\cdot}5$) is seen to provide excellent convergence with respect to q and N. The derivatives, calculated from equations (32) for the mid-root-chord axis in Table 46, show good convergence with respect to N for the gothic wing, but not for the slender delta wing. Such is the effect of violating the condition of zero loading at the trailing edge. It is well summarized in Fig. 16 by the curves of $-m_{\dot\theta}/A$ against x_0/c_r. The discrepancies between $N = 4$ and exact theory are more than twenty times greater for the delta than for the gothic planform.

4.6. *Wings with Curved Tips.*

In Section 3.1 the lift slope and centres of lift of Planform 16 are used to illustrate a case in which the previous version of Multhopp's theory ($q = 1$) is in serious error. Moreover, Fig. 2 shows adequate convergence of overall forces with respect to the parameters m, N and q. From the full solutions in Tables 20 and 21 for this wing at $M = 0$ the local convergence is less satisfactory, especially in the region of the curved tip. Associated features in the last three columns of Table 21 ($q = 8$) are the irregular spanwise distributions of μ_n, κ_n and λ_n, which can be attributed partly to the high sweepback ($\Lambda = 60°$) and partly to the curved tip. In Table 22 the same features are found for Planform 17, another curved-tipped wing of slightly lower sweepback ($\Lambda = 55°$) but at $M = 0{\cdot}8$. Here the lift slope with $m = 11$ and $N = 3$ falls by over 10 per cent as q is increased from 1 to 8. Attention is also drawn to the third and last solutions in Table 22, which differ only in the amount of central rounding; this is seen to influence the lift slope by 2 per cent and the local lift at $\eta = 0$ by 8 per cent. The behaviour of the calculated $\partial C_L/\partial\alpha$ is plotted in the upper diagrams of Fig. 17, which demonstrate the effect of q and suggest that the aerodynamic effect of the artificial rounding may need to be taken into account (Section 6).

There are eleven solutions with $N = 3$ for Planform 17 in low-frequency pitching motion at $M = 0{\cdot}8$. The coefficients in Table 42 and the derivatives for the mid-root-chord axis in Table 47 show a marked effect of q with satisfactory convergence, but there are considerable differences between the five results with $\bar{m} = 95$ as the rounding and number of collocation sections are changed. The pitching damping about the axis $x_0 = 1{\cdot}5\bar{c}$ just forward of the aerodynamic centre is plotted against $(\bar{m}+1)$ and $(m+1)$ in the lower part of Fig. 17. By increasing the parameter q the discrepancies are reduced from 30 per cent ($\bar{m} = m = 11$) to ± 3 per cent.

A peculiarity of curved tips is the behaviour of local aerodynamic centres in Tables 33 and 34. Previous solutions with $q = 1$ had indicated a rapidly falling value of X_{ac} as $\eta \to 1$ in common with the accepted characteristic of sweptback wings of non-zero tip chord, *viz.*, Fig. 8. Spanwise distributions of X_{ac} for the two curved-tipped wings are drawn in Fig. 18, where the upper diagram for Planform 17 shows a marked effect of q such that the fall in X_{ac} virtually disappears; there remains, however, the irregular waviness already noted. The lower diagram supports the progressive effect of q on X_{ac} by experimental data from Ref. 34 calculated from observed pressure distributions on two half-models of Planform 16 with different aerofoil thickness. Apart from the slender delta wing (Section 4.5), planforms with curved tips have presented the greatest difficulties regarding convergence. They have, nevertheless, provided convincing examples of the need for the improved programme of Ref. 18 and some experimental confirmation of its success.

5. *Criteria for Selecting m, N and* $\bar{m}$.

The preceding sub-sections have demonstrated that the rate of convergence of solutions by the Algol programme of Ref. 18 is highly dependent on the type of planform. From the wide range of results available it should be possible to recommend a suitable set of values of the parameters m, N and $\bar{m}$ for other planforms, but discretion is needed according to the scope of the aerodynamic quantities to be evaluated and the required accuracy.

The difficulty in choosing the number of collocation sections is that in the standard procedure for kinked planforms the odd integer m has the added role of defining the artificial central rounding. Where this complication does not arise, i.e. for Planforms 1, 2, 3, 4 and 6, $(m+1)$ can safely be taken below the value $4A \sec \Lambda_1$ recommended as a minimum in Section 2.4 of Ref. 18, unless accurate results are required close to the wing tip. It is probably best to relate the choice of m to the length of the trailing edge and, in view of the factors β^{-2} in the square brackets of the last two of equations (32), not to reduce its value in compressible flow. In general, the recommendation of Ref. 18 should be followed and the number of collocation sections should satisfy the condition

$$m+1 \geqslant 4A \sec \Lambda_1 \tag{41}$$

where for curved trailing edges $\sec \Lambda_1$ may be regarded as the length of the trailing edge as a fraction of the span. However, it is undesirable to take $m < 11$, and this is the recommended minimum value whenever $A \sec \Lambda_1 < 3$. From Section 6 it will appear that, when artificial rounding is necessary, the standard y_1 in equations (18) to (20) should be replaced by

$$y_2 = s \sin \frac{2\pi}{m+1}. \tag{42}$$

The results then involve smaller collocation error but need some allowance for the rounding itself.

An increase in the number of chordwise terms causes slower convergence with respect to $\overline{m}$. It is therefore desirable to choose the smallest value of N that ensures theoretical data to the required accuracy. In practice the choice rests between $N = 3$ and $N = 4$. For the simple mode of rigid pitching oscillation there is little evidence in Tables 43 to 47 to suggest that appreciable errors would result from using $N = 3$. Only in the case of the slender gothic wing in Table 46c would $N = 4$ seem to be overwhelmingly advantageous. In steady flow at uniform incidence, however, it is essential to take $N = 4$ when the chordwise loading is to be calculated near a tip or a central kink. A glance at the magnitude of λ_n, when it appears in Tables 3 to 22, gives the best indication of the importance of the fourth chordwise term. At the central section, for example, it is only for wings of leading-edge sweepback $\tan \Lambda_0 \geqslant \beta$ that $|\lambda_0|$ exceeds 0·01. For applications to more complicated oscillatory modes or camber distributions the four terms may prove inadequate and the method of Ref. 18 must be used with discretion.

In the course of the present work convergence with respect to $\overline{m}$ or q has naturally been a major preoccupation. One criterion embracing a wide range of planforms is that the lift slope $\partial C_L/\partial\alpha$ should be within $\frac{1}{2}$ per cent of its value for the highest attainable value of q. The upper part of Fig. 19 shows for ten planforms the roughly estimated values of the quantity

$$\frac{\overline{m}+1}{\beta A}\sin^2\left(\frac{\pi}{2N+1}\right) = \frac{q(m+1)}{\beta A}\sin^2\left(\frac{\pi}{2N+1}\right)$$

above which this is achieved. The critical values depend to some extent on N, but the values are mainly for $N = 3$ and lie reasonably close to a curve against $\beta^{-1}\tan\Lambda_{\frac{1}{2}}$, where $\Lambda_{\frac{1}{2}}$ is the angle of mid-chord sweepback. In producing a criterion for selecting $\overline{m}$, the compressibility factor is retained in the sweepback but, to ensure extra accuracy of the coefficients in equations (32), it is omitted in the aspect ratio. The full curves in the lower part of Fig. 19 give the corresponding critical values of $(\overline{m}+1)/A$ for $N = 3$ and 4 and offer one lower limit to $\overline{m}$ as an alternative to the tentative equation (5). Another consideration from Sections 4.1 and 4.4 is that there is usually a substantial improvement in a solution when q is increased from 1 to 2, and $q = 2$ should be regarded as a minimum value. It therefore follows from the recommended choice of m that

$$\left.\begin{aligned} \overline{m}+1 &\geqslant 24 \\ \overline{m}+1 &\geqslant 8A\sec\Lambda_1 \end{aligned}\right\} \qquad (43)$$

which for $N = 3$ will usually be more restrictive than the condition set in Fig. 19.

The following table lists the minimum odd values of $\overline{m}$ from the conditions (43) and any larger values that may be required by equation (5) or Fig. 19.

Planform				Minimum $\bar{m}$ ($N = 3$)			
No.	A	$A \sec \Lambda_1$	$\tan \Lambda_{\frac{1}{2}}$	Eqn. (43)	Eqn. (5)	Fig. 19 $M = 0$	Fig. 19 $M = 0{\cdot}8$
2	4·00	4·00	0	31	43	—	—
3	8·00	8·00	0	63	85	—	—
5	4·33	4·48	0	35	47	—	—
7	4·00	5·66	1·00	45	61	—	61
9	2·83	3·37	1·00	27	35	29	43
10	1·45	1·53	0·58	23	—	—	—
11	2·00	2·24	1·12	23	23	—	33
12	8·00	10·54	0·95	85	111	—	115
13	1·50	1·50	1·33	23	—	—	(31)
16	3·90	7·80	1·73	63	83	—	?
17	3·56	6·20	1·43	49	65	—	(79)

Equation (5) usually overrides conditions (43) and can be recommended for $M = 0$. The larger values of $\bar{m}$ from Fig. 19 for $M = 0{\cdot}8$ are thought to be essential. For the tapered sweptback wings of moderately small aspect ratio the pitching damping derivatives tend to converge more slowly than the lift slope on which Fig. 19 is based. Table 45a for Planform 9 suggests that $\bar{m} = 63$ is desirable when $M = 0{\cdot}8$. This is met by modifying conditions (43) to become

$$\left.\begin{aligned} \bar{m}+1 &\geqslant 24/\beta^2 \\ \bar{m}+1 &\geqslant 8A \sec \Lambda_1 \end{aligned}\right\}. \qquad (44)$$

Then equations (5) and Fig. 19 only enter into consideration when both aspect ratio and sweepback are moderately high or when in applications to detailed load distributions in steady flow it is necessary to take $N = 4$. The following sets of maximum permissible values of m, q and $\bar{m}$ will then apply.

m	11	15	21	27
q	14	8	4	2
$\bar{m}$	167	127	87	55

The tables in Section 1 of Ref. 18 indicate other upper restrictions on m, N and q, which are imposed to keep within the capacity of the KDF9 computer and an arbitrary maximum running time of 45 minutes. For planforms of high aspect ratio where these restrictions prohibit the use of the recommended values of m, N and $\bar{m}$, N should be reduced to 3 or $(m+1)$ should be lowered from $4A \sec \Lambda_1$ until a satisfactory value of $\bar{m}$ can be accommodated.

6. *Central Rounding of Sweptback Planforms.*

Earlier sections have foreshadowed the need to study the influence of the central rounding on the solutions. It may be asked what happens when the rounding in equations (18) to (20) is increased, reduced or removed. It may be wondered whether such a study can shed light on the discrepancy between direct and reverse flow in the lower half of Fig. 9. In Figs. 11, 12 and 17 the rounding has been kept constant while the number of collocation sections has been increased, and crucial uncertainty lies in the aerodynamic influence of the rounding itself. It remains to clarify these three matters and to re-interpret certain of the theoretical data already discussed.

There are four planforms for which the rounding has been systematically varied without changing the collocation sections and spanwise integration points. The solutions at steady unit incidence in Tables 9, 14 and 19 include a fixed value of m to denote the number of collocation sections and a variable m to define y_1 in equation (18); in Table 9, for example, $m = \infty$ denotes zero rounding and $m = 7$ is virtually twice the standard rounding $m = 15$, and their respective effects are to reduce C_L by $7\frac{1}{2}$ per cent and to increase it by 2 per cent. Naturally there are marked changes in the loading functions γ_0, μ_0, κ_0 and λ_0 at the centre section. For the slender gothic wing there is no difficulty in computing the exact central chordwise loading from equation (36)

$$\Delta C_p/\alpha = 4\, s'(x) \text{ at } y = 0 \tag{45}$$

so as to include the effect of the rounding. Fig. 20 shows full curves from exact theory with the standard $m = 11$ rounding and also with $m = 5$ and $m = 23$, to compare with the distributions when γ_0, μ_0 and κ_0 from Table 19 are substituted into equation (15). There is a remarkable diminution in collocation error with twice the standard rounding, and as decisive a worsening when the standard rounding is halved. It follows from equation (45) that the distance of the local aerodynamic centre from the trailing edge is precisely the geometric mean chord. Referred to the actual root chord c_r,

$$X_{ac} = 1 - \frac{S'}{2sc_r} \tag{46}$$

where S' is the area of the rounded planform. The top left diagram of Fig. 21 compares the result

$$X_{ac} = \frac{1}{c_r}\left[x_{l0} + c_0\left(\frac{1}{4} - \frac{\mu_0}{\gamma_0}\right)\right] \tag{47}$$

from the solutions in Table 19 with equation (46) and shows that with twice the standard rounding $(m+1 = 6)$ the collocation and rounding errors are nearly equal. Against the same diagrammatic scale of the rounding parameter $(m+1)$, Fig. 21 shows for each of the four wings the central X_{ac} and the ratio of C_L to its value with the standard rounding. Especially for Planforms 7 and 9 with sweptback trailing edges, there is no sign of convergence at either end of the scale. The conclusion is reached that solutions with less than the standard rounding are useless, while those with greater rounding may need some correction to offset its genuine aerodynamic influence.

Fig. 7 of Ref. 36 indicates excellent agreement between damping derivatives $-z_{\dot\theta}$ and $-m_{\dot\theta}$ against pitching axis calculated from direct-flow and reverse-flow solutions for Planform 11 at $M = 0{\cdot}781$. These calculations correspond to $m, N, q = 15, 3, 1$ in the present method and are now seen to give misleading satisfaction. The effects of q in direct and reverse flow are given by coefficients in Table 39, by derivatives in Table 48 and graphically in Fig. 22. Although both solutions converge with respect to q, they diverge from each other until with $q \geqslant 4$ there are constant discrepancies of 0·1 in $z_{\dot\theta}$ and 0·03 in $m_{\dot\theta}$. These discrepancies are repeated when the number of chordwise terms is increased to $N = 4$. Spanwise collocation error due to the irregularity of the planform with $m = 15$ rounding is suspected, and further solutions have been obtained with the same rounding but $m, N, q = 31, 3, 2$. The points (O and X) for $\bar{m}+1 = 64$ in Fig. 22 show that the discrepancies between direct and reverse flow are reduced by the factor 0·18 to a satisfactory level. An even better result can be achieved with $m, N, q = 15, 3, 6$ and the rounding used in Ref. 23 which amounts to equations (19) with a different square bracket, *viz.*,

$$\left.\begin{aligned} x_l(y) &= x_l(y_1)\left[\frac{1}{3} + \left(\frac{|y|}{y_1}\right)^2 - \frac{1}{3}\left(\frac{|y|}{y_1}\right)^3\right] \\ c(y) &= c_r + \left[\frac{1}{3} + \left(\frac{|y|}{y_1}\right)^2 - \frac{1}{3}\left(\frac{|y|}{y_1}\right)^3\right]\{c(y_1) - c_r\} \end{aligned}\right\}. \tag{48}$$

The lower order of the polynomial in $|y|/y_1$ gives rounded leading and trailing edges with larger displacement and smaller curvature. The only misgiving is that the displacement may be influencing the answer and that the effect, though apparently small in Fig. 22, may be important for more highly swept trailing edges.

An attempt has been made to estimate the genuine effect of the rounding by considering only solutions in which the standard rounding is doubled. Thus y_2 in equation (42) is used in place of y_1 in equations (18) to (20). The ratio of the displacement of the leading edge to the root chord

$$\xi_0 = \frac{x_{l0}}{c_r} = \frac{y_2 \tan \Lambda_0}{6\, c_r} \tag{49}$$

is taken as a measure of the rounding. Such solutions are available for Planforms 7, 9, 13 and 16 each with two different roundings and will be found in Tables 9, 14 and 49. Corresponding values of overall forces, spanwise loading and local aerodynamic centres are presented in Table 50. For the Planform 7 of constant chord there are three solutions in Table 9 with $N = 3$ and the following results are obtained.

Rounding m, N, q ξ_0	$m = 15$ 31, 3, 2 0·0650	$m = 11$ 23, 3, 4 0·0863	$m = 7$ 15, 3, 6 0·1276
C_L $\bar{\eta}$ $x_{ac}/\bar{c}$	3·0042 0·4653 1·1748	3·0080 0·4649 1·1743	3·0215 0·4640 1·1764
C_{LL} at $\eta = 0$ X_{ac} at $\eta = 0$	3·0460 0·4034	3·0740 0·4170	3·1322 0·4464

Since the values tabulated above are roughly linear in ξ_0, it is permissible to think in terms of gradients

$$\frac{1}{C_L}\frac{\partial C_L}{\partial \xi_0}, \frac{\partial \bar{\eta}}{\partial \xi_0}, \frac{\partial}{\partial \xi_0}\left(\frac{x_{ac}}{\bar{c}}\right), \frac{1}{C_{LL}}\frac{\partial C_{LL}}{\partial \xi_0}, \frac{\partial X_{ac}}{\partial \xi_0},$$

and these are estimated for the four wings and plotted against $A \tan \Lambda_1$ in Fig. 23. To the rough accuracy now envisaged the straight lines adequately represent the known data and can be used to re-interpret some of the discrepancies that have already arisen.

First we consider Fig. 2 in relation to the appreciably different results in Table 50d with doubled rounding and small collocation error. When the overall forces in Table 50d for the $m = 15$ rounding are corrected by subtraction of the contributions from Fig. 23 with $\xi_0 = 0{\cdot}103$ and $A \tan \Lambda_1 = 6{\cdot}75$, the final values are

$$\left.\begin{aligned} \partial C_L/\partial\alpha &= 2{\cdot}3500\,[1-(0{\cdot}18 \times 0{\cdot}103)] = 2{\cdot}306 \\ \bar{\eta} &= 0{\cdot}4684+(0{\cdot}032 \times 0{\cdot}103) \quad = 0{\cdot}4717 \\ x_{ac}/\bar{c} &= 1{\cdot}8981+(0{\cdot}06 \times 0{\cdot}103) \quad\;\; = 1{\cdot}904 \end{aligned}\right\}.$$

It may be concluded that in Fig. 2 there are opposing effects of collocation error and rounding error, so that the standard results with sufficient $\bar{m}$ are better than would be expected.

Next there is the discrepancy in pitching damping between direct and reverse flow for Planform 7 in Fig. 9. There are some further calculations for this wing with twice the standard rounding in Table 51, which illustrate the transformation in equations (33) and (34) from coefficients $\bar{I}_{Lr}$, $-\bar{I}_{mr}$ and $-\bar{I}^*_{mr}$ for the reversed wing to I_{Lr}, $-I_{mr}$ and $-I^*_{mr}$ from reverse flow. The worst discrepancies in m_a for the rearward axes are reduced from 10 per cent to an acceptable 2 per cent. Tables 51a and 51c suggest that the pitching derivatives are not linear in ξ_0, but that the corrections to allow for the smaller roundings are negligible in this case.

From the solution in the last column of Table 15 and the last row of Table 31 we may comment on the results in Figs. 11 and 12 for Planform 12. Since $\xi_0 = 0{\cdot}0988$ and $A \tan \Lambda_1 = 6{\cdot}86$, the final estimated theoretical values of total and local loads at $\eta = 0$ are

$$\left.\begin{aligned} \partial C_L/\partial\alpha &= 3{\cdot}7634\,[1-(0{\cdot}18 \times 0{\cdot}0988)] &&= 3{\cdot}696 \\ x_{ac}/\bar{c} &= 2{\cdot}1745+(0{\cdot}055 \times 0{\cdot}0988) &&= 2{\cdot}180 \\ cC_{LL}/\bar{c}C_L &= 1{\cdot}0981 \times \frac{1-(0{\cdot}71 \times 0{\cdot}0988)}{1-(0{\cdot}18 \times 0{\cdot}0988)} &&= 1{\cdot}040 \\ X_{ac} &= 0{\cdot}4214-(0{\cdot}85 \times 0{\cdot}0988) &&= 0{\cdot}337 \end{aligned}\right\}.$$

The lift slope and aerodynamic centre in Fig. 11, corresponding to $\bar{m} = 95$ and the standard rounding, are again fairly consistent with the new values. In the case of the lift slope the collocation and rounding errors due to m almost cancel, while the rounding correction to $x_{ac}/\bar{c}$ takes it half-way back to its value with the standard rounding. The load grading $(cC_{LL}/\bar{c}C_L)$ at $\eta = 0$ in Fig. 12 is not improved by considering collocation error alone as the rounding error is now estimated to be larger and of opposite sign; the new value is fairly consistent with the trend of the full curve for $\bar{m} = 95$ and the standard rounding. It is perhaps premature to discuss the local X_{ac} at the centre section, but the facts suggest that Fig. 12 is quite misleading and that the rapid increases as $\eta \to 0$, plotted in Fig. 8 for example, are grossly exaggerated. Moreover, there is experimental evidence for this wing in Fig. 14 of Ref. 32 to support the new value $X_{ac} = 0{\cdot}337$.

The next discrepancy to consider is that for the slender gothic planform at $\eta = 0$ in Fig. 14. The solution in Table 19 with twice the standard rounding gives the local $X_{ac} = 0{\cdot}4110$ when $\xi_0 = 0{\cdot}0617$. The corrected value is

$$X_{ac} = 0{\cdot}4110-(0{\cdot}28 \times 0{\cdot}0617) = 0{\cdot}394$$

in better agreement with the exact value 0·4 than the result $X_{ac} = 0{\cdot}424$ in Fig. 14.

It is suggested in Section 4.6 that the behaviour of $\partial C_L/\partial\alpha$ in the top right diagram of Fig. 17 is evidence that the aerodynamic effect of the artificial rounding may need to be taken into account. The solution with twice the standard rounding and $\xi_0 = 0{\cdot}0977$ for Planform 17 ($A \tan \Lambda_1 = 5{\cdot}08$) at $M = 0{\cdot}8$ is now corrected to give

$$\partial C_L/\partial\alpha = 2{\cdot}7918\,[1-(0{\cdot}13 \times 0{\cdot}0977)] = 2{\cdot}756\,,$$

a value in keeping with the trend of the results labelled $\bar{m} = 95$ in Fig. 17.

A final instance of the importance of considering both collocation and rounding error concerns the value of X_{ac} at $\eta = 0{\cdot}195$ in the lower diagram of Fig. 18. The result in Table 50d for the smaller doubled rounding is now corrected to give

$$X_{ac} = 0{\cdot}2771-(0{\cdot}08 \times 0{\cdot}103) = 0{\cdot}269$$

which is seen to be in better agreement with experiment than the standard solution with $m, N, q = 15, 4, 8$.

7. *Concluding Remarks.*

(1) A parallel investigation is reported in Ref. 39, where Planforms 1, 4, 6 and 9 in steady incompressible flow are treated by the methods of Refs. 18, 23 and 24. By comparison with the present investigation a higher degree of accuracy is sought and remarkably good agreement is found between the three methods. There is no doubt about the increasing superiority of Ref. 23 for wings of higher aspect ratio and of Ref. 24 when much larger numbers of chordwise terms are necessary.

(2) The present investigation establishes that large errors can result from previous extensions of the steady-flow theory of Ref. 19 or the low-frequency theory of Ref. 20 to three and four chordwise terms. The refinements in Ref. 18 reduce these errors to meet practical requirements in theoretical spanwise loading, local aerodynamic centres and oscillatory pitching derivatives.

(3) The properties of numerical convergence differ throughout the range of planforms. Rectangular wings require remarkably few, say $A =$ aspect ratio, collocation sections on the half-wing. For more general planforms, provided the leading and trailing edges are smooth and of low curvature, $2A$ collocation sections on the half-wing are adequate. The central kink of a sweptback wing leads to a situation in which the balance between artificial rounding and number of collocation sections becomes crucial, with further complication in the convergence of wing loading near curved tips.

(4) To define a calculation for a particular planform and Mach number, the following choice of parameters is recommended:

$$m+1 \geqslant 4A \sec \Lambda_1 ,$$

where $\sec \Lambda_1$ is generalized to be the length of the trailing edge as a fraction of the span.

$N = 3$ for calculations of pitching derivatives unless $\beta A \leqslant 1$, say,

$N = 4$ for elastic modes of oscillation or detailed wing loading.

$q \geqslant 2$ and related conditions

$$\left.\begin{array}{l} \bar{m}+1 \geqslant 24/\beta^2 \\ \bar{m}+1 \geqslant 8A \sec \Lambda_1 \\ \bar{m}+1 \geqslant 2A \sec \Lambda_1 \operatorname{cosec}^2 \dfrac{\pi}{2N+1} \\ (\bar{m}+1) \quad \text{to satisfy Fig. 19} \end{array}\right\}$$

(5) Errors are likely to persist near a kinked centre section or crank and near a tip. For chordwise loading the maximum $N = 4$ is inadequate locally if the kink is severe or the tip is too closely explored, but it should suffice elsewhere unless the camber or deformation of the wing warrants a larger value from two-dimensional considerations. Checks by reverse flow have proved that a severe central kink must be given adequate rounding if collocation error is to be acceptable; the standard rounding in Ref. 18 falls short in this respect. If the leading-edge sweepback is of order 45 deg, then the doubled extent of rounding

$$0 < y < y_2 = \sin \frac{2\pi}{m+1}$$

is recommended in place of equation (18) or, following Ref. 23, the rounding from equation (48) may be used.

(6) Fig. 23 has been prepared on the hypotheses that the doubled displacement of the leading edge

$$\xi_0 \, c_r = x_{l0} = \tfrac{1}{6} y_2 \tan \Lambda_0$$

eliminates collocation error, and that the rounding itself introduces an aerodynamic effect proportional to ξ_0. Thus the solutions with doubled rounding may be corrected roughly for rounding error which is quite as important as the collocation error with the standard rounding. Section 6 includes several examples to suggest that the standard solutions with both collocation and rounding errors are closer to the true solution for the planform with leading apex than the others with only rounding error; local aerodynamic centres from the latter, corrected for rounding error, are found to lie closer to exact theory or experiment.

(7) The method of Ref. 18 and the present results have been applied or developed along the following lines:

(i) As suggested in Section 1, the same principles now under discussion apply equally to certain subsonic theories with general frequency parameter and have led to the significant improvements in Ref. 40.

(ii) The present low-frequency method has been extended to treat slowly oscillating part-span control surfaces, in particular the derivatives of hinge moment (Ref. 41).

(iii) The AGARD Manual on Aeroelasticity is to include an extra chapter, in which the results of numerous oscillatory theories are compared for wings including Planforms 4, 5, 10 and 11 (Ref. 42).

(iv) The influence of central rounding on local loading is so large that it requires more systematic study; the few solutions with doubled rounding in Tables 9, 14, 15, 19, 22 and 49 are suitable for further analysis.

(v) Half-models of Planforms 8, 9, 12, 16 and 17 without twist or camber or fuselage have been extensively pressure plotted, and theoretical solutions for these wings can be extended to include effects of aerofoil thickness.

Acknowledgements.

The author acknowledges the assistance of Mrs. S. Inch of the Aerodynamics Division, N.P.L., who has been responsible for the preparation of data tapes and the tabulated results. She and Mrs. S. Lucas have shared the task of numerical analysis and have helped to prepare the illustrations. Acknowledgments are also due to the operators of the KDF9 computer in the Central Computer Unit, N.P.L.

LIST OF SYMBOLS

A	Aspect ratio; $2s/\bar{c}$
c	Local chord
$\bar{c}$	Geometric mean chord; $S/2s$
c_n	Local chord at station n including any artificial rounding
c_r	Root chord
C_L	Lift coefficient; lift$/\frac{1}{2}\rho U^2 S$
C_{LL}	Local lift coefficient; local lift$/\frac{1}{2}\rho U^2 c$
C_m	Nose-up pitching moment about root leading edge$/\frac{1}{2}\rho U^2 S\bar{c}$
C_p	Pressure coefficient; $\Delta C_p =$ pressure difference$/\frac{1}{2}\rho U^2$
I_{Lr}, I_{mr}	Lift and pitching-moment coefficients in equations (16)
$\bar{I}_{Lr}, \bar{I}_{mr}$	Equivalent of I_{Lr}, I_{mr} for reversed planform
$I^*_{mr}, \bar{I}^*_{mr}$	Second moment coefficient in equation (17) for direct, reversed planform
	Kernel function
l	Non-dimensional load distribution; ΔC_p
$\bar{l}$	Complex load distribution from expression (1)
l_r	Loading l corresponding to $\alpha = \alpha_r$ in equations (13) and (14)
m	Number of collocation sections; rounding parameter in equation (18)
$\bar{m}$	Number of spanwise integration points; $q(m+1)-1$
$m_\theta, m_{\dot{\theta}}$	Oscillatory pitching-moment derivatives in equation (31)
M	Mach number of free stream
n	Subscript or integer denoting loading station in equation (11)
N	Number of chordwise functions or collocation points
q	Factor; $(\bar{m}+1)/(m+1)$
r	Subscript or integer denoting incidence in equations (13) and (14)
s	Semi-span of wing
$s(x)$	Local semi-span of wing
S	Area of planform
t	Time
U	Velocity of free stream
x, y ; x', y'	Rectangular co-ordinates referred to root leading edge
x_0	Location of pitching axis
x_{ac}	Aerodynamic centre referred to $\bar{c}$; $-C_m/C_L$
x_l	Ordinate of leading edge

x_{ln}	Ordinate of leading edge at station n including any artificial rounding
X_{ac}	Local aerodynamic centre referred to leading edge in equation (23)
y_1, y_2	Semi-span of artificial rounding; $s \sin \dfrac{\pi}{m+1}, s \sin \dfrac{2\pi}{m+1}$
z	$\frac{1}{2}(m-1)$
$\bar{z}$	Complex upward displacement of wing surface
$z_\theta, z_{\dot{\theta}}$	Lift derivatives for pitching oscillations in equation (31)
α	Incidence of wing (radians)
α_r	Distribution of incidence in equations (13) and (14)
β	Compressibility factor; $(1-M^2)^{1/2}$
γ	Non-dimensional circulation; $\frac{1}{4}\, cC_{LL}/s$
γ_n	First chordwise loading function in equation (10)
η	Spanwise ordinate; y/s
$\bar{\eta}$	Spanwise centre of pressure in equations (25) and (27)
θ	Spanwise parameter; $\cos^{-1} \eta$
θ_0	Amplitude of pitching oscillation (radians)
κ_n	Third chordwise loading function in equation (10)
λ	$c_r/\bar{c}$
λ_n	Fourth chordwise loading function in equation (10)
Λ	Angle of sweepback
Λ_ξ	Local sweepback at chordwise position $\xi = 0, \frac{1}{2}, 1$
μ_n	Second chordwise loading function in equation (10)
ν	Subscript or integer denoting collocation section in equation (7)
$\bar{\nu}$	Frequency parameter; $\omega\bar{c}/U$
ξ	Local chordwise position; $(x-x_l)/c$
ξ_0	Leading-edge rounding parameter; x_{l0}/c_r
ρ	Density of free stream
ϕ	Chordwise parameter; $\cos^{-1}(1-2\xi)$
ω	Circular frequency of oscillation

REFERENCES

No.	*Author(s)*	*Title, etc.*
1	I. E. Garrick	Non steady wing characteristics. *High Speed Aerodynamics and Jet Propulsion*, Vol. VII, Aerodynamic Components of Aircraft at High speeds, Section F (Ed. A. F. Donovan and H. R. Lawrence). Oxford University Press, 1957.
2	D. E. Williams..	Some mathematical methods in three-dimensional subsonic flutter-derivative theory. A.R.C. R. & M. 3302, February, 1961.
3	A. I. van de Vooren and W. Eckhaus ..	Strip theory for oscillating swept wings in incompressible flow. N.L.L. Report F.146, April, 1954.
4	W. Eckhaus	Strip theory for oscillating swept wings in compressible subsonic flow. N.L.L. Report F.159, October, 1955.
5	D. E. Lehrian	Calculation of flutter derivatives for wings of general plan-form. A.R.C. R. & M. 2961, January, 1954.
6	H. L. Runyan and D. S. Woolston	Method for calculating the aerodynamic loading on an oscillating finite wing in subsonic and sonic flow. N.A.C.A. Report 1322, 1957.
7	V. J. E. Stark	A method for solving the subsonic problem of the oscillating finite wing with the aid of high-speed digital computers. S.A.A.B. Tech. Note 41, December, 1958.
8	I. E. Garrick	Some research on high-speed flutter. Third Anglo-American Aeronautical Conference, Brighton, 4th–7th September, 1951, pp. 419–446. (The Royal Aeronautical Society).
9	B. Mazelsky	Theoretical aerodynamic properties of vanishing aspect ratio harmonically oscillating rigid airfoils in a compressible medium. *J. Aero. Sci.*, Vol. 23, pp. 639–652, July, 1956.
10	H. R. Lawrence and E. H. Gerber	The aerodynamic forces on low-aspect-ratio wings oscillating in an incompressible flow. *J. Aero Sci.*, Vol. 19, pp. 769–781, November, 1952.
11	P. Cicala	La teoria e l'esperienza nel fenomeno delle vibrazioni alari. L'Aerotechnica, Vol. 18, pp. 412–433, April, 1938. Translation in N.A.C.A. Tech. Memo. 887, 1939.
12	E. Reissner	On the theory of oscillating airfoils of finite span in subsonic compressible flow. N.A.C.A. Report 1002, 1950.

No.	*Author(s)*	*Title, etc.*
13	C. E. Watkins, H. L. Runyan and D. S. Woolston	On the kernel function of the integral equation relating the lift and downwash distributions of oscillating finite wings in subsonic flow. N.A.C.A. Report 1234, 1955.
14	J. R. Richardson	A method for calculating the lifting forces on wings (Unsteady subsonic and supersonic lifting-surface theory). A.R.C. R. & M. 3157, April, 1955.
15	P. T. Hsu	Some recent developments in the flutter analysis of low-aspect-ratio wings. *Proceedings of the National Specialists Meeting on Dynamics and Aeroelasticity*, Fort Worth, Texas, 6th–7th November, 1958, pp.7–26. (Institute of the Aeronautical Sciences).
16	B. Laschka	Zur Theorie der harmonisch schwingenden tragenden Fläche bei Unterschallanströmung. *Z. Flugwiss.*, Vol. 11, pp. 265–292, July, 1963.
17	D. E. Davies	Calculation of unsteady generalised airforces on a thin wing oscillating harmonically in subsonic flow. A.R.C. R. & M. 3409, August, 1963.
18	H. C. Garner and D. A. Fox	Algol 60 programme for Multhopp's low-frequency subsonic lifting-surface theory. A.R.C. R. & M. 3517, April, 1966.
19	H. Multhopp	Methods for calculating the lift distribution of wings. (Subsonic lifting-surface theory). A.R.C. R. & M. 2884, January, 1950.
20	H. C. Garner	Multhopp's subsonic lifting-surface theory of wings in slow pitching oscillations. A.R.C. R. & M. 2885, July, 1952.
21	K. W. Mangler and B. F. R. Spencer	Some remarks on Multhopp's subsonic lifting-surface theory. A.R.C. R. & M. 2926, August, 1952.
22	H. C. Garner	Accuracy of downwash evaluation by Multhopp's lifting-surface theory. A.R.C. R. & M. 3431, July, 1964.
23	P. J. Zandbergen, T. E. Labrujere and J. G. Wouters	A new approach to the numerical solution of the equation of subsonic lifting surface theory. N.L.R. Report TR G.49, November, 1967.

No.	Author(s)	Title, etc.
24	B. L. Hewitt and W. Kellaway	A new treatment of the subsonic lifting surface problem using curvilinear co-ordinates. Part I—Details of the method as applied to regular surfaces with finite tip chords and a preliminary set of numerical results. B.A.C. Preston Division Report Ae. 290. S. & T. Memo. 20/68, August, 1968.
25	V. J. E. Stark	Aerodynamic forces on rectangular wings oscillating in subsonic flow. S.A.A.B. Tech. Note 44, February, 1960.
26	E. van Spiegel	Boundary value problems in lifting surface theory. N.L.L. Tech. Report W.1, March, 1959.
27	J. P. Benthem and J. G. Wouters	The calculation of aerodynamic forces on the circular wing in unsteady incompressible flow. N.L.R. Tech. Note W.25, November, 1963.
28	E. W. E. Rogers, I. M. Hall and C. J. Berry	An investigation of the flow about a plane half-wing of cropped-delta planform and 6 per cent symmetrical section at stream Mach numbers between 0·8 and 1·41. A.R.C. R. & M. 3286, September, 1960.
29	I. M. Hall and E. W. E. Rogers	Experiments with a tapered sweptback wing of Warren 12 planform at Mach numbers between 0·6 and 1·6. A.R.C. R. & M. 3271, Part 2, July, 1960.
30	B. Laschka	Die Druck-, Auftriebs- und Momentenverteilungen an einem harmonisch schwingenden Pfeilflügel kleiner Streckung im niedrigen Unterschallbereich. Vergleich zwischen Theorie und Messung. *Proceedings of the International Council of the Aeronautical Sciences.* Fourth Congress, Paris, 1964. R.A.E. Library Translation 1223, 1967.
31	D. E. Lehrian	Calculation of subsonic flutter derivatives for an arrowhead wing with control surfaces. A.R.C. R. & M. 3561, March, 1967.
32	R. R. Graham	Low-speed characteristics of a 45° sweptback wing of aspect ratio 8 from pressure distributions and force tests at Reynolds numbers from 1,500,000 to 4,800,000. N.A.C.A. RM L51 H13 (T.I.B. 2920), 1951.
33	L. Woodgate and P. G. Pugh	Measurements of the pitching-moment derivatives on a sharp-edged delta wing in incompressible flow. A.R.C. R. & M. 3379, October, 1963.

No.	*Author(s)*	*Title, etc.*
34	H. C. Garner and D. E. Walshe	Pressure distribution and surface flow on 5% and 9% thick wings with curved tip and 60° sweepback. A.R.C. R. & M. 3244. January, 1960.
35	R. C. Lock	The loading of swept wings at transonic speeds. Proceedings of a Seminar in Aeronautical Sciences, Bangalore, December, 1961. A.R.C. 23 352, December, 1961.
36	D. E. Lehrian and H. C. Garner	Comparative numerical applications of the reverse-flow theorem to oscillating wings and control surfaces. A.R.C. R. & M. 3488, August, 1965.
37	D. L. Woodcock	On the accuracy of collocation solutions of the integral equation of linearised subsonic flow past an oscillating aerofoil. *Proceedings of the International Symposium on Analogue and Digital Techniques Applied to Aeronautics*, Liège, 9th–12th September, 1963.
38	R. Dat, J. Leclerc and Y. Akamatsu	Optimisation de l'emploi de la théorie de la surface portante en aéroélasticité subsonique. *La Recherche Aérospatiale* No. 113, pp. 37–52, July-August, 1966.
39	H. C. Garner, B. L. Hewitt T. E. Labrujere ..	Comparison of three methods for the evaluation of subsonic lifting-surface theory. A.R.C. R. & M. 3597, June, 1968.
40	G. Long	An improved method for calculating generalised airforces on oscillating wings in subsonic flow. R.A.E. Tech. Report 69 073. A.R.C. 31 480, April 1969.
41	H. C. Garner and D. E. Lehrian	The theoretical treatment of slowly oscillating part-span control surfaces in subsonic flow. N.P.L. Aero Report 1303. A.R.C. 31 490, October, 1969.
42	D. L. Woodcock	A comparison of methods used in lifting-surface theory. (Chapter to appear in Vol. VI of AGARD Manual on Aeroelasticity).

TABLE 1

Details of Planforms and Mach Numbers Used.

No.	Planform	$A = \frac{2s}{\bar{c}}$	$\frac{c_r}{\bar{c}}$	$\tan\Lambda_0$	$\tan\Lambda_1$	M	Ref.
1	Rectangular	2·00000	1·00000	0	0	0	25
2	Rectangular	4·00000	1·00000	0	0	0	-
3	Rectangular	8·00000	1·00000	0	0	0	-
4	Circular	1·27324	1·27324	-	-	0	27
5	Symmetrical taper	4·32921	1·58000	0·26795	-0·26795	0	-
6	Hyperbolic edges	4·00000	1·00000	-	-	0	-
7	Constant chord	4·00000	1·00000	1·00000	1·00000	0	-
8	Cropped delta	1·97035	1·66667	1·35340	0	0·8	28
9	Arrowhead	2·82843	1·50000	1·35355	0·64645	0,0·6,0·8	29
10	Arrowhead	1·45033	1·16969	0·81000	0·34200	0·8	30
11	Arrowhead	2·00000	1·61603	1·73205	0·50000	0·78062	31
12	Arrowhead	8·00000	1·37931	1·04741	0·85776	0	32
13	Delta	1·50000	2·00000	2·66667	0	0	33
14	Slender delta	0·00010	2·00000	40000	0	0	-
15	Slender gothic	0·00010	1·66667	-	0	0	-
16	Curved tip	3·89927	1·06829	-	1·73205	0	34
17	Curved tip	3·55645	1·12120	-	1·42815	0·8	35

Planform 4 $\quad c = c_r(1-\eta^2)^{1/2}$

Planform 6 $\quad \left.\begin{array}{l} c = c_r(\text{constant}) \\ x_\ell = \frac{3}{4}\, c_r[(1+8\eta^2)^{1/2}-1] \end{array}\right\}$

Planform 15 $\quad c = (1-|\eta|)^{2/3}$

Planform 16 $\quad \left.\begin{array}{ll} c = c_r(\text{constant}) & 0 < \eta < 0\cdot616438 \\ c = c_r\left[1-\left(\dfrac{1-\eta}{0\cdot383562}\right)^{1/2}\right]^2 & 0\cdot616438 < \eta < 1 \end{array}\right\}$

Planform 17 $\quad \left.\begin{array}{ll} c = c_r(\text{constant}) & 0 < \eta < 0\cdot4415 \\ \text{and in following table} & 0\cdot4415 < \eta < 1 \end{array}\right\}$

η	0·5000	0·6088	0·7071	0·7934	0·8660	0·9239	0·9659	0·9914
c/c_r	0·9947	0·9588	0·8954	0·8059	0·6916	0·5535	0·3922	0·2077

TABLE 2

Summary of Numerical Results.

Planform (Table 1)			Tables					Figures
No.	A	M	Solns. $\alpha = 1$	C_{LL}	X_{ac}	Coeffs.	$-z_\theta, -m_\theta$ $-\dot{z}_\theta, -\dot{m}_\theta$	
1	2·000	0	3	-	23(a)	-	-	1,5
2	4·000	0	4,5	-	23(b)	35(a)	43(a)*	1,5,6,7,8
3	8·000	0	-	24	24	-	-	5
4	1·273	0	6	-	25(a)	35(b)	43(b)*	6
5	4·329	0	-	-	25(b)	35(c)	43(c)*	6,7
6	4·000	0	7	-	26(a)	36	44(a)*	3,8,9
7	4·000	0	8,9+	50	26(b),50	37,51*	44(b)*	8,9,21
8	1·970	0·8	10	-	27(a)	-	-	-
9	2·828	0	11,14+	50	50	38(b)	45(a)	10,21
9	2·828	0·6	11	-	-	-	-	10
9	2·828	0·8	12,13	-	27(b)	38(c)	45(a)	10
10	1·450	0·8	-	28	28	38(a)	45(b)	13
11	2·000	0·781	-	-	-	39*	48*	22
12	8·000	0	15+	29	30,31	40	45(c)	4,11,12
13	1·500	0	16,19+,49+	50	32(a),50	41(a)	46(a)	15,21
14	0·000	0	17	-	32(b)	41(b)	46(b)	14,15,16
15	0·000	0	18,19+,49+	-	32(c)	41(c)	46(c)	14,16,20,21
16	3·899	0	20,21	50	33(a),50	-	-	2,18
17	3·556	0·8	22+	34	33(b),34	42	47	17,18

+ Table includes solutions with non-standard central rounding.

* Table includes results calculated from solutions for the wing in reverse flow.

TABLE 3

Solutions for Rectangular Wing ($A = 2, M = 0$) at Unit Incidence.

m	7	7	7	7	7	7	15
N	4	4	4	4	4	4	4
q	1	2	4	6	8	16	8
$\bar{m}$	7	15	31	47	63	127	127
y_0	0·768119	0·775501	0·776399	0·776225	0·776098	0·775928	0·775927
y_1							0·762796
y_2	0·716825	0·723068	0·723723	0·723545	0·723431	0·723287	0·723287
y_3							0·657277
y_4	0·561516	0·565323	0·565551	0·565401	0·565324	0·565241	0·565240
y_5							0·448964
y_6	0·310660	0·312161	0·312188	0·312116	0·312083	0·312051	0·312051
y_7							0·160025
μ_0	0·019207	0·025362	0·024073	0·023502	0·023366	0·023329	0·023327
μ_1							0·023876
μ_2	0·022852	0·027271	0·025947	0·025489	0·025389	0·025364	0·025366
μ_3							0·027262
μ_4	0·029096	0·029855	0·028781	0·028566	0·028526	0·028517	0·028511
μ_5							0·027549
μ_6	0·024028	0·023126	0·022746	0·022687	0·022675	0·022672	0·022672
μ_7							0·013042
K_0	−0·036737	0·014748	0·015386	0·013065	0·012257	0·011661	0·011633
K_1							0·012786
K_2	−0·019325	0·021020	0·019551	0·017584	0·016955	0·016501	0·016536
K_3							0·023519
K_4	0·027926	0·038961	0·035166	0·034177	0·033909	0·033722	0·033666
K_5							0·043842
K_6	0·056507	0·047712	0·046118	0·045907	0·045850	0·045810	0·045834
K_7							0·030619
λ_0	−0·020904	0·003481	0·001687	−0·000013	−0·000471	−0·000656	−0·000678
λ_1							−0·000533
λ_2	−0·015414	0·004599	0·001927	0·000553	0·000221	0·000093	0·000124
λ_3							0·002046
λ_4	0·005009	0·010446	0·007199	0·006620	0·006515	0·006475	0·006416
λ_5							0·013362
λ_6	0·029308	0·019877	0·018726	0·018644	0·018628	0·018619	0·018688
λ_7							0·014607
C_L	2·453985	2·473974	2·475899	2·475294	2·474923	2·474470	2·474468
$-C_m$	0·518486	0·511936	0·516773	0·518009	0·518219	0·518184	0·518188
$\bar{\eta}$	0·428613	0·428254	0·428167	0·428163	0·428167	0·428177	0·428176
$\frac{x_{ac}}{\bar{c}}$	0·211283	0·206929	0·208721	0·209272	0·209388	0·209412	0·209414

TABLE 4

Solutions for Rectangular Wing ($A = 4, M = 0$) at Unit Incidence ($m = 7$).

m	7	7	7	7	7	7
N	4	4	4	4	4	4
q	1	2	4	8	12	16
$\bar{m}$	7	15	31	63	95	127
γ_0	0·51206	0·53994	0·54890	0·55006	0·54985	0·54970
γ_1	0·49030	0·51308	0·52051	0·52133	0·52113	0·52099
γ_2	0·40776	0·42052	0·42470	0·42494	0·42477	0·42468
γ_3	0·23798	0·24336	0·24491	0·24492	0·24484	0·24480
μ_0	-0·00884	0·00335	0·00644	0·00540	0·00500	0·00491
μ_1	-0·00536	0·00547	0·00770	0·00666	0·00635	0·00629
μ_2	0·00554	0·01128	0·01158	0·01080	0·01067	0·01066
μ_3	0·01446	0·01373	0·01319	0·01298	0·01295	0·01295
κ_0	-0·08672	-0·02901	0·00311	0·00395	0·00248	0·00194
κ_1	-0·07686	-0·02075	0·00497	0·00439	0·00312	0·00269
κ_2	-0·03969	0·00240	0·01140	0·00917	0·00853	0·00835
κ_3	0·03135	0·02704	0·02415	0·02334	0·02323	0·02320
λ_0	-0·02583	-0·01053	0·00298	0·00136	0·00025	-0·00003
λ_1	-0·02509	-0·00795	0·00298	0·00095	0·00006	-0·00014
λ_2	-0·01923	-0·00060	0·00279	0·00075	0·00040	0·00034
λ_3	0·01265	0·01063	0·00779	0·00730	0·00727	0·00727
C_L	3·41936	3·56408	3·61085	3·61562	3·61421	3·61332
$-C_m$	0·85458	0·82831	0·82866	0·83650	0·83800	0·83813
$\bar{\eta}$	0·43951	0·43689	0·43607	0·43590	0·43590	0·43590
$\frac{x_{ac}}{\bar{c}}$	0·24992	0·23240	0·22949	0·23136	0·23186	0·23196

TABLE 5

Solutions for Rectangular Wing ($A = 4, M = 0$) at Unit Incidence ($m = 15$)

m	15	15	15	15	15	15
N	2	3	4	4	4	4
q	4	6	1	2	4	8
$\bar{m}$	63	95	15	31	63	127
y_0	0·54968	0·54971	0·53994	0·54891	0·55006	0·54970
y_1	0·54268	0·54271	0·53344	0·54200	0·54306	0·54270
y_2	0·52095	0·52099	0·51308	0·52051	0·52133	0·52099
y_3	0·48249	0·48255	0·47650	0·48235	0·48287	0·48255
y_4	0·42457	0·42468	0·42052	0·42470	0·42495	0·42468
y_5	0·34506	0·34530	0·34272	0·34542	0·34550	0·34531
y_6	0·24437	0·24484	0·24336	0·24492	0·24493	0·24481
y_7	0·12680	0·12729	0·12656	0·12726	0·12727	0·12721
μ_0	0·00490	0·00488	0·00334	0·00644	0·00539	0·00490
μ_1	0·00524	0·00522	0·00388	0·00675	0·00570	0·00524
μ_2	0·00630	0·00629	0·00548	0·00771	0·00667	0·00630
μ_3	0·00812	0·00815	0·00808	0·00937	0·00840	0·00815
μ_4	0·01049	0·01065	0·01127	0·01156	0·01078	0·01064
μ_5	0·01246	0·01289	0·01387	0·01346	0·01297	0·01291
μ_6	0·01210	0·01281	0·01375	0·01324	0·01301	0·01299
μ_7	0·00771	0·00831	0·00892	0·00872	0·00864	0·00863
κ_0		0·00173	−0·02902	0·00309	0·00392	0·00191
κ_1		0·00192	−0·02693	0·00358	0·00401	0·00208
κ_2		0·00262	−0·02074	0·00500	0·00443	0·00274
κ_3		0·00436	−0·01076	0·00738	0·00570	0·00439
κ_4		0·00821	0·00233	0·01127	0·00904	0·00821
κ_5		0·01504	0·01687	0·01771	0·01590	0·01550
κ_6		0·02157	0·02728	0·02467	0·02382	0·02368
κ_7		0·01783	0·02242	0·02119	0·02098	0·02094
λ_0			−0·01053	0·00298	0·00136	−0·00003
λ_1			−0·00988	0·00300	0·00125	−0·00006
λ_2			−0·00796	0·00299	0·00096	−0·00013
λ_3			−0·00484	0·00283	0·00060	−0·00016
λ_4			−0·00062	0·00274	0·00069	0·00028
λ_5			0·00487	0·00405	0·00270	0·00255
λ_6			0·01085	0·00821	0·00770	0·00767
λ_7			0·01070	0·00955	0·00946	0·00945
C_L	3·61242	3·61340	3·56408	3·61087	3·61563	3·61334
$-C_m$	0·83927	0·83838	0·82830	0·82862	0·83648	0·83810
$\bar{\eta}$	0·43582	0·43591	0·43689	0·43607	0·43590	0·43591
$\frac{x_{ac}}{\bar{c}}$	0·23233	0·23202	0·23240	0·22948	0·23135	0·23195

TABLE 6

Solutions for Circular Wing (A = 1·2732, M = 0) at Unit Incidence.

m	11	5	11	5	11	11	11
N	2	2	3	3	4	4	4
q	4	8	6	12	4	6	8
$\bar{m}$	47	47	71	71	47	71	95
y_0	0·90246	0·90280	0·90302	0·90349	0·90296	0·90297	0·90300
y_1	0·87018		0·87086		0·87080	0·87081	0·87084
y_2	0·77595	0·77625	0·77686	0·77724	0·77676	0·77678	0·77681
y_3	0·62742		0·62846		0·62827	0·62827	0·62832
y_4	0·43690	0·43818	0·43759	0·43902	0·43727	0·43720	0·43724
y_5	0·22142		0·22098		0·22070	0·22063	0·22063
μ_0	0·04888	0·04875	0·04688	0·04677	0·04688	0·04692	0·04694
μ_1	0·04826		0·04608		0·04608	0·04613	0·04614
μ_2	0·04623	0·04616	0·04358	0·04355	0·04356	0·04366	0·04369
μ_3	0·04216		0·03894		0·03903	0·03917	0·03921
μ_4	0·03488	0·03402	0·03150	0·03094	0·03133	0·03196	0·03218
μ_5	0·02181		0·01982		0·01761	0·01993	0·02093
K_0			0·00516	0·00508	0·00460	0·00448	0·00445
K_1			0·00594		0·00532	0·00514	0·00508
K_2			0·00820	0·00813	0·00694	0·00689	0·00689
K_3			0·01131		0·00950	0·00919	0·00908
K_4			0·01441	0·01268	0·00983	0·01051	0·01075
K_5			0·01463		−0·00589	0·00651	0·01212
λ_0					−0·00737	−0·00745	−0·00747
λ_1					−0·00826	−0·00843	−0·00849
λ_2					−0·01094	−0·01120	−0·01130
λ_3					−0·01367	−0·01477	−0·01523
λ_4					−0·01663	−0·01724	−0·01770
λ_5					−0·02519	−0·01508	−0·01054
C_L	1·78878	1·79032	1·79057	1·79248	1·79020	1·79019	1·79028
$-C_m$	0·53940	0·54001	0·54653	0·54715	0·54650	0·54605	0·54592
$\bar{\eta}$	0·42175	0·42199	0·42180	0·42209	0·42175	0·42174	0·42174
$\frac{x_{ac}}{\bar{c}}$	0·30155	0·30163	0·30522	0·30525	0·30527	0·30502	0·30494

TABLE 7

Solutions for Planform 6 with Hyperbolic Edges ($A = 4$, $M = 0$) *at Unit Incidence.*

m	15	15	15	15	15	15	7
N	2	3	4	4	4	4	4
q	4	6	1	2	4	8	16
$\bar{m}$	63	95	15	31	63	127	127
y_0	0·45611	0·45642	0·45082	0·45767	0·45668	0·45642	0·45566
y_1	0·45584	0·45607	0·45204	0·45796	0·45648	0·45609	
y_2	0·45201	0·45231	0·45099	0·45504	0·45293	0·45238	0·45262
y_3	0·43880	0·43931	0·43999	0·44216	0·44001	0·43944	
y_4	0·40683	0·40719	0·40861	0·40947	0·40772	0·40725	0·40678
y_5	0·34453	0·34404	0·34518	0·34560	0·34435	0·34405	
y_6	0·24836	0·24835	0·24924	0·24956	0·24881	0·24865	0·24876
y_7	0·12881	0·13027	0·13014	0·13040	0·13007	0·12999	
μ_0	−0·01057	−0·01089	−0·00954	−0·00930	−0·01068	−0·01091	−0·01106
μ_1	−0·00731	−0·00751	−0·00514	−0·00523	−0·00744	−0·00754	
μ_2	−0·00180	−0·00196	0·00173	0·00106	−0·00218	−0·00204	−0·00234
μ_3	0·00372	0·00351	0·00793	0·00641	0·00301	0·00342	
μ_4	0·01140	0·01152	0·01616	0·01354	0·01105	0·01153	0·01200
μ_5	0·02134	0·02260	0·02653	0·02335	0·02234	0·02260	
μ_6	0·02656	0·02854	0·03074	0·02867	0·02844	0·02849	0·02790
μ_7	0·01871	0·01964	0·02154	0·02067	0·02054	0·02054	
K_0		0·00175	−0·01858	0·00220	0·00317	0·00209	0·00279
K_1		−0·00150	−0·01027	0·00585	0·00000	−0·00144	
K_2		−0·00409	0·00324	0·01196	−0·00271	−0·00423	−0·00481
K_3		−0·00606	0·01277	0·01194	−0·00588	−0·00615	
K_4		−0·00838	0·01630	0·00465	−0·01034	−0·00917	−0·00774
K_5		0·00157	0·02431	0·00641	−0·00017	0·00090	
K_6		0·03408	0·05196	0·03893	0·03783	0·03808	0·03308
K_7		0·04286	0·05588	0·05040	0·04978	0·04978	
λ_0			−0·00118	0·00199	−0·00039	−0·00112	−0·00110
λ_1			0·00207	0·00569	0·00040	−0·00000	
λ_2			0·00701	0·00983	0·00006	0·00002	0·00058
λ_3			0·01216	0·01040	−0·00071	−0·00012	
λ_4			0·01406	0·00684	−0·00279	−0·00160	−0·00318
λ_5			0·00783	−0·00280	−0·00751	−0·00654	
λ_6			0·01534	0·00592	0·00517	0·00540	0·00720
λ_7			0·03333	0·02711	0·02655	0·02655	
C_L	3·23039	3·23298	3·22444	3·24924	3·23673	3·23347	3·23216
$-C_m$	2·47938	2·47941	2·45347	2·47635	2·48371	2·47990	2·47962
$\bar{\eta}$	0·45324	0·45324	0·45469	0·45338	0·45328	0·45326	0·45336
$\frac{x_{ac}}{\bar{c}}$	0·76740	0·76691	0·76090	0·76213	0·76735	0·76695	0·76717

TABLE 8

Solutions for Planform 7 (A = 4, Λ = 45°, M = 0) at Unit Incidence.

m N q $\overline{m}$	15 2 4 63	15 3 6 95	15 4 1 15	15 4 2 31	15 4 4 63	15 4 8 127	7 4 16 127
y_0	0·36447	0·36538	0·37810	0·37240	0·36646	0·36516	0·37308
y_1	0·39874	0·39916	0·40700	0·40526	0·40042	0·39915	
y_2	0·41678	0·41709	0·42451	0·42308	0·41836	0·41712	0·41655
y_3	0·41621	0·41696	0·42309	0·42184	0·41807	0·41709	
y_4	0·39164	0·39204	0·39767	0·39583	0·39286	0·39209	0·39150
y_5	0·33436	0·33399	0·33772	0·33649	0·33448	0·33400	
y_6	0·24176	0·24175	0·24450	0·24362	0·24233	0·24204	0·24219
y_7	0·12562	0·12712	0·12779	0·12754	0·12697	0·12684	
μ_0	-0·03354	-0·03589	-0·02339	-0·03135	-0·03603	-0·03630	-0·02683
μ_1	-0·00944	-0·00988	-0·00180	-0·00542	-0·00997	-0·01009	
μ_2	0·00008	0·00032	0·00478	0·00402	-0·00004	0·00016	-0·00307
μ_3	0·00410	0·00364	0·00932	0·00708	0·00305	0·00352	
μ_4	0·01177	0·01206	0·01673	0·01416	0·01152	0·01206	0·01305
μ_5	0·02120	0·02226	0·02672	0·02317	0·02203	0·02228	
μ_6	0·02640	0·02846	0·03068	0·02860	0·02835	0·02840	0·02705
μ_7	0·01846	0·01930	0·02140	0·02040	0·02020	0·02020	
K_0		0·01100	0·00556	0·00840	0·01005	0·01212	0·01286
K_1		-0·01307	0·00906	0·01028	-0·01051	-0·01310	
K_2		-0·00172	0·01616	0·02308	0·00036	-0·00225	-0·00927
K_3		-0·00673	0·01943	0·01439	-0·00665	-0·00670	
K_4		-0·00676	0·01913	0·00763	-0·00897	-0·00770	-0·00507
K_5		0·00098	0·02518	0·00570	-0·00083	0·00042	
K_6		0·03445	0·05207	0·03956	0·03813	0·03832	0·03126
K_7		0·04219	0·05558	0·04964	0·04907	0·04908	
λ_0			0·01762	-0·00172	-0·01090	-0·01116	-0·00630
λ_1			0·00919	0·01449	0·00152	0·00144	
λ_2			0·01122	0·01486	-0·00078	-0·00127	0·00080
λ_3			0·01505	0·01250	-0·00046	0·00029	
λ_4			0·01570	0·00785	-0·00321	-0·00192	-0·00358
λ_5			0·00836	-0·00261	-0·00723	-0·00617	
λ_6			0·01538	0·00574	0·00477	0·00500	0·00749
λ_7			0·03310	0·02691	0·02634	0·02634	
C_L	2·95962	2·96296	3·01519	3·00061	2·97070	2·96314	2·95591
$-C_m$	3·49192	3·49550	3·50157	3·51075	3·50594	3·49677	3·49657
$\bar{\eta}$	0·46789	0·46782	0·46639	0·46690	0·46768	0·46786	0·46836
$\frac{x_{ac}}{\bar{c}}$	1·17985	1·17973	1·16131	1·17001	1·18017	1·18009	1·18291

TABLE 9

Solutions for Planform 7 ($A = 4, \Lambda = 45°, M = 0, \alpha = 1$) with Different Rounding.

Rounding	$m = \infty$	$m = 31$	$m = 15$	$m = 7$	$m = 7$	$m = 11$*	$m = 15$*
m	15	15	15	15	15	23	31
N	4	4	4	4	3	3	3
q	8	8	8	8	6	4	2
$\bar{m}$	127	127	127	127	95	95	63
γ_0	0·27348	0·33564	0·36516	0·39152	0·39153	0·38425	0·38075
γ_1	0·35649	0·38558	0·39915	0·41019	0·41012		0·40647
γ_2	0·39324	0·40939	0·41712	0·42341	0·42332	0·42226	0·42194
γ_3	0·40030	0·41175	0·41709	0·42136	0·42120		0·42008
γ_4	0·38002	0·38820	0·39209	0·39528	0·39521	0·39461	0·39459
γ_5	0·32530	0·33125	0·33400	0·33620	0·33618		0·33553
γ_6	0·23638	0·24022	0·24204	0·24354	0·24324	0·24301	0·24291
γ_7	0·12408	0·12597	0·12684	0·12755	0·12782		0·12759
μ_0	-0·04990	-0·04373	-0·03630	-0·02710	-0·02688	-0·03100	-0·03366
μ_1	-0 01336	-0·01150	-0·01009	-0·00979	-0·00961		-0·00815
μ_2	0·00042	0·00032	0·00016	-0·00035	-0·00019	-0·00060	-0·00100
μ_3	0·00271	0·00321	0·00352	0·00381	0·00393		0·00378
μ_4	0·01202	0·01208	0·01206	0·01197	0·01197	0·01185	0·01158
μ_5	0·02151	0·02202	0·02228	0·02253	0·02252		0·02260
μ_6	0·02797	0·02828	0·02840	0·02846	0·02852	0·02836	0·02840
μ_7	0·01972	0·02005	0·02020	0·02034	0·01944		0·01948
K_0	0 04200	0·02294	0·01212	0·00530	0·00439	0·00083	-0·00273
K_1	-0·01365	-0·01429	-0·01310	-0·01056	-0·01032		-0·00896
K_2	-0·00196	-0·00187	-0·00225	-0·00370	-0·00322	-0·00463	-0·00479
K_3	-0·00661	-0·00688	-0·00670	-0·00610	-0·00610		-0·00596
K_4	-0·00758	-0·00751	-0·00770	-0·00826	-0·00735	-0·00767	-0·00836
K_5	0·00088	0·00032	0·00042	0·00076	0·00135		0·00169
K_6	0·03752	0·03808	0·03832	0·03829	0·03438	0·03395	0·03405
K_7	0·04830	0·04879	0·04908	0·04940	0·04250		0·04263
λ_0	-0·03204	-0·01803	·0·01116	-0.00630			
λ_1	0·00304	0·00213	0·00144	0·00087			
λ_2	-0·00161	-0·00147	-0·00127	-0·00105			
λ_3	0·00064	0·00047	0·00029	0·00011			
λ_4	-0·00217	-0·00205	-0·00192	-0·00179			
λ_5	-0·00627	-0·00602	-0·00617	-0·00632			
λ_6	0·00477	0·00486	0·00500	0·00513			
λ_7	0·02589	0·02612	0·02634	0·02641			
$C_{L'}$	2·74359	2·89280	2·96314	3·02217	3·02152	3·00800	3·00424
$-C_m$	3·32468	3·44054	3·49677	3·55583	3·55438	3·53227	3·52926
$\bar{\eta}$	0·48320	0·47254	0·46786	0·46397	0·46395	0·46487	0·46525
$\frac{x_{ac}}{\bar{c}}$	1·21180	1·18935	1·18009	1·17658	1·17636	1·17429	1·17476

*The subscripts to γ, μ, etc., refer to the $m = 15$ collocation sections.

TABLE 10

Solutions for Cropped Delta Planform 8 (A = 1·9704, M = 0·8) at Unit Incidence.

m	15	7*	15	31*	15	15	15
N	2	3	3	3	4	4	4
q	1	4	2	1	1	2	4
$\bar{m}$	15	31	31	31	15	31	63
y_0	0·87369	0·86600	0·86912	0·87143	0·87740	0·86840	0·86946
y_1	0·85544		0·85286	0·85522	0·86062	0·85220	0·85321
y_2	0·80560	0·80165	0·80447	0·80644	0·81147	0·80380	0·80475
y_3	0·72598		0·72550	0·72715	0·73172	0·72507	0·72594
y_4	0·61886	0·61712	0·61894	0·62019	0·62414	0·61866	0·61941
y_5	0·48718		0·48818	0·48912	0·49228	0·48814	0·48872
y_6	0·33534	0·33719	0·33796	0·33856	0·34040	0·33764	0·33799
y_7	0·17050		0·17328	0·17358	0·17371	0·17240	0·17260
μ_0	−0·08488	−0·09624	−0·09915	−0·09269	−0·08542	−0·10218	−0·10291
μ_1	−0·04845		−0·05189	−0·04581	−0·03768	−0·05688	−0·05338
μ_2	−0·02034	−0·02318	−0·01833	−0·01640	−0·00322	−0·02294	−0·01806
μ_3	−0·00107		0·00154	0·00273	0·01906	−0·00199	0·00247
μ_4	0·01520	0·01803	0·01751	0·01792	0·03443	0·01590	0·01910
μ_5	0·02998		0·03079	0·03110	0·04412	0·02949	0·03205
μ_6	0·03698	0·03669	0·03781	0·03801	0·04493	0·03672	0·03870
μ_7	0·02598		0·02735	0·02742	0·03159	0·02872	0·02907
K_0		−0·14120	−0·17908	−0·18493	−0·21492	−0·17424	−0·18038
K_1			−0·11026	−0·10233	−0·09639	−0·12444	−0·11169
K_2		−0·08827	−0·07098	−0·07151	−0·02893	−0·08857	−0·06619
K_3			−0·06534	−0·06298	0·00816	−0·08011	−0·05851
K_4		−0·04428	−0·05267	−0·05398	0·03083	−0·05737	−0·04225
K_5			−0·02195	−0·02060	0·05306	−0·02880	−0·01613
K_6		0·03497	0·04433	0·04372	0·08445	0·03511	0·04782
K_7			0·06588	0·06669	0·09433	0·07495	0·07708
λ_0					−0·05411	0·01506	0·00696
λ_1					−0·00562	−0·00009	0·00463
λ_2					0·01936	−0·00334	0·01054
λ_3					0·03286	−0·01688	−0·00218
λ_4					0·03206	−0·02427	−0·01424
λ_5					0·01706	−0·04136	−0·03384
λ_6					0·02110	−0·01962	−0·00863
λ_7					0·05762	0·03705	0·03940
C_L	2·70319	2·69118	2·70002	2·70652	2·72352	2·69809	2·70130
$-C_m$	2·37747	2·39703	2·38487	2·37318	2·34649	2·39743	2·38801
$\bar{\eta}$	0·42474	0·42556	0·42546	0·42538	0·42532	0·42548	0·42547
$\frac{x_{ac}}{\bar{c}}$	0·87950	0·89070	0·88328	0·87684	0·86157	0·88857	0·88402

*The subscripts to y, μ, etc., refer to the m = 15 collocation sections.

TABLE 11

Solutions for Arrowhead Planform 9 ($A = 2\sqrt{2}$, $M = 0$ and 0·6) at Unit Incidence.

M	0	0	0	0·6	0·6	0·6
m	15	15	15	15	15	15
N	2	3	4	2	3	4
q	4	6	8	4	6	8
$\bar{m}$	63	95	127	63	95	127
γ_0	0·56616	0·56842	0·56877	0·60266	0·60620	0·60693
γ_1	0·57519	0·57531	0·57532	0·61461	0·61515	0·61529
γ_2	0·55772	0·55787	0·55788	0·59807	0·59834	0·59841
γ_3	0·51760	0·51798	0·51805	0·55690	0·55749	0·55767
γ_4	0·45682	0·45712	0·45718	0·49217	0·49250	0·49257
γ_5	0·37464	0·37448	0·37449	0·40239	0·40192	0·40191
γ_6	0·26640	0·26629	0·26652	0·28413	0·28390	0·28427
γ_7	0·13757	0·13892	0·13872	0·14587	0·14757	0·14733
μ_0	−0·06364	−0·06841	−0·06911	−0·07904	−0·08487	−0·08584
μ_1	−0·02805	−0·02847	−0·02846	−0·03821	−0·03914	−0·03917
μ_2	−0·00899	−0·00838	−0·00836	−0·01417	−0·01340	−0·01333
μ_3	−0·00111	−0·00122	−0·00125	−0·00302	−0·00311	−0·00307
μ_4	0·00659	0·00672	0·00673	0·00764	0·00804	0·00816
μ_5	0·01580	0·01603	0·01607	0·01968	0·02035	0·02048
μ_6	0·02410	0·02540	0·02533	0·02901	0·03086	0·03072
μ_7	0·01932	0·02038	0·02119	0·02224	0·02341	0·02448
κ_0		−0·01686	−0·01411		−0·00810	−0·00214
κ_1		−0·02380	−0·02369		−0·02882	−0·02853
κ_2		−0·00761	−0·00725		−0·01346	−0·01332
κ_3		−0·01157	−0·01147		−0·01834	−0·01776
κ_4		−0·01038	−0·01024		−0·01851	−0·01850
κ_5		−0·01230	−0·01347		−0·01877	−0·02023
κ_6		0·01914	0·01973		0·02475	0·02589
κ_7		0·04288	0·05003		0·05118	0·06070
λ_0			−0·01505			−0·01835
λ_1			0·00039			0·00253
λ_2			0·00195			0·00325
λ_3			0·00048			0·00219
λ_4			−0·00002			0·00084
λ_5			−0·00629			−0·00982
λ_6			−0·00715			−0·01026
λ_7			0·02421			0·03009
C_L	2·72437	2·72665	2·72704	2·91950	2·92312	2·92408
$-C_m$	3·09773	3·10294	3·10379	3·34758	3·35443	3·35579
$\bar{\eta}$	0·43932	0·43920	0·43918	0·43998	0·43971	0·43967
$\frac{x_{ac}}{\bar{c}}$	1·13705	1·13800	1·13815	1·14663	1·14755	1·14764

TABLE 12

Solutions for Arrowhead Planform 9 ($A = 2\sqrt{2}, M = 0{\cdot}8$) at Unit Incidence ($N = 2, 3$).

m	15	15	15	15	15	15	15
N	2	2	2	3	3	3	3
q	1	2	4	1	2	4	6
$\bar{m}$	15	31	63	15	31	63	95
y_0	0·64730	0·64526	0·64156	0·67364	0·64605	0·64814	0·64702
y_1	0·65644	0·65944	0·65754	0·67915	0·65660	0·65971	0·65901
y_2	0·64012	0·64365	0·64239	0·66052	0·64068	0·64359	0·64306
y_3	0·59724	0·60085	0·60001	0·61476	0·59889	0·60143	0·60105
y_4	0·52897	0·53114	0·53057	0·54162	0·52935	0·53118	0·53090
y_5	0·43063	0·43230	0·43198	0·43772	0·42970	0·43109	0·43089
y_6	0·30196	0·30299	0·30274	0·30706	0·30157	0·30239	0·30224
y_7	0·15413	0·15465	0·15453	0·15885	0·15625	0·15669	0·15662
μ_0	−0·09149	−0·09566	−0·09888	−0·09736	−0·10293	−0·10525	−0·10586
μ_1	−0·05362	−0·05066	−0·05218	−0·04383	−0·05655	−0·05359	−0·05416
μ_2	−0·02952	−0·02085	−0·02192	−0·01183	−0·02601	−0·02049	−0·02118
μ_3	−0·01394	−0·00532	−0·00625	0·00589	−0·01156	−0·00562	−0·00639
μ_4	0·00126	0·00922	0·00853	0·01935	0·00484	0·01006	0·00948
μ_5	0·02011	0·02467	0·02429	0·03236	0·02289	0·02613	0·02584
μ_6	0·03357	0·03490	0·03475	0·03912	0·03654	0·03751	0·03747
μ_7	0·02532	0·02565	0·02558	0·02814	0·02672	0·02691	0·02688
κ_0				−0·06408	0·01406	0·01087	0·01303
κ_1				−0·03214	−0·03558	−0·03093	−0·03071
κ_2				−0·00404	−0·03374	−0·02039	−0·02164
κ_3				0·01080	−0·04373	−0·02714	−0·02915
κ_4				0·00630	−0·04814	−0·03029	−0·03237
κ_5				−0·00062	−0·04233	−0·02747	−0·02882
κ_6				0·03972	0·02635	0·03188	0·03160
κ_7				0·06864	0·05990	0·06116	0·06106
C_L	3·12597	3·13836	3·13137	3·21994	3·12757	3·14019	3·13750
$-C_m$	3·63730	3·62714	3·62863	3·66767	3·64287	3·63772	3·63848
$\bar{\eta}$	0·43990	0·44021	0·44055	0·43824	0·44003	0·43995	0·44004
$\frac{x_{ac}}{\bar{c}}$	1·16357	1·15574	1·15880	1·13905	1·16476	1·15844	1·15968

TABLE 13

Solutions for Arrowhead Planform 9 ($A = 2\sqrt{2}, M = 0{\cdot}8$) at Unit Incidence ($N = 4$).

m	15	15	15	15	15
N	4	4	4	4	4
q	1	2	4	6	8
$\overline{m}$	15	31	63	95	127
γ_0	0·67685	0·65370	0·64800	0·64897	0·64842
γ_1	0·68097	0·66324	0·65853	0·65973	0·65937
γ_2	0·66171	0·64669	0·64244	0·64351	0·64321
γ_3	0·61568	0·60398	0·60075	0·60161	0·60138
γ_4	0·54218	0·53287	0·53048	0·53110	0·53092
γ_5	0·43836	0·43211	0·43051	0·43096	0·43084
γ_6	0·30801	0·30371	0·30264	0·30291	0·30284
γ_7	0·15838	0·15675	0·15627	0·15641	0·15637
μ_0	−0·08321	−0·10657	−0·10647	−0·10705	−0·10743
μ_1	−0·03198	−0·05487	−0·05477	−0·05389	−0·05440
μ_2	−0·00387	−0·02044	−0·02276	−0·02073	−0·02120
μ_3	0·01170	−0·00425	−0·00839	−0·00594	−0·00634
μ_4	0·02526	0·01152	0·00797	0·01004	0·00972
μ_5	0·03897	0·02619	0·02531	0·02632	0·02606
μ_6	0·04338	0·03593	0·03714	0·03721	0·03717
μ_7	0·03083	0·02818	0·02824	0·02827	0·02826
κ_0	−0·00779	0·00590	0·02692	0·02392	0·02496
κ_1	0·04631	−0·03943	−0·03013	−0·02867	−0·02988
κ_2	0·07009	−0·02004	−0·02801	−0·02108	−0·02306
κ_3	0·07424	−0·01850	−0·03722	−0·02696	−0·02846
κ_4	0·05745	−0·02037	−0·04311	−0·03230	−0·03370
κ_5	0·04761	−0·02689	−0·03587	−0·02940	−0·03094
κ_6	0·07476	0·02530	0·03386	0·03405	0·03386
κ_7	0·08856	0·07267	0·07387	0·07385	0·07383
λ_0	−0·05595	−0·02444	−0·02239	−0·02427	−0·02386
λ_1	0·04432	0·00017	0·00758	0·00804	0·00743
λ_2	0·07393	0·00379	0·00343	0·00751	0·00616
λ_3	0·08565	0·00856	0·00064	0·00677	0·00568
λ_4	0·07997	0·00927	−0·00335	0·00349	0·00271
λ_5	0·04285	−0·01003	−0·02034	−0·01495	−0·01609
λ_6	0·01910	−0·02143	−0·01548	−0·01478	−0·01509
λ_7	0·05528	0·03527	0·03706	0·03700	0·03699
C_L	3·22693	3·15520	3·13612	3·14077	3·13931
$-C_m$	3·62379	3·65324	3·64260	3·64042	3·64127
$\overline{\eta}$	0·43801	0·43956	0·43997	0·43990	0·43994
$\frac{x_{ac}}{\overline{c}}$	1·12298	1·15785	1·16150	1·15909	1·15989

TABLE 14

Solutions for Planform 9 ($A = 2\sqrt{2}, M = 0, \alpha = 1$) with Different Rounding.

Rounding	$m = \infty$	$m = 31$	$m = 15$	$m = 7$	$m = 7$	$m = 15$
m	15	15	15	15	7	31
N	4	4	4	4	4	3
q	8	8	8	8	16	2
$\bar{m}$	127	127	127	127	127	63
γ_0	0·49918	0·54959	0·56877	0·58284	0·56495	0·57894
γ_1	0·53645	0·56447	0·57532	0·58247		0·58162
γ_2	0·53332	0·55092	0·55788	0·56239	0·55532	0·56216
γ_3	0·50125	0·51332	0·51805	0·52106		0·52072
γ_4	0·44499	0·45371	0·45718	0·45945	0·45476	0·45935
γ_5	0·36623	0·37217	0·37449	0·37595		0·37578
γ_6	0·26097	0·26494	0·26652	0·26757	0·26647	0·26732
γ_7	0·13615	0·13800	0·13872	0·13918		0·13931
μ_0	-0·10797	-0·08536	-0·06911	-0·05198	-0·05686	-0·06018
μ_1	-0·03906	-0·03247	-0·02846	-0·02628		-0·02470
μ_2	-0·00959	-0·00879	-0·00836	-0·00854	-0·01241	-0·00858
μ_3	-0·00257	-0·00170	-0·00125	-0·00096		-0·00090
μ_4	0·00681	0·00676	0·00673	0·00662	0·00811	0·00626
μ_5	0·01530	0·01583	0·01607	0·01626		0·01625
μ_6	0·02512	0·02529	0·02533	0·02532	0·02293	0·02534
μ_7	0·02065	0·02102	0·02119	0·02132		0·02053
κ_0	0·06188	0·00180	-0·01411	-0·01475	0·00840	-0·03023
κ_1	-0·02218	-0·02604	-0·02369	-0·01898		-0·01743
κ_2	-0·00774	-0·00707	-0·00725	-0·00869	-0·01909	-0·01008
κ_3	-0·01290	-0·01240	-0·01147	-0·01014		-0·00948
κ_4	-0·00949	-0·00968	-0·01024	-0·01128	-0·00807	-0·01293
κ_5	-0·01387	-0·01389	-0·01347	-0·01267		-0·01107
κ_6	0·01968	0·01996	0·01973	0·01912	0·01174	0·01810
κ_7	0·04906	0·04958	0·05003	0·05060		0·04379
λ_0	-0·04179	-0·02027	-0·01505	-0·00991	-0·00704	
λ_1	0·00510	0·00171	0·00039	-0·00015		
λ_2	0·00202	0·00209	0·00195	0·00144	0·00264	
λ_3	0·00133	0·00064	0·00048	0·00064		
λ_4	-0·00082	-0·00021	-0·00002	-0·00006	-0·00285	
λ_5	-0·00541	-0·00606	-0·00629	-0·00632		
λ_6	-0·00777	-0·00732	-0·00715	-0·00712	-0·00113	
λ_7	0·02436	0·02426	0·02421	0·02420		
C_L	2·58774	2·68807	2·72704	2·75328	2·70807	2·74991
$-C_m$	3·01907	3·08217	3·10379	3·12600	3·09472	3·11289
$\bar{\eta}$	0·44674	0·44118	0·43918	0·43777	0·44014	0·43805
$\frac{x_{ac}}{\bar{c}}$	1·16668	1·14661	1·13815	1·13537	1·14278	1·13199

TABLE 15

Solutions for Arrowhead Planform 12 ($A = 8, M = 0, N = 3$) *at Unit Incidence.*

	Rounding	m = 7	m = 11	m = 15	m = 23	m = 15	m = 15
	η	m = 7 $\bar{m}$ = 95	m = 11 $\bar{m}$ = 95	m = 15 $\bar{m}$ = 95	m = 23 $\bar{m}$ = 95	m = 23 $\bar{m}$ = 95	m = 31 $\bar{m}$ = 63
Values of γ	0	0·25744	0·24963	0·24660	0·24513	0·25410	0·25828
	0·13053				0·26166	0·26542	
	0·19509			0·26497			0·27093
	0·25882		0·26577		0·26626	0·26833	
	0·38268	0·26142		0·26154	0·26206	0·26338	0·26587
	0·50000		0·25194		0·25198	0·25294	
	0·55557			0·24591			0·24911
	0·60876				0·23929	0·23993	
	0·70711	0·22490	0·22424	0·22408	0·22422	0·22472	0·22674
	0·79335				0·20776	0·20783	
	0·83147			0·19826			0·19978
	0·86602		0·18699		0·18712	0·18731	
	0·92388	0·15680		0·15737	0·15763	0·15779	0·15854
	0·96593		0·11436		0·11410	0·11423	
	0·98078			0·08813			0·08850
Values of μ	0	−0·01444	−0·01811	−0·02090	−0·02452	−0·02077	−0·02029
	0·13053				−0·00791	−0·00762	
	0·19509			−0·00528			−0·00316
	0·25882		−0·00390		−0·00214	−0·00230	
	0·38268	−0·00244		−0·00101	−0·00192	−0·00182	−0·00046
	0·50000		−0·00054		−0·00086	−0·00092	
	0·55557			−0·00134			0·00024
	0·60876				−0·00096	−0·00089	
	0·70711	0·00004	−0·00076	0·00002	−0·00014	−0·00017	0·00059
	0·79335				0·00037	0·00055	
	0·83147			0·00099			0·00163
	0·86602		0·00300		0·00264	0·00263	
	0·92388	0·00580		0·00694	0·00654	0·00657	0·00658
	0·96593		0·01008		0·01089	0·01088	
	0·98078			0·01066			0·01088
Values of K	0	0·00566	0·00725	0·00758	0·00563	0·00316	−0·00090
	0·13053				−0·00817	−0·00715	
	0·19509			−0·00628			0·00022
	0·25882		−0·00480		−0·00058	−0·00108	
	0·38268	−0·00304		0·00010	−0·00244	−0·00216	0·00321
	0·50000		−0·00006		−0·00039	−0·00062	
	0·55557			−0·00210			0·00359
	0·60876				−0·00178	−0·00161	
	0·70711	−0·00106	−0·00194	−0·00063	−0·00082	−0·00102	0·00254
	0·79335				−0·00239	−0·00264	
	0·83147			−0·00315			−0·00051
	0·86602		−0·00300		−0·00290	−0·00298	
	0·92388	−0·00096		−0·00243	−0·00346	−0·00338	−0·00329
	0·96593		0·00718		0·00843	0·00837	
	0·98078			0·01518			0·01588

TABLE 16

Solutions for Complete Delta Wing ($A = 1{\cdot}5, M = 0$) at Unit Incidence.

m	11	11	11	11	11	11	11
N	2	3	3	3	3	3	4
q	12	4	6	8	10	12	12
$\bar{m}$	143	47	71	95	119	143	143
y_0	0·78099	0·77708	0·77750	0·77753	0·77746	0·77745	0·77707
y_1	0·74935	0·74654	0·74688	0·74696	0·74690	0·74689	0·74688
y_2	0·65931	0·65796	0·65810	0·65826	0·65824	0·65822	0·65818
y_3	0·52086	0·52005	0·51976	0·51989	0·51985	0·51984	0·51996
y_4	0·34674	0·34764	0·34645	0·34607	0·34586	0·34586	0·34623
y_5	0·16160	0·16385	0·16258	0·16097	0·16023	0·16027	0·16124
μ_0	-0·11823	-0·11396	-0·11525	-0·11554	-0·11572	-0·11580	-0·11448
μ_1	-0·05931	-0·05473	-0·05563	-0·05568	-0·05570	-0·05572	-0·05601
μ_2	-0·02638	-0·02437	-0·02265	-0·02322	-0·02323	-0·02324	-0·02297
μ_3	-0·01327	-0·01649	-0·01206	-0·01136	-0·01169	-0·01164	-0·01154
μ_4	-0·00630	-0·00614	-0·00843	-0·00581	-0·00476	-0·00484	-0·00592
μ_5	-0·00315	0·00386	-0·00030	-0·00354	-0·00495	-0·00485	-0·00288
K_0		-0·07139	-0·07350	-0·07270	-0·07304	-0·07300	-0·06461
K_1		-0·03406	-0·04190	-0·04050	-0·04048	-0·04046	-0·04593
K_2		-0·00114	-0·00378	-0·00654	-0·00551	-0·00568	-0·00818
K_3		-0·02506	-0·00606	-0·00915	-0·01243	-0·01212	-0·01039
K_4		-0·00833	-0·01000	0·00072	0·00447	0·00421	-0·00324
K_5		0·02524	0·00326	-0·00368	-0·00679	-0·00677	-0·00181
λ_0							0·03281
λ_1							0·00462
λ_2							0·00761
λ_3							0·00583
λ_4							-0·00122
λ_5							0·00263
C_L	1·78190	1·77767	1·77731	1·77708	1·77674	1·77673	1·77694
$-C_m$	2·17764	2·16575	2·16427	2·16388	2·16351	2·16358	2·16340
$\bar{\eta}$	0·41474	0·41536	0·41508	0·41496	0·41489	0·41490	0·41503
$\frac{x_{ac}}{\bar{c}}$	1·22209	1·21831	1·21773	1·21766	1·21768	1·21773	1·21748

TABLE 17

Solutions for Slender Delta Wing (A = 0·0001, M = 0) at Unit Incidence.

m / N / q / $\bar{m}$	11 / 2 / 6 / 71	11 / 3 / 1 / 11	11 / 3 / 2 / 23	11 / 3 / 4 / 47	11 / 3 / 6 / 71	11 / 4 / 6 / 71
y_0	0·94128	0·98408	0·99193	0·98125	0·97986	0·99306
y_1	0·91921	0·95074	0·95794	0·94888	0·94733	0·95908
y_2	0·82759	0·85267	0·85671	0·85208	0·84913	0·85886
y_3	0·67406	0·69200	0·69574	0·69753	0·69366	0·70096
y_4	0·47392	0·50032	0·48694	0·49337	0·48992	0·49428
y_5	0·24268	0·25970	0·24832	0·25524	0·25281	0·25428
μ_0	-0·06920	-0·20997	-0·23848	-0·23137	-0·23492	-0·21540
μ_1	-0·08681	-0·11122	-0·17859	-0·16091	-0·16331	-0·14519
μ_2	-0·06787	-0·02916	-0·11830	-0·10037	-0·10221	-0·10685
μ_3	-0·04085	0·02386	-0·05170	-0·07327	-0·06287	-0·07707
μ_4	-0·02425	0·01217	0·00575	-0·04745	-0·03930	-0·04553
μ_5	-0·01628	0·04200	0·00827	0·00086	-0·01353	-0·00389
κ_0		-0·09969	0·41401	0·33766	0·33275	0·18757
κ_1		-0·06043	0·19567	0·20374	0·19162	0·36248
κ_2		-0·00728	0·03534	0·16861	0·11694	0·26000
κ_3		0·08920	-0·01387	0·10256	0·09923	0·11339
κ_4		0·41664	0·03500	0·01593	0·05211	0·04117
κ_5		0·13783	0·19565	0·02261	0·01790	0·06645
λ_0						-0·74582
λ_1						-0·27653
λ_2						-0·05710
λ_3						-0·05819
λ_4						-0·00644
λ_5						-0·01153
C_L/A	1·49312	1·54750	1·55138	1·54518	1·54003	1·55788
$-C_m/A$	1·83920	1·95535	2·07726	2·05841	2·05306	2·05462
$\bar{\eta}$	0·42491	0·42500	0·42291	0·42491	0·42438	0·42400
$x_{ac}/\bar{c}$	1·23179	1·26356	1·33898	1·33216	1·33313	1·31885

TABLE 18

Solutions for Slender Gothic Planform 15 (A = 0·0001, M = 0) at Unit Incidence.

m	11	11	11	11	11	11
N	2	3	3	3	3	4
q	6	1	2	4	6	6
$\bar{m}$	71	11	23	47	71	71
y_0	1·00385	1·00044	1·00144	1·00068	0·99847	1·00117
y_1	0·96906	0·96510	0·96772	0·96678	0·96436	0·96722
y_2	0·86847	0·86358	0·86760	0·86704	0·86478	0·86720
y_3	0·70904	0·70342	0·70577	0·70844	0·70536	0·70786
y_4	0·50121	0·50205	0·49607	0·50123	0·49900	0·50067
y_5	0·25869	0·26084	0·25724	0·25955	0·25870	0·25927
μ_0	-0·15522	-0·13672	-0·14798	-0·15411	-0·15630	-0·15596
μ_1	-0·09837	-0·08295	-0·09098	-0·09189	-0·09355	-0·09411
μ_2	-0·05481	-0·01955	-0·05532	-0·04644	-0·04654	-0·04596
μ_3	-0·02756	0·02767	-0·03683	-0·02032	-0·02370	-0·02186
μ_4	-0·00957	0·03482	0·00425	-0·01105	-0·00724	-0·01173
μ_5	0·00070	0·04437	0·01428	0·00386	-0·01347	0·00513
K_0		-0·28257	-0·02211	-0·10656	-0·11422	-0·10266
K_1		-0·23216	0·01670	-0·04858	-0·06315	-0·05332
K_2		-0·16255	-0·00595	-0·01007	-0·01150	0·00483
K_3		-0·03377	-0·11846	0·01313	-0·02445	0·00629
K_4		0·22198	-0·04315	-0·01370	0·03080	-0·03576
K_5		0·14505	0·13372	-0·01273	-0·00504	-0·00226
λ_0						-0·03072
λ_1						-0·03097
λ_2						0·00055
λ_3						0·02521
λ_4						-0·00623
λ_5						0·00595
C_L/A	1·57551	1·56883	1·57106	1·57278	1·56812	1·57281
$-C_m/A$	1·47139	1·40978	1·45957	1·45884	1·45768	1·46117
$\bar{\eta}$	0·42426	0·42437	0·42380	0·42455	0·42436	0·42440
$x_{ac}/\bar{c}$	0·93391	0·89862	0·92904	0·92755	0·92957	0·92902

TABLE 19

Solutions for Complete Delta and Slender Gothic Wings with Different Rounding.

	Planform 13 ($A = 1 \cdot 5$, $M = 0$, $\alpha = 1$)				Planform 15 ($A = 0 \cdot 0001$, $M = 0$, $\alpha = 1$)		
Rounding	$m = \infty$	$m = 23$	$m = 11$	$m = 5$	$m = 23$	$m = 11$	$m = 5$
m	11	11	11	11	11	11	11
N	3	3	3	3	3	3	3
q	8	8	8	8	6	6	6
$\bar{m}$	95	95	95	95	71	71	71
γ_0	0·75477	0·77162	0·77753	0·78058	0·99884	0·99847	0·99868
γ_1	0·72679	0·74158	0·74696	0·74973	0·96457	0·96436	0·96449
γ_2	0·64338	0·65427	0·65826	0·66026	0·86494	0·86478	0·86478
γ_3	0·51022	0·51727	0·51989	0·52122	0·70544	0·70536	0·70540
γ_4	0·34012	0·34441	0·34607	0·34700	0·49915	0·49900	0·49884
γ_5	0·15855	0·16036	0·16097	0·16121	0·25895	0·25870	0·25844
μ_0	-0·19434	-0·14449	-0·11554	-0·08783	-0·19068	-0·15630	-0·12216
μ_1	-0·08166	-0·06410	-0·05568	-0·05035	-0·10803	-0·09355	-0·08436
μ_2	-0·02826	-0·02475	-0·02322	-0·02261	-0·05263	-0·04654	-0·04372
μ_3	-0·01372	-0·01202	-0·01136	-0·01096	-0·02659	-0·02370	-0·02235
μ_4	-0·00492	-0·00558	-0·00581	-0·00601	-0·00805	-0·00724	-0·00680
μ_5	-0·00414	-0·00374	-0·00354	-0·00334	-0·01389	-0·01347	-0·01314
K_0	0·08954	-0·05626	-0·07270	-0·05883	-0·09436	-0·11422	-0·07425
K_1	-0·02350	-0·04247	-0·04050	-0·03436	-0·05562	-0·06315	-0·05180
K_2	0·00049	-0·00428	-0·00654	-0·00961	-0·00693	-0·01150	-0·01117
K_3	-0·01459	-0·01160	-0·00915	-0·00609	-0·02580	-0·02445	-0·02075
K_4	0·00338	0·00220	0·00072	-0·00141	0·03384	0·03080	0·02648
K_5	-0·00393	-0·00418	-0·00368	-0·00275	-0·00573	-0·00504	-0·00290
C_L	1·73453	1·76574	1·77708	1·78290	1·56849	1·56812	1·56817
$-C_m$	2·19901	2·17704	2·16388	2·15922	1·48259	1·45768	1·44439
$\bar{\eta}$	0·41608	0·41523	0·41496	0·41482	0·42436	0·42436	0·42432
$\frac{x_{ac}}{\bar{c}}$	1·26778	1·23293	1·21766	1·21107	0·94523	0·92957	0·92106

TABLE 20

Solutions for Curved Planform 16 ($A = 3{\cdot}8993$, $\Lambda = 60°$, $M = 0$) *at Unit Incidence* ($N = 2, 4$).

m N q $\bar{m}$	15 2 1 15	15 2 2 31	15 2 8 127	15 4 1 15	15 4 2 31	15 4 4 63	15 4 8 127
y_0	0·30491	0·27392	0·27286	0·30024	0·28636	0·27679	0·27381
y_1	0·33750	0·31441	0·31501	0·33488	0·32755	0·31933	0·31594
y_2	0·35767	0·33580	0·33670	0·35696	0·34964	0·33989	0·33693
y_3	0·35734	0·33596	0·33905	0·35799	0·35165	0·34176	0·33959
y_4	0·33441	0·31126	0·31665	0·33531	0·32819	0·31852	0·31654
y_5	0·28651	0·26328	0·26965	0·28650	0·27925	0·27226	0·26940
y_6	0·21214	0·19414	0·19752	0·21281	0·20332	0·20006	0·19658
y_7	0·11273	0·10486	0·10567	0·11413	0·10772	0·10686	0·10482
μ_0	−0·02957	−0·03321	−0·03392	−0·02375	−0·03068	−0·03564	−0·03524
μ_1	0·00178	−0·01233	−0·00914	0·00292	−0·00376	−0·00968	−0·01107
μ_2	0·00655	−0·00369	−0·00034	0·00868	0·00578	0·00027	−0·00046
μ_3	0·00707	−0·00041	0·00206	0·01146	0·00779	0·00067	0·00118
μ_4	0·00660	0·00165	0·00388	0·01300	0·01035	0·00270	0·00419
μ_5	0·00772	0·00027	0·00353	0·01461	0·01074	0·00154	0·00303
μ_6	0·01288	−0·00131	0·00406	0·01642	0·01244	0·00556	0·00356
μ_7	0·02010	0·00387	0·00233	0·02225	0·00892	0·00689	0·00050
K_0				0·04342	0·02630	0·02662	0·03164
K_1				0·04764	0·02943	−0·00789	−0·01602
K_2				0·05974	0·04690	0·00541	−0·00431
K_3				0·06378	0·03709	−0·00189	−0·00395
K_4				0·07248	0·03918	−0·00212	−0·00061
K_5				0·07687	0·03589	−0·00669	−0·00191
K_6				0·08916	0·04430	−0·00294	−0·00501
K_7				0·05909	0·04566	0·01772	−0·00463
λ_0				0·03021	−0·00286	−0·01641	−0·01621
λ_1				0·01397	0·03131	0·00359	0·00128
λ_2				0·02530	0·03252	−0·00094	−0·00477
λ_3				0·03886	0·02596	0·00004	−0·00005
λ_4				0·05531	0·02306	−0·00440	−0·00186
λ_5				0·06931	0·02587	−0·00120	0·00136
λ_6				0·04830	0·03563	−0·00235	−0·00286
λ_7				0·03158	0·05309	0·00951	−0·00168
C_L	2·46507	2·29017	2·30956	2·45916	2·39772	2·33308	2·31153
$-C_m$	4·62727	4·37158	4·40506	4·59775	4·51734	4·45080	4·41059
$\bar{\eta}$	0·47032	0·47085	0·47287	0·47170	0·47187	0·47239	0·47237
$\dfrac{x_{ac}}{\bar{c}}$	1·87713	1·90884	1·90732	1·86965	1·88402	1·90769	1·90808

TABLE 21

Solutions for Curved Planform 16 ($A = 3{\cdot}8993$, $\Lambda = 60°$, $M = 0$) at Unit Incidence.

m N q $\bar{m}$	15 3 1 15	15 3 2 31	15 3 4 63	31 3 2 63	15 2 8 127	15 3 8 127	15 4 8 127
y_0	0·30580	0·28543	0·27354	0·27305	0·27286	0·27441	0·27381
y_1	0·34052	0·32733	0·31509	0·31642	0·31501	0·31616	0·31594
y_2	0·36266	0·34812	0·33612	0·33770	0·33670	0·33688	0·33693
y_3	0·36367	0·34890	0·33752	0·33906	0·33905	0·33940	0·33959
y_4	0·34027	0·32460	0·31214	0·31632	0·31665	0·31661	0·31654
y_5	0·28898	0·27788	0·26497	0·26816	0·26965	0·26988	0·26940
y_6	0·21559	0·20245	0·19362	0·19739	0·19752	0·19708	0·19658
y_7	0·11562	0·10709	0·10264	0·10575	0·10567	0·10518	0·10482
μ_0	−0·02375	−0·03416	−0·03468	−0·04175	−0·03392	−0·03476	−0·03524
μ_1	0·00354	−0·00636	−0·01211	−0·00820	−0·00914	−0·00987	−0·01107
μ_2	0·00940	0·00297	−0·00197	−0·00306	−0·00034	0·00059	−0·00046
μ_3	0·01209	0·00336	0·00011	0·00099	0·00206	0·00175	0·00118
μ_4	0·01359	0·00502	0·00326	0·00233	0·00388	0·00437	0·00419
μ_5	0·01504	0·00466	0·00128	0·00214	0·00353	0·00335	0·00303
μ_6	0·01281	0·01105	0·00147	0·00016	0·00406	0·00502	0·00356
μ_7	0·02062	0·00874	0·00328	0·00436	0·00233	0·00125	0·00050
K_0	0·05922	0·01328	0·02923	0·01571		0·03035	0·03164
K_1	0·07004	0·00231	−0·01790	−0·01169		−0·01464	−0·01602
K_2	0·07938	0·02069	−0·00640	−0·00732		−0·00035	−0·00431
K_3	0·07433	0·00790	−0·00738	−0·00556		−0·00318	−0·00395
K_4	0·07543	0·00847	−0·00304	−0·00408		0·00074	−0·00061
K_5	0·08258	−0·00006	−0·00534	−0·00471		−0·00294	−0·00191
K_6	0·10927	0·00317	−0·01285	−0·00956		0·00090	−0·00501
K_7	0·04915	0·04717	−0·00390	−0·01087		−0·00211	−0·00463
λ_0							−0·01621
λ_1							0·00128
λ_2							−0·00477
λ_3							−0·00005
λ_4							−0·00186
λ_5							0·00136
λ_6							−0·00286
λ_7							−0·00168
C_L	2·49672	2·38527	2·29504	2·31746	2·30956	2·31290	2·31153
$-C_m$	4·66180	4·51805	4·37512	4·41884	4·40506	4·40757	4·41059
$\bar{\eta}$	0·47117	0·47130	0·47095	0·47134	0·47287	0·47239	0·47237
$\frac{x_{ac}}{\bar{c}}$	1·86717	1·89414	1·90634	1·90676	1·90732	1·90564	1·90808

TABLE 22

Solutions for Curved Planform 17 ($A = 3{\cdot}5564$, $\Lambda = 55°$, $M = 0{\cdot}8$) at Unit Incidence.

Rounding	m = 11	m = 23	m = 23	m = 15	m = 11	m = 11	m = 11
m	11	23	23	15	11	15	23
N	3	3	3	3	3	3	3
q	1	1	4	6	8	6	4
$\bar{m}$	11	23	95	95	95	95	95
γ_0	0·44690	0·41654	0·38630	0·38512	0·38548	0·40462	0·41720
γ_1		0·44232	0·42050				0·43622
γ_2	0·48610	0·46122	0·44026		0·43868		0·45080
γ_3		0·46595	0·44681	0·44474		0·45030	0·45453
γ_4	0·48299	0·45859	0·43915		0·43634		0·44530
γ_5		0·43889	0·42025				0·42500
γ_6	0·42765	0·40751	0·38864	0·38782	0·38852	0·39061	0·39256
γ_7		0·36421	0·34642				0·34941
γ_8	0·32871	0·30907	0·29266		0·29112		0·29508
γ_9		0·24020	0·23070	0·22837		0·22965	0·23234
γ_{10}	0·17983	0·17020	0·15955		0·15829		0·16085
γ_{11}		0·08754	0·08195				0·08254
μ_0	−0·04664	−0·06364	−0·06682	−0·06175	−0·05592	−0·05854	−0·05718
μ_1		−0·02502	−0·03091				−0·03027
μ_2	0·00254	−0·00638	−0·00706		−0·01489		−0·00778
μ_3		0·00122	−0·00057	0·00217		0·00200	−0·00012
μ_4	0·01480	0·00372	0·00243		0·00424		0·00235
μ_5		0·00617	0·00249				0·00281
μ_6	0·01704	0·00895	0·00429	0·00498	0·00182	0·00489	0·00422
μ_7		0·01223	0·00436				0·00459
μ_8	0·01860	0·01595	0·00571		0·00713		0·00562
μ_9		0·02000	0·00356	0·00583		0·00567	0·00378
μ_{10}	0·03340	0·01148	0·00214		−0·00010		0·00189
μ_{11}		0·01529	0·00209				0·00233
K_0	0·09548	−0·01934	0·03754	0·05341	0·05797	0·04212	0·02007
K_1		−0·02423	−0·03515				−0·02951
K_2	0·12558	−0·00723	−0·02194		−0·03155		−0·02307
K_3		0·00318	−0·00915	−0·00573		−0·00610	−0·00895
K_4	0·16210	0·00561	−0·00214		−0·00086		−0·00272
K_5		0·00756	−0·00335				−0·00291
K_6	0·19117	0·00953	−0·00015	0·00001	−0·00405	−0·00014	−0·00058
K_7		0·01227	−0·00174				−0·00128
K_8	0·19229	0·01758	0·00303		0·00258		0·00255
K_9		0·02784	0·00225	0·00326		0·00346	0·00282
K_{10}	0·08025	0·10213	−0·00899		−0·00454		−0·00908
K_{11}		0·04055	−0·00352				−0·00416
C_L	3·02517	2·86766	2·73191	2·72135	2·71057	2·76421	2·79176
$-C_m$	4·50467	4·32481	4·15612	4·14903	4·14377	4·19662	4·22267
$\bar{\eta}$	0·45636	0·45605	0·45674	0·45724	0·45798	0·45454	0·45300
$\frac{x_{ac}}{\bar{c}}$	1·48906	1·50813	1·52132	1·52462	1·52874	1·51820	1·51255

TABLE 23

Local Aerodynamic Centres of Rectangular Wings at M = 0.

Solution	Values of X_{ac} for η =							
m, N, q		0·1951	0·3827	0·5556	0·7071	0·8315	0·9239	0·9808
7, 2, 1	0·2169		0·2122		0·1985		0·1817	
7, 2, 2	0·2195		0·2148		0·2011		0·1832	
7, 2, 4	0·2200		0·2152		0·2013		0·1834	
15, 2, 1	0·2195	0·2183	0·2149	0·2090	0·2011	0·1920	0·1832	0·1769
7, 3, 1	0·2181		0·2121		0·1952		0·1753	
7, 3, 2	0·2177		0·2129		0·1984		0·1786	
7, 3, 4	0·2197		0·2147		0·1996		0·1792	
7, 3, 6	0·2199		0·2149		0·1997		0·1792	
15, 3, 1	0·2177	0·2165	0·2129	0·2068	0·1984	0·1884	0·1786	0·1714
7, 4, 1	0·2250		0·2181		0·1982		0·1727	
7, 4, 2	0·2173		0·2123		0·1972		0·1759	
7, 4, 4	0·2190		0·2141		0·1991		0·1771	
7, 4, 6	0·2197		0·2148		0·1995		0·1773	
7, 4, 8	0·2199		0·2149		0·1995		0·1773	
7, 4, 16	0·2199		0·2149		0·1995		0·1773	
15, 4, 1	0·2173	0·2161	0·2123	0·2059	0·1972	0·1867	0·1759	0·1674
15, 4, 2	0·2190	0·2178	0·2141	0·2079	0·1991	0·1883	0·1771	0·1683
15, 4, 8	0·2199	0·2187	0·2149	0·2085	0·1996	0·1886	0·1773	0·1685

(b) A = 4

Solution	Values of X_{ac} for η =							
m, N, q	0	0·1951	0·3827	0·5556	0·7071	0·8315	0·9239	0·9808
15, 2, 1	0·2377	0·2371	0·2349	0·2307	0·2234	0·2126	0·1998	0·1888
15, 2, 2	0·2407	0·2400	0·2376	0·2330	0·2252	0·2139	0·2005	0·1892
15, 2, 4	0·2411	0·2403	0·2379	0·2332	0·2253	0·2139	0·2005	0·1892
15, 3, 1	0·2380	0·2372	0·2344	0·2292	0·2209	0·2091	0·1951	0·1832
15, 3, 2	0·2389	0·2382	0·2360	0·2316	0·2239	0·2121	0·1974	0·1845
15, 3, 4	0·2409	0·2402	0·2378	0·2330	0·2249	0·2127	0·1977	0·1847
15, 3, 6	0·2411	0·2404	0·2379	0·2331	0·2249	0·2127	0·1977	0·1847
7, 3, 12	0·2411		0·2380		0·2249		0·1977	
7, 4, 1	0·2673		0·2609		0·2364		0·1892	
7, 4, 2	0·2438		0·2393		0·2232		0·1936	
7, 4, 4	0·2383		0·2352		0·2227		0·1961	
7, 4, 8	0·2402		0·2372		0·2246		0·1970	
7, 4, 12	0·2409		0·2378		0·2249		0·1971	
7, 4, 16	0·2411		0·2379		0·2249		0·1971	
15, 4, 1	0·2438	0·2427	0·2393	0·2331	0·2232	0·2095	0·1935	0·1795
15, 4, 4	0·2402	0·2395	0·2372	0·2326	0·2246	0·2125	0·1969	0·1821
15, 4, 8	0·2411	0·2403	0·2379	0·2331	0·2249	0·2126	0·1969	0·1821

TABLE 24

Spanwise Loading and Local Aerodynamic Centres of Rectangular Wing ($A = 8, M = 0$).

m, N, q	21, 3, 1	21, 3, 2	21, 3, 4	21, 3, 6
η	Values of $cC_{LL}/\bar{c}C_L$			
0	1·1533	1·1607	1·1623	1·1622
0·1423	1·1495	1·1563	1·1577	1·1576
0·2817	1·1375	1·1423	1·1433	1·1432
0·4154	1·1149	1·1170	1·1173	1·1172
0·5406	1·0785	1·0771	1·0767	1·0767
0·6549	1·0218	1·0177	1·0168	1·0168
0·7557	0·9395	0·9326	0·9313	0·9314
0·8413	0·8216	0·8148	0·8134	0·8136
0·9096	0·6662	0·6591	0·6580	0·6582
0·9595	0·4697	0·4657	0·4649	0·4651
0·9898	0·2443	0·2416	0·2412	0·2413
$\partial C_L/\partial \alpha$	4·4864	4·5912	4·5950	4·5909
$-\partial C_m/\partial \alpha$	1·0848	1·0972	1·1097	1·1110
η	Values of X_{ac}			
0	0·2498	0·2441	0·2470	0·2478
0·1423	0·2495	0·2440	0·2469	0·2477
0·2817	0·2484	0·2437	0·2466	0·2473
0·4154	0·2466	0·2430	0·2458	0·2464
0·5406	0·2436	0·2417	0·2444	0·2448
0·6549	0·2401	0·2393	0·2418	0·2421
0·7557	0·2337	0·2350	0·2370	0·2372
0·8413	0·2270	0·2276	0·2289	0·2290
0·9096	0·2144	0·2158	0·2166	0·2166
0·9595	0·2055	0·2009	0·2013	0·2013
0·9898	0·1902	0·1875	0·1878	0·1878

TABLE 25

Local Aerodynamic Centres of Unswept Planforms 4 and 5 at $M = 0$.

(a) Circular ($A = 1 \cdot 2732$)

Solution m, N, q	Values of X_{ac} for η =					
	0	0·2588	0·5000	0·7071	0·8660	0·9659
11, 2, 4 5, 2, 8	0·1958 0·1960	0·1945	0·1904 0·1905	0·1828	0·1702 0·1724	0·1515
11, 3, 6 5, 3, 12	0·1981 0·1982	0·1971	0·1939 0·1940	0·1880	0·1780 0·1795	0·1603
11, 4, 4 11, 4, 6 11, 4, 8 5, 4, 16	0·1981 0·1980 0·1980 0·1982	0·1971 0·1970 0·1970	0·1939 0·1938 0·1938 0·1938	0·1879 0·1877 0·1876	0·1783 0·1769 0·1764 0·1784	0·1702 0·1597 0·1551

(b) Symmetrically tapered ($A = 4 \cdot 3292$)

Solution m, N, q	Values of X_{ac} for η =					
	0	0·2588	0·5000	0·7071	0·8660	0·9659
11, 3, 1 11, 3, 2 11, 3, 4 11, 3, 8	0·2506 0·2559 0·2581 0·2583	0·2349 0·2368 0·2394 0·2396	0·2354 0·2331 0·2362 0·2366	0·2341 0·2300 0·2333 0·2340	0·2202 0·2182 0·2216 0·2223	0·1806 0·1896 0·1928 0·1932
23, 3, 1 23, 3, 2 23, 3, 4	0·2514 0·2548 0·2553	0·2356 0·2384 0·2386	0·2331 0·2363 0·2367	0·2298 0·2332 0·2338	0·2183 0·2218 0·2224	0·1896 0·1926 0·1930

TABLE 26

Local Aerodynamic Centres of Constant-Chord Sweptback Wings ($A = 4, M = 0$).

Solution	Values of X_{ac} for η =							
m, N, q	0	0·1951	0·3827	0·5556	0·7071	0·8315	0·9239	0·9808
15, 2, 1	0·2718	0·2636	0·2507	0·2395	0·2215	0·1870	0·1408	0·1032
15, 2, 2	0·2737	0·2671	0·2557	0·2431	0·2229	0·1882	0·1430	0·1047
15, 2, 4	0·2732	0·2660	0·2540	0·2415	0·2220	0·1880	0·1430	0·1048
7, 2, 8	0·2736		0·2543		0·2217		0·1427	
15, 3, 1	0·2675	0·2574	0·2422	0·2293	0·2108	0·1767	0·1304	0·0958
15, 3, 2	0·2724	0·2650	0·2530	0·2417	0·2227	0·1854	0·1355	0·0992
15, 3, 4	0·2740	0·2669	0·2552	0·2429	0·2222	0·1845	0·1351	0·0992
15, 3, 6	0·2739	0·2665	0·2543	0·2420	0·2217	0·1843	0·1351	0·0992
7, 3,12	0·2742		0·2550		0·2205		0·1370	
15, 4, 1	0·2712	0·2614	0·2462	0·2320	0·2104	0·1731	0·1266	0·0845
15, 4, 2	0·2703	0·2614	0·2477	0·2355	0·2169	0·1824	0·1351	0·0915
15, 4, 4	0·2734	0·2663	0·2548	0·2432	0·2229	0·1851	0·1357	0·0921
15, 4, 6	0·2739	0·2667	0·2550	0·2428	0·2221	0·1845	0·1355	0·0920
15, 4, 8	0·2739	0·2665	0·2545	0·2422	0·2217	0·1843	0·1354	0·0920
7, 4,16	0·2743		0·2552		0·2204		0·1378	

(b) Planform 7 with straight edges

Solution	Values of X_{ac} for η =							
m, N, q	0	0·1951	0·3827	0·5556	0·7071	0·8315	0·9239	0·9808
15, 2, 1	0·3897	0·2604	0·2445	0·2362	0·2197	0·1852	0·1389	0·1013
15, 2, 2	0·4050	0·2766	0·2529	0·2424	0·2211	0·1868	0·1408	0·1030
15, 2, 4	0·4070	0·2737	0·2498	0·2401	0·2200	0·1866	0·1408	0·1030
7, 2, 8	0·4471		0·2556		0·2185		0·1419	
15, 3, 1	0·3746	0·2499	0·2343	0·2250	0·2082	0·1746	0·1284	0·0940
15, 3, 2	0·4062	0·2703	0·2472	0·2406	0·2204	0·1844	0·1329	0·0981
15, 3, 4	0·4132	0·2764	0·2510	0·2425	0·2198	0·1835	0·1324	0·0982
15, 3, 6	0·4133	0·2748	0·2492	0·2413	0·2192	0·1833	0·1323	0·0982
7, 3,12	0·4491		0·2570		0·2165		0·1375	
15, 4, 1	0·3769	0·2544	0·2387	0·2280	0·2079	0·1709	0·1245	0·0826
15, 4, 2	0·3992	0·2634	0·2405	0·2332	0·2142	0·1811	0·1326	0·0901
15, 4, 4	0·4133	0·2749	0·2501	0·2427	0·2207	0·1841	0·1330	0·0909
15, 4, 6	0·4145	0·2762	0·2506	0·2424	0·2197	0·1834	0·1327	0·0908
15, 4, 8	0·4144	0·2753	0·2496	0·2416	0·2192	0·1833	0·1327	0·0908
7, 4,16	0·4495		0·2574		0·2167		0·1383	

TABLE 27

Local Aerodynamic Centres of Tapered Sweptback Wings at $M = 0{\cdot}8$.

(a) Cropped delta Planform 8 ($A = 1{\cdot}9704$)

Solution	Values of X_{ac} for η =							
m, N, q	0	0·1951	0·3827	0·5556	0·7071	0·8315	0·9239	0·9808
15, 2, 1	0·3641	0·3066	0·2752	0·2515	0·2254	0·1885	0·1397	0·0976
7, 3, 4	0·3937		0·2789		0·2208		0·1412	
15, 3, 2	0·3806	0·3108	0·2728	0·2479	0·2217	0·1869	0·1381	0·0922
31, 3, 1	0·3648	0·3036	0·2703	0·2462	0·2211	0·1864	0·1377	0·0920
15, 4, 4	0·3848	0·3126	0·2724	0·2466	0·2192	0·1844	0·1355	0·0816

(b) Arrowhead Planform 9 ($A = 2\sqrt{2}$)

Solution	Values of X_{ac} for η =							
m, N, q	0	0·1951	0·3827	0·5556	0·7071	0·8315	0·9239	0·9808
15, 2, 1	0·4244	0·3317	0·2961	0·2733	0·2476	0·2033	0·1388	0·0857
15, 2, 2	0·4311	0·3268	0·2824	0·2589	0·2326	0·1929	0·1348	0·0842
15, 2, 4	0·4369	0·3294	0·2841	0·2604	0·2339	0·1938	0·1352	0·0845
15, 3, 1	0·4275	0·3145	0·2679	0·2404	0·2143	0·1761	0·1226	0·0729
15, 3, 2	0·4419	0·3361	0·2906	0·2693	0·2409	0·1967	0·1288	0·0790
15, 3, 4	0·4449	0·3312	0·2818	0·2594	0·2311	0·1894	0·1259	0·0783
15, 3, 6	0·4461	0·3322	0·2829	0·2606	0·2321	0·1900	0·1260	0·0784
15, 4, 1	0·4063	0·2970	0·2558	0·2310	0·2034	0·1611	0·1092	0·0554
15, 4, 2	0·4456	0·3327	0·2816	0·2570	0·2284	0·1894	0·1317	0·0702
15, 4, 4	0·4468	0·3332	0·2854	0·2640	0·2350	0·1912	0·1273	0·0693
15, 4, 6	0·4475	0·3317	0·2822	0·2599	0·2311	0·1889	0·1272	0·0692
15, 4, 8	0·4482	0·3325	0·2830	0·2605	0·2317	0·1895	0·1273	0·0693

TABLE 28

Spanwise Loading and Local Aerodynamic Centres of Planform 10 (A = 1·4503, M = 0·8).

m N q $\bar{m}$	7 4 12 95	11 4 8 95	15 4 6 95
η	Values of $cC_{LL}/\bar{c}C_L$		
0	1·2590	1·2595	1·2597
0·1951			1·2407
0·2588		1·2239	
0·3827	1·1749		1·1747
0·5000		1·1050	
0·5556			1·0626
0·7071	0·9084	0·9080	0·9077
0·8315			0·7156
0·8660		0·6447	
0·9239	0·4943		0·4937
0·9659		0·3341	
0·9808			0·2518
$\partial C_L/\partial\alpha$	2·1270	2·1314	2·1335
$-\partial C_m/\partial\alpha$	0·9791	0·9739	0·9708
$\bar{\eta}$	0·4266	0·4264	0·4264
$\frac{x_{ac}}{\bar{c}}$	0·4603	0·4569	0·4550

m N q $\bar{m}$	7 4 12 95	11 4 8 95	15 4 6 95
η	Values of X_{ac}		
0	0·3108	0·3050	0·3013
0·1951			0·2389
0·2588		0·2269	
0·3827	0·2052		0·1993
0·5000		0·1789	
0·5556			0·1687
0·7071	0·1403	0·1404	0·1395
0·8315			0·1121
0·8660		0·1038	
0·9239	0·0900		0·0886
0·9659		0·0780	
0·9808			0·0736

TABLE 29

Spanwise Loading of Arrowhead Planform 12 ($A = 8, M = 0$).

m, N, q	15, 3, 1	23, 3, 1	31, 3, 1	41, 3, 1
η	Values of $cC_{LL}/\bar{c}C_L$			
0	1·0707	1·0818	1·0806	1·0776
0·1305		1·1371		
0·1490				1·1446
0·1951	1·1445		1·1526	
0·2588		1·1529		
0·2948				1·1513
0·3827	1·1327	1·1305	1·1320	
0·4339				1·1164
0·5000		1·0876		1·0894
0·5556	1·0648		1·0613	
0·5633				1·0581
0·6088		1·0316		
0·6802				0·9862
0·7071	0·9735	0·9679	0·9670	
0·7818				0·9036
0·7934		0·8960		
0·8315	0·8610		0·8516	
0·8660		0·8069		0·8012
0·9239	0·6850	0·6774	0·6736	
0·9309				0·6490
0·9659		0·4895		
0·9749				0·4235
0·9808	0·3810		0·3751	
0·9914		0·2567		
0·9972				0·1473

m, N, q	7, 3, 12	11, 3, 8	15, 3, 6	23, 3, 4
η	Values of $cC_{LL}/\bar{c}C_L$			
0	1·1125	1·0819	1·0686	1·0606
0·1305				1·1321
0·1951			1·1482	
0·2588		1·1518		1·1520
0·3827	1·1297		1·1334	1·1339
0·5000		1·0919		1·0903
0·5556			1·0656	
0·6088				1·0354
0·7071	0·9719	0·9718	0·9710	0·9702
0·7934				0·8989
0·8315			0·8592	
0·8660		0·8104		0·8096
0·9239	0·6776		0·6819	0·6820
0·9659		0·4956		0·4937
0·9808			0·3819	
0·9914				0·2594

TABLE 30

Local Aerodynamic Centres of Arrowhead Planform 12 ($A = 8, M = 0$).

m, N, q	15, 3, 1	23, 3, 1	31, 3, 1	41, 3, 1
η	Values of X_{ac}			
0	0·3764	0·3733	0·3746	0·3777
0·1305		0·2498		
0·1490				0·2584
0·1951	0·2378		0·2452	
0·2588		0·2351		
0·2948				0·2444
0·3827	0·2335	0·2312	0·2356	
0·4339				0·2405
0·5000		0·2297		0·2395
0·5556	0·2334		0·2331	
0·5633				0·2387
0·6088		0·2289		
0·6802				0·2376
0·7071	0·2316	0·2278	0·2315	
0·7818				0·2358
0·7934		0·2250		
0·8315	0·2235		0·2265	
0·8660		0·2164		0·2283
0·9239	0·1878	0·1917	0·1983	
0·9309				0·1995
0·9659		0·1448		
0·9749				0·1400
0·9808	0·1060		0·1237	
0·9914		0·0982		
0·9972				0·0965

m, N, q	7, 3, 12	11, 3, 8	15, 3, 6	23, 3, 4
η	Values of X_{ac}			
0	0·4891	0·4459	0·4275	0·4119
0·1305				0·2802
0·1951			0·2699	
0·2588		0·2647		0·2580
0·3827	0·2593		0·2538	0·2573
0·5000		0·2522		0·2534
0·5556			0·2554	
0·6088				0·2540
0·7071	0·2498	0·2534	0·2499	0·2506
0·7934				0·2482
0·8315			0·2450	
0·8660		0·2339		0·2359
0·9239	0·2130		0·2059	0·2085
0·9659		0·1619		0·1546
0·9808			0·1291	
0·9914				0·1065

TABLE 31

Local Aerodynamic Centres of Planform 12 ($A = 8, M = 0$) with Fixed $\bar{m}$, q or Rounding.

			Values of X_{ac} for η =					
Rounding	m, N, q	$\bar{m}$	0	0·1951	0·3827	0·7071	0·8315	0·9239
m = 7	7,3,12	95	0·4891		0·2593	0·2498		0·2130
m = 11	11,3, 8	95	0·4459			0·2534		
m = 15	15,3, 6	95	0·4275	0·2699	0·2538	0·2499	0·2450	0·2059
m = 23	23,3, 4	95	0·4119		0·2573	0·2506		0·2085
m = 15	15,3, 1	15	0·3764	0·2378	0·2335	0·2316	0·2235	0·1878
m = 23	23,3, 1	23	0·3733		0·2312	0·2278		0·1917
m = 31	31,3, 1	31	0·3746	0·2452	0·2356	0·2315	0·2265	0·1983
m = 15	15,3, 1	15	0·3764	0·2378	0·2335	0·2316	0·2235	0·1878
m = 15	15,3, 4	63	0·4274	0·2675	0·2499	0·2462	0·2435	0·2069
m = 15	15,3, 6	95	0·4275	0·2699	0·2538	0·2499	0·2450	0·2059
m = 15	15,3, 8	127	0·4274	0·2685	0·2527	0·2488	0·2438	0·2052
m = 15	15,3, 6	95	0·4275	0·2699	0·2538	0·2499	0·2450	0·2059
m = 15	23,3, 4	95	0·4246		0·2569	0·2508		0·2083
m = 15	15,3, 4	63	0·4274	0·2675	0·2499	0·2462	0·2435	0·2069
m = 15	31,3, 2	63	0·4214	0·2617	0·2517	0·2474	0·2418	0·2085

TABLE 32

Local Aerodynamic Centres of Slender Wings.

Solution m, N, q	Values of X_{ac} for η = 0	0·2588	0·5000	0·7071	0·8660	0·9659
11, 2, 1	0·4198	0·3393	0·2988	0·2527	0·1907	0·1658
11, 2, 8	0·4262	0·3285	0·2896	0·2749	0·2678	0·2770
11, 2,12	0·4272	0·3292	0·2900	0·2755	0·2682	0·2695
11, 3, 1	0·4004	0·2940	0·2436	0·2169	0·1860	0·1829
11, 3, 2	0·4231	0·3329	0·2904	0·2579	0·2202	0·1811
11, 3, 4	0·4227	0·3233	0·2870	0·2817	0·2677	0·2265
11, 3, 6	0·4242	0·3245	0·2844	0·2732	0·2743	0·2518
11, 3, 8	0·4245	0·3245	0·2853	0·2719	0·2668	0·2720
11, 3,10	0·4248	0·3246	0·2853	0·2725	0·2638	0·2809
11, 3,12	0·4249	0·3246	0·2853	0·2724	0·2640	0·2803
11, 4, 1	0·3794	0·2826	0·2492	0·2239	0·1900	0·1982
11, 4, 8	0·4227	0·3245	0·2844	0·2760	0·2713	0·2465
11, 4,12	0·4233	0·3250	0·2849	0·2722	0·2671	0·2679

(b) Complete delta (A = 0·0001, M = 0)

Solution m, N, q	Values of X_{ac} for η = 0	0·2588	0·5000	0·7071	0·8660	0·9659
11, 2, 6	0·3527	0·3444	0·3320	0·3106	0·3012	0·3171
11, 3, 1	0·4865	0·3670	0·2842	0·2155	0·2257	0·0883
11, 3, 2	0·5124	0·4364	0·3881	0·3243	0·2382	0·2167
11, 3, 4	0·5080	0·4196	0·3678	0·3550	0·3462	0·2466
11, 3, 6	0·5118	0·4224	0·3704	0·3406	0·3302	0·3035
11, 4, 6	0·4899	0·4014	0·3744	0·3599	0·3421	0·2653
Exact	0·5000	0·4203	0·3802	0·3568	0·3430	0·3357

(c) Gothic Planform 15 (A = 0·0001, M = 0)

Solution m, N, q	Values of X_{ac} for η = 0	0·2588	0·5000	0·7071	0·8660	0·9659
11, 2, 4	0·4167	0·3451	0·3077	0·2809	0·2648	0·2900
11, 2, 6	0·4226	0·3515	0·3131	0·2889	0·2691	0·2473
11, 3, 1	0·4052	0·3360	0·2726	0·2107	0·1806	0·0799
11, 3, 2	0·4159	0·3440	0·3138	0·3022	0·2414	0·1945
11, 3, 4	0·4220	0·3450	0·3036	0·2787	0·2720	0·2351
11, 3, 6	0·4244	0·3470	0·3038	0·2836	0·2645	0·3021
11, 4, 4	0·4189	0·3422	0·3028	0·2894	0·2696	0·2022
11, 4, 6	0·4237	0·3473	0·3030	0·2809	0·2734	0·2302
Exact	0·4000			0·2808		

TABLE 33

Local Aerodynamic Centres of Planforms 16 and 17 with Curved Tips.

(a) $A = 3{\cdot}8993,\ \Lambda = 60°,\ M = 0$

Solution m, N, q	Values of X_{ac} for η = 0	0·1951	0·3827	0·5556	0·7071	0·8315	0·9239	0·9808
15, 2, 1	0·4498	0·2447	0·2317	0·2302	0·2303	0·2231	0·1893	0·0717
15, 2, 2	0·4740	0·2892	0·2610	0·2512	0·2447	0·2490	0·2567	0·2131
15, 2, 8	0·4771	0·2790	0·2510	0·2439	0·2378	0·2369	0·2294	0·2280
15, 3, 1	0·4304	0·2396	0·2241	0·2168	0·2100	0·1979	0·1906	0·0716
15, 3, 2	0·4725	0·2694	0·2415	0·2404	0·2346	0·2332	0·1954	0·1684
15, 3, 4	0·4796	0·2884	0·2558	0·2497	0·2396	0·2452	0·2424	0·2180
31, 3, 2	0·4546	0·2759	0·2591	0·2471	0·2426	0·2420	0·2492	0·2088
15, 3, 8	0·4794	0·2812	0·2483	0·2449	0·2362	0·2376	0·2245	0·2381
15, 4, 1	0·4319	0·2413	0·2257	0·2180	0·2112	0·1990	0·1728	0·0551
15, 4, 2	0·4599	0·2615	0·2335	0·2279	0·2185	0·2115	0·1888	0·1672
15, 4, 4	0·4815	0·2803	0·2492	0·2480	0·2415	0·2443	0·2222	0·1856
15, 4, 8	0·4815	0·2850	0·2514	0·2465	0·2368	0·2388	0·2319	0·2452
15, 4, 8*	0·5449	0·2851	0·2530	0·2451	0·2376	0·2377	0·2334	0·2426

(b) $A = 3{\cdot}5564,\ \Lambda = 55°,\ M = 0{\cdot}8$

Solution m, N, q	Values of X_{ac} for η = 0	0·2588	0·5000	0·7071	0·8660	0·9659
11, 3, 1	0·4521	0·2448	0·2194	0·2101	0·1934	0·0643
11, 3, 2	0·4947	0·2780	0·2374	0·2339	0·1856	0·1790
11, 3, 4	0·4898	0·2904	0·2479	0·2604	0·2534	0·2160
11, 3, 6	0·4924	0·2835	0·2389	0·2447	0·2314	0·2663
11, 3, 8	0·4928	0·2840	0·2403	0·2453	0·2255	0·2506
23, 3, 1	0·4521	0·2638	0·2419	0·2280	0·1984	0·1825
23, 3, 2	0·4697	0·2739	0·2523	0·2537	0·2589	0·1998
23, 3, 4	0·4723	0·2660	0·2445	0·2390	0·2305	0·2366
23, 3, 4+	0·4847	0·2673	0·2447	0·2393	0·2309	0·2382

*m = 7 rounding is used with the m = 15 collocation sections.

+m = 11 rounding is used with the m = 23 collocation sections.

TABLE 34

Spanwise Loading and Aerodynamic Centres of Planform 17 (A = 3·5564, Λ = 55°, M = 0·8).

m	11	15	23	m	11	15	23
N	3	3	3	N	3	3	3
q	8	6	4	q	8	6	4
$\bar{m}$	95	95	95	$\bar{m}$	95	95	95
η	Values of $cC_{LL}/\bar{c}C_L$			η	Values of X_{ac}		
0	1·0115	1·0066	1·0058	0	0·4928	0·4839	0·4723
0·1305			1·0948	0·1305			0·3235
0·1951		1·1283		0·1951		0·2993	
0·2588	1·1511		1·1463	0·2588	0·2840		0·2660
0·3827		1·1624	1·1633	0·3827		0·2451	0·2513
0·5000	1·1450		1·1434	0·5000	0·2403		0·2445
0·5556		1·1266		0·5556		0·2476	
0·6088			1·0942	0·6088			0·2441
0·7071	1·0195	1·0137	1·0119	0·7071	0·2453	0·2372	0·2390
0·7934			0·9019	0·7934			0·2374
0·8315		0·8387		0·8315		0·2368	
0·8660	0·7639		0·7620	0·8660	0·2255		0·2305
0·9239		0·5969	0·6006	0·9239		0·2245	0·2346
0·9659	0·4154		0·4154	0·9659	0·2506		0·2366
0·9808		0·3133		0·9808		0·2674	
0·9914			0·2134	0·9914			0·2245

Rounding	m = 11	m = 11	m = 11	Rounding	m = 11	m = 11	m = 11
m	11	15	23	m	11	15	23
N	3	3	3	N	3	3	3
q	8	6	4	q	8	6	4
$\bar{m}$	95	95	95	$\bar{m}$	95	95	95
η	Values of $cC_{LL}/\bar{c}C_L$			η	Values of X_{ac}		
0	1·0115	1·0412	1·0629	0	0·4928	0·4924	0·4847
0·1305			1·1114	0·1305			0·3209
0·1951		1·1343		0·1951		0·2967	
0·2588	1·1511		1·1485	0·2588	0·2840		0·2673
0·3827		1·1587	1·1580	0·3827		0·2456	0·2503
0·5000	1·1450		1·1345	0·5000	0·2403		0·2447
0·5556		1·1191		0·5556		0·2469	
0·6088			1·0828	0·6088			0·2434
0·7071	1·0195	1·0051	1·0002	0·7071	0·2453	0·2375	0·2393
0·7934			0·8902	0·7934			0·2369
0·8315		0·8305		0·8315		0·2362	
0·8660	0·7639		0·7518	0·8660	0·2255		0·2309
0·9239		0·5909	0·5919	0·9239		0·2253	0·2337
0·9659	0·4154		0·4098	0·9659	0·2506		0·2382
0·9808		0·3102		0·9808		0·2663	
0·9914			0·2103	0·9914			0·2217

TABLE 35

Coefficients for Unswept Planforms 2, 4 and 5 in Oscillatory Motion.

m N q $\bar{m}$	15 2 1 15	15 2 2 31	15 3 1 15	15 3 2 31	15 3 4 63	15 3 6 95	7 3 12 95
I_{L1}	3·62517	3·61734	3·60000	3·61900	3·61517	3·61340	3·61338
I_{L2}	2·77908	2·78285	2·73255	2·77839	2·77924	2·77663	2·77660
I_{L3}	-0·31439	-0·31356	-0·33022	-0·31296	-0·31414	-0·31534	-0·31536
I_{L4}	2·34099	2·34815	2·29239	2·34891	2·34952	2·34581	2·34575
I_{L5}	-0·61521	-0·60933	-0·60892	-0·60749	-0·60729	-0·60735	-0·60737
$-I_{m1}$	0·83280	0·83957	0·82266	0·83382	0·83843	0·83838	0·83835
$-I_{m2}$	1·00988	1·01455	0·98859	1·01201	1·01473	1·01366	1·01363
$-I_{m3}$	0·29864	0·29464	0·28298	0·29587	0·29310	0·29196	0·29195
$-I_{m4}$	1·00209	1·00582	0·97509	1·00674	1·00899	1·00727	1·00722
$-I_{m5}$	0·08948	0·08828	0·08204	0·09022	0·08869	0·08800	0·08798
$-I^*_{m1}$	0·39803	0·40359	0·39502	0·40363	0·40645	0·40635	0·40633
$-I^*_{m2}$	0·58371	0·58698	0·57022	0·58739	0·58918	0·58840	0·58838

(b) Circular (A = 1·2732, M = 0)

m N q $\bar{m}$	11 2 4 47	11 3 6 71	11 4 8 95	5 4 16 95
I_{L1}	1·78878	1·79057	1·79028	1·79216
I_{L2}	1·73248	1·73376	1·73357	1·73824
I_{L3}	0·93945	0·93285	0·93345	0·94084
I_{L4}	1·78391	1·78608	1·78596	1·79134
I_{L5}	0·54990	0·54612	0·54650	0·55078
$-I_{m1}$	0·53940	0·54653	0·54592	0·54664
$-I_{m2}$	0·89898	0·90379	0·90341	0·90597
$-I_{m3}$	0·64617	0·64136	0·64189	0·64639
$-I_{m4}$	1·12178	1·12903	1·12876	1·13184
$-I_{m5}$	0·45110	0·45170	0·45200	0·45473
$-I^*_{m1}$	0·26646	0·27466	0·27387	0·27409
$-I^*_{m2}$	0·63273	0·63578	0·63536	0·63694

TABLE 35—*continued*

Coefficient for Unswept Planforms 2, 4 and 5 in Oscillatory Motion.

(c) Symmetrically tapered (A = 4·3292, M = 0)

m N q $\overline{m}$	11 3 1 11	11 3 2 23	11 3 4 47	11 3 8 95	23 3 1 23	23 3 2 47	23 3 4 95
I_{L1}	3·82039	3·85786	3·85505	3·85124	3·85987	3·85517	3·85144
I_{L2}	4·05122	4·15371	4·16424	4·15792	4·14995	4·15958	4·15347
I_{L3}	-0·41536	-0·34173	-0·33358	-0·33425	-0·37299	-0·35626	-0·35604
I_{L4}	4·62196	4·79860	4·81981	4·80852	4·78734	4·80816	4·79731
I_{L5}	-0·86904	-0·82901	-0·82286	-0·82250	-0·85040	-0·83798	-0·83708
$-I_{m1}$	1·91069	1·93356	1·94384	1·94310	1·92985	1·94083	1·94032
$-I_{m2}$	2·48319	2·56099	2·57762	2·57399	2·55395	2·57103	2·56774
$-I_{m3}$	0·21580	0·27799	0·27945	0·27697	0·26353	0·26819	0·26610
$-I_{m4}$	3·15210	3·29861	3·32429	3·31644	3·28625	3·31225	3·30489
$-I_{m5}$	-0·03099	0·01873	0·01981	0·01760	0·00924	0·01223	0·01022
$-I^*_{m1}$	1·26491	1·28539	1·29757	1·29737	1·28117	1·29434	1·29429
$-I^*_{m2}$	1·92797	2·00255	2·02002	2·01677	1·99553	2·01349	2·01049

TABLE 36

Coefficients for Planform 6 with Hyperbolic Edges ($A = 4, M = 0$) in Oscillatory Motion.

m N q $\bar{m}$	15 2 1 15	15 2 2 31	15 2 4 63	7 2 8 63	15 3 6 95	15 4 1 15	15 4 6 95
I_{L1}	3·25706	3·23454	3·23089	3·22967	3·23298	3·22444	3·23422
I_{L2}	3·98728	3·95396	3·93994	3·93716	3·94374	3·91073	3·94804
I_{L3}	-0·34127	-0·35390	-0·35857	-0·35251	-0·35670	-0·35253	-0·35545
I_{L4}			5·48373	5·48280	5·48901	5·44338	5·49857
I_{L5}			-0·51502	-0·50981	-0·51477	-0·48916	-0·51373
$-I_{m1}$	2·49307	2·48547	2·47938	2·47881	2·47941	2·45347	2·48161
$-I_{m2}$	3·72458	3·69483	3·67910	3·67866	3·68105	3·63631	3·68664
$-I_{m3}$	-0·04475	-0·06820	-0·07182	-0·06863	-0·06592	-0 04401	-0·06423
$-I_{m4}$			5·88338	5·88322	5·88962	5·83784	5·90169
$-I_{m5}$			0·02390	0·02781	0·03105	0·07463	0·03316
$-I^*_{m1}$		2·59413	2·58596	2·58605	2·58105	2·53449	2·58385
$-I^*_{m2}$		4·31540	4·29646	4·29526	4·29245	4·23164	4·29967

m N q $\bar{m}$	15 3 1 15	15 3 2 31	15 3 4 63	15 3 6 95	7 3 12 95
I_{L1}	3·25878	3·24466	3·23449	3·23298	3·23201
I_{L2}	3·96455	3·96604	3·94937	3·94374	3·94135
I_{L3}	-0·34144	-0·34881	-0·35512	-0·35670	-0·35090
I_{L4}			5·50134	5·48901	5·48849
I_{L5}			-0·51379	-0·51477	-0·51017
$-I_{m1}$	2·46998	2·48651	2·48227	2·47941	2·47892
$-I_{m2}$	3·68294	3·70463	3·68807	3·68105	3·68080
$-I_{m3}$	-0·02922	-0·05504	-0·06449	-0·06592	-0·06291
$-I_{m4}$			5·90414	5·88962	5·88946
$-I_{m5}$			0·03247	0·03105	0·03419
$-I^*_{m1}$	2·55510	2·59047	2·58503	2·58105	2·58108
$-I^*_{m2}$	4·28990	4·32517	4·30154	4·29245	4·29152

TABLE 37

Coefficients for Planform 7 ($A = 4, \Lambda = 45°, M = 0$) *in Oscillatory Motion.*

m N q $\bar{m}$	15 2 1 15	15 2 2 31	15 2 4 63	7 2 8 63	15 3 6 95	15 4 1 15	15 4 6 95
I_{L1}	3·04301	2·96838	2·95962	2·95345	2·96296	3·01519	2·96430
I_{L2}	4·81615	4·69471	4·66353	4·65673	4·67057	4·74238	4·67740
I_{L3}	-0·31971	-0·27629	-0·27200	-0·19912	-0·26878	-0·31876	-0·26751
I_{L4}			8·33354	8·35376	8·34417	8·45565	8·36267
I_{L5}			-0·37126	-0·30521	-0·36982	-0·41880	-0·36853
$-I_{m1}$	3·55371	3·50520	3·49192	3·49281	3·49550	3·50157	3·49999
$-I_{m2}$	6·47725	6·36293	6·32362	6·33616	6·33111	6 35473	6·34395
$-I_{m3}$	-0·23057	-0·20379	-0·19974	-0·12680	-0·19101	-0·21656	-0·18840
$-I_{m4}$			12·53971	12·58562	12·55405	12·62271	12·58616
$-I_{m5}$			0·04503	0·11719	0·05458	0·05160	0·05807
$-I^*_{m1}$	5·07490	5·02898	5·00627	5·01949	5·00365	4·97812	5·01142
$-I^*_{m2}$	10·11892	9·97076	9·90926	9·93639	9·91017	9·90088	9·93187

m N q $\bar{m}$	15 3 1 15	15 3 2 31	15 3 4 63	15 3 6 95	7 3 12 95
I_{L1}	3·05183	2·99198	2·96534	2·96296	2·95601
I_{L2}	4·80837	4·72904	4·68077	4·67057	4·66299
I_{L3}	-0·31230	-0·27076	-0·26913	-0·26878	-0·19666
I_{L4}			8·36947	8·34417	8·36529
I_{L5}			-0·37069	-0·36982	-0·30333
$-I_{m1}$	3·53251	3·51940	3·50105	3·49550	3·49546
$-I_{m2}$	6·43229	6·39749	6·34715	6·33111	6·34250
$-I_{m3}$	-0·20551	-0·18640	-0·19083	-0·19101	-0·11995
$-I_{m4}$			12·59292	12·55405	12·59884
$-I_{m5}$			0·05452	0·05458	0·12388
$-I^*_{m1}$	5·02065	5·03654	5·01367	5·00365	5·01746
$-I^*_{m2}$	10·02059	10·01328	9·93689	9·91017	9·93945

TABLE 38

Coefficients for Arrowhead Planforms 10 *and* 9 *in Oscillatory Motion.*

m	7	11	15	m	15	15	15
N	4	4	4	N	3	3	3
q	12	8	6	q	1	2	4
$\bar{m}$	95	95	95	$\bar{m}$	15	31	63
I_{L1}	1·27618	1·27886	1·28011	I_{L1}	2·79562	2·72847	2·72743
I_{L2}	1·40638	1·41251	1·41541	I_{L2}	4·55539	4·44966	4·43656
I_{L3}	0·76379	0·75794	0·75539	I_{L3}	0·31604	0·32090	0·33046
I_{L4}	1·60764	1·61616	1·62030	I_{L4}	7·79674	7·62431	7·58813
I_{L5}	0·56333	0·56193	0·56124	I_{L5}	0·12177	0·13800	0·14614
$-I_{m1}$	0·58747	0·58434	0 58247	$-I_{m1}$	3·11765	3·11066	3·10369
$-I_{m2}$	0·92456	0·92261	0·92148	$-I_{m2}$	5·67319	5·63463	5·61348
$-I_{m3}$	0·60680	0·60171	0·59933	$-I_{m3}$	0·43298	0·42222	0·43213
$-I_{m4}$	1·23471	1·23477	1·23467	$-I_{m4}$	10·41763	10·32702	10·27236
$-I_{m5}$	0·49724	0·49533	0·49440	$-I_{m5}$	0·38531	0·37110	0·38044
$-I^*_{m1}$	0·33882	0·33457	0·33237	$-I^*_{m1}$	4·13629	4·17935	4·16485
$-I^*_{m2}$	0·72175	0·71745	0·71527	$-I^*_{m2}$	7·99757	8·01972	7·98278

(c) $A = 2\sqrt{2}$, $M = 0·8$

m	15	15	15	15	15	15
N	3	3	3	4	4	4
q	1	2	4	1	2	4
$\bar{m}$	15	31	63	15	31	63
I_{L1}	1·93197	1·87654	1·88411	1·93616	1·89312	1·88167
I_{L2}	3·18877	3·08709	3·09063	3·19536	3·11500	3·09058
I_{L3}	0·57013	0·55079	0·56780	0·60202	0·57006	0·56439
I_{L4}	5·47405	5·29084	5 28655	5·48591	5·34031	5·29063
I_{L5}	0·63463	0·60569	0·62195	0·66347	0·62849	0·61717
$-I_{m1}$	2·20060	2·18572	2·18263	2·17427	2·19195	2·18556
$-I_{m2}$	4·06147	4·00127	3·99271	4·04093	4·02101	4·00078
$-I_{m3}$	0·72374	0·69282	0·71502	0·75514	0·72150	0·71131
$-I_{m4}$	7·48721	7·33900	7·31557	7·46933	7·38608	7·33353
$-I_{m5}$	0·93422	0·88387	0·90752	0·96991	0·92012	0·90209
$-I^*_{m1}$	2·92488	2·95194	2·93382	2·88113	2·94368	2·94362
$-I^*_{m2}$	5·75222	5·73211	5·70261	5·70953	5·74088	5·72208

TABLE 39

Coefficients for Direct and Reversed Planform 11 (A = 2, M = 0·7806) *in Oscillatory Motion.*

m N q $\bar{m}$	15 3 1 15	15 3 2 31	15 3 4 63	15 3 6 95	15 3 8 127	15 4 6 95	31+ 3 2 63
I_{L1}	1·60072	1·57616	1·58065	1·57982	1·57971	1·58128	1·59065
I_{L2}	2·61862	2·57048	2·57412	2·57259	2·57227	2·57603	2·60056
I_{L3}	0·65493	0·65923	0·67118	0·67152	0·67176	0·67346	0·65112
I_{L4}	4·38293	4·29460	4·29672	4·29417	4·29351	4·30088	4·34959
I_{L5}	0·76019	0·75151	0·76423	0·76427	0·76450	0·76564	0·74878
$-I_{m1}$	1·72638	1·72155	1·72169	1 72169	1·72181	1·72286	1·71989
$-I_{m2}$	3·16868	3·14880	3·14791	3·14762	3·14757	3·15201	3·15783
$-I_{m3}$	0·81971	0·81960	0·83643	0·83684	0·83724	0·83999	0·80924
$-I_{m4}$	5·67414	5·61774	5·61362	5·61274	5·61237	5·62329	5·64848
$-I_{m5}$	1·04352	1·02825	1·04706	1·04711	1·04749	1·05015	1·02395
$-I^*_{m1}$	2·13742	2·15966	2·15092	2·15186	2·15205	2·15289	2·14293
$-I^*_{m2}$	4·19911	4·21220	4·20135	4·20256	4·20263	4·20871	4·20161

(b) Reversed wing

m N q $\bar{m}$	15 3 1 15	15 3 2 31	15 3 4 63	15 3 6 95	15 3 8 127	15 4 6 95	31+ 3 2 63
$\bar{I}_{L1}$	1·59960	1·60063	1·59854	1·59915	1·59984	1·59884	1·59160
$\bar{I}_{L2}$	0·88600	0·87743	0·87132	0·87407	0·87610	0·87373	0·85146
$\bar{I}_{L3}$	0·67414	0·65246	0·64334	0·64531	0·64694	0·64774	0·64317
$\bar{I}_{L4}$	0·78499	0·77910	0·77551	0·77991	0·78246	0·77777	0·74072
$\bar{I}_{L5}$	0·26282	0·25189	0·24889	0·25067	0·25172	0·24999	0·24031
$-\bar{I}_{m1}$	-0·02405	-0·03564	-0·03675	-0·03694	-0·03691	-0·04050	-0·03220
$-\bar{I}_{m2}$	0·34516	0·32965	0·32547	0·32645	0·32708	0·32553	0·32741
$-\bar{I}_{m3}$	0·31581	0·30178	0·29724	0·29828	0·29891	0·29870	0·29954
$-\bar{I}_{m4}$	0·43192	0·41506	0·41240	0·41476	0·41592	0·41287	0·40296
$-\bar{I}_{m5}$	0·22027	0·21016	0·20831	0·20963	0·21028	0·20912	0·20347
$-\bar{I}^*_{m1}$	0·09907	0·09463	0·09464	0·09456	0·09459	0·09246	0·09641
$-\bar{I}^*_{m2}$	0·23636	0·22273	0·21940	0·22011	0·22050	0·21930	0·22274

+m = 15 rounding is used with the m = 31 collocation sections.

TABLE 40

Coefficients for Arrowhead Planform 12 ($A = 8, M = 0$) in Oscillatory Motion.

m N q $\bar{m}$	15 3 1 15	23 3 1 23	31 3 1 31	41 3 1 41
I_{L1}	3·78526	3·80421	3·82004	3·80436
I_{L2}	9·28996	9·37563	9·42324	9·39283
I_{L3}	-1·90009	-1·89103	-1·91614	-1·91496
I_{L4}	26·54324	26·82521	26·96339	26·88033
I_{L5}	-4·18363	-4·20574	-4·26574	-4·26436
$-I_{m1}$	8·17964	8·19481	8·24075	8·22893
$-I_{m2}$	23·35384	23·50402	23·63626	23·59934
$-I_{m3}$	-4·94786	-4·91054	-4·97419	-4·97844
$-I_{m4}$	74·42268	75·06482	75·47354	75·33802
$-I_{m5}$	-10·13499	-10·14691	-10·31067	-10·34665
$-I^*_{m1}$	22·27321	22·26277	22·39012	22·3769[illegible]
$-I^*_{m2}$	69·02922	69·35102	69·75066	69·69991

m N q $\bar{m}$	7 3 12 95	11 3 8 95	15 3 6 95	23 3 4 95
I_{L1}	3·70248	3·69185	3·69228	3·69788
I_{L2}	9·16025	9·14628	9·14862	9·15952
I_{L3}	-1·59159	-1·67928	-1·72368	-1·77126
I_{L4}	26·42059	26·32185	26·30473	26·30862
I_{L5}	-3·80720	-3·88693	-3·93798	-4·00041
$-I_{m1}$	8·09149	8·08062	8·07993	8·08394
$-I_{m2}$	23·27614	23·22472	23·21636	23·21918
$-I_{m3}$	-4·46445	-4·58034	-4·64520	-4·71971
$-I_{m4}$	74·52614	74·31138	74·26697	74·24980
$-I_{m5}$	-9·60185	-9·71397	-9·79510	-9·89912
$-I^*_{m1}$	22·17816	22·08754	22·07341	22·07538
$-I^*_{m2}$	69·11261	68·88816	68·85689	68·85592

TABLE 41

Coefficients for Slender Planforms 13, 14 and 15 in Oscillatory Motion.

(a) Complete delta (A = 1·5, M = 0)

m N q $\bar{m}$	11 2 12 143	11 3 1 11	11 3 2 23	11 3 4 47	11 3 8 95	11 3 12 143	11 4 12 143
I_{L1}	1·78190	1·82891	1·79115	1·77767	1·77708	1·77673	1·77694
I_{L2}	3·22896	3·31482	3·25175	3·22480	3·22268	3·22190	3·22203
I_{L3}	0·81459	0·82890	0·80752	0·82070	0·82520	0·82566	0·82634
I_{L4}	5·94293	6·11610	6·00732	5·95546	5·95000	5·94837	5·94786
I_{L5}	0·96087	1·02508	0·98487	0·99100	0·99716	0·99768	0·99869
$-I_{m1}$	2·17764	2·15880	2·18775	2·16575	2·16388	2·16358	2·16340
$-I_{m2}$	4·40365	4·39113	4·41578	4·38268	4·37755	4·37670	4·37612
$-I_{m3}$	1·10011	1·12868	1·10324	1·11406	1·12222	1·12298	1·12323
$-I_{m4}$	8·57446	8·63703	8·64344	8·58378	8·57124	8·56911	8·56924
$-I_{m5}$	1·45781	1·52101	1·46864	1·46906	1·48042	1·48127	1·48267
$-I^*_{m1}$	3·05227	2·93675	3·04774	3·02240	3·01476	3·01419	3·01433
$-I^*_{m2}$	6·47631	6·37639	6·51247	6·48062	6·46566	6·46424	6·46363

TABLE 41—*continued*

Coefficients for Slender Planforms 13, 14 *and* 15 *in Oscillatory Motion.*

(*b*) *Complete delta* ($A = 0{\cdot}0001$, $M = 0$)

m N q $\bar{m}$	11 2 6 71	11 3 1 11	11 3 2 23	11 3 4 47	11 3 6 71	11 4 6 71
I_{L1}/A	1·49312	1·54750	1·55138	1·54518	1·54003	1·55788
I_{L2}/A	2·80550	3·04113	3·03929	3·02787	3·01834	3·09702
I_{L3}/A	1·08366	1·08284	1·03192	1·04942	1 04678	1·13118
I_{L4}/A	5·28094	5·95596	5·94195	5·91969	5·90172	6·13178
I_{L5}/A	1·99318	1·60136	1·51019	1·51782	1·51710	1·87884
$-I_{m1}/A$	1·83920	1·95535	2·07726	2·05841	2·05306	2·05462
$-I_{m2}/A$	3·53770	4·36438	4·53503	4·51826	4·50395	4·41960
$-I_{m3}/A$	1·05571	1·60246	1·53043	1·54867	1·54948	1·45400
$-I_{m4}/A$	6·78904	9·17043	9·38720	9·37158	9·34176	9·20699
$-I_{m5}/A$	1·92907	2·51424	2·38170	2·38246	2·38745	2·42526
$-I^*_{m1}/A$	2·63155	2·75634	3·09752	3·07234	3·05903	3·06421
$-I^*_{m2}/A$	5·18576	6·67078	7·16978	7·16850	7·13734	6·94545

(c) Gothic Planform 15 ($A = 0{\cdot}0001$, $M = 0$)

m N q $\bar{m}$	11 2 6 71	11 3 1 11	11 3 2 23	11 3 4 47	11 3 6 71	11 4 6 71
I_{L1}/A	1·57551	1·56883	1·57106	1·57278	1·56812	1·57281
I_{L2}/A	2·49843	2·56642	2·56370	2·56804	2·56092	2·58818
I_{L3}/A	1·08921	1·15266	1·14286	1·15681	1·15186	1·17776
I_{L4}/A	3·92420	4·18350	4·17248	4·18052	4·16946	4·25789
I_{L5}/A	1·22804	1·36058	1·32426	1·33758	1·33341	1·37192
$-I_{m1}/A$	1·47139	1·40978	1·45957	1·45884	1·45768	1·46117
$-I_{m2}/A$	2·78803	2·82766	2·89700	2·90194	2·89609	2·93970
$-I_{m3}/A$	1·23781	1·35841	1·33649	1·35829	1·35405	1·39654
$-I_{m4}/A$	4·73537	5·09820	5·17368	5·18968	5·17708	5·32993
$-I_{m5}/A$	1·53679	1·72275	1·67665	1·69644	1·69182	1·75986
$-I^*_{m1}/A$	1·61405	1·46352	1·59582	1·58452	1·58392	1·58851
$-I^*_{m2}/A$	3·31873	3·38261	3·55611	3·56079	3·55415	3·62715

TABLE 42

Coefficients for Curved Planform 17 (A = 3·5564, Λ = 55°, M = 0·8) in Oscillatory Motion.

m N q $\bar{m}$	11 3 1 11	11 3 2 23	11 3 4 47	11 3 6 71	11 3 8 95
I_{L1}	1·81510	1·68403	1·61672	1·62651	1·62634
I_{L2}	3·32355	3·07132	2·93000	2·93494	2·93551
I_{L3}	0·22810	0·23111	0·19900	0·20799	0·20690
I_{L4}					
I_{L5}					
$-I_{m1}$	2·70280	2·56266	2·48546	2·48350	2·48626
$-I_{m2}$	5·80744	5·44215	5·24803	5·22633	5·23309
$-I_{m3}$	0·16233	0·19135	0·11600	0·13464	0·13431
$-I_{m4}$					
$-I_{m5}$					
$-I^*_{m1}$	5·13689	4·86806	4·78543	4·74991	4·75729
$-I^*_{m2}$	12·05945	11·30461	11·03937	10·93474	10·95281

Rounding m N q $\bar{m}$	m = 15 15 3 6 95	m = 11 15 3 6 95	m = 23 23 3 1 23	m = 23 23 3 2 47	m = 23 23 3 4 95	m = 11 23 3 4 95
I_{L1}	1·63281	1·65853	1·72060	1·63121	1·63915	1·67505
I_{L2}	2·94453	2·99545	3·13298	2·95190	2·95291	3·02777
I_{L3}	0·18376	0·17608	0·17791	0·15970	0·16800	0·16017
I_{L4}						
I_{L5}						
$-I_{m1}$	2·48942	2·51797	2·59488	2·49533	2·49367	2·53360
$-I_{m2}$	5·23438	5·29365	5·50819	5·25976	5·24037	5·32800
$-I_{m3}$	0·09703	0·07956	0·09784	0·05446	0·07271	0·05233
$-I_{m4}$						
$-I_{m5}$						
$-I^*_{m1}$	4·75764	4·79973	4·92976	4·79617	4·76669	4·82638
$-I^*_{m2}$	10·94722	11·03580	11·43812	11·05332	10·96430	11·09639

TABLE 43

Oscillatory Pitching Derivatives of Wings with Streamwise Symmetry.

(a) Rectangular $(A = 4, M = 0, x_o = 0{\cdot}5\bar{c})$

Solution m, N, q	$-z_\theta$	$-m_\theta$	$-z_{\dot\theta}$	$-m_{\dot\theta}$
15, 2, 1	1·81259	-0·48990	0·32606	0·28303
15, 2, 2	1·80867	-0·48456	0·33032	0·27955
15, 3, 1	1·80000	-0·48867	0·30117	0·27954
15, 3, 2	1·80950	-0·48784	0·32797	0·28150
15, 3, 4	1·80758	-0·48458	0·32876	0·27994
15, 3, 6	1·80670	-0·48416	0·32729	0·27957
7, 3, 12	1·80669	-0·48416	0·32728	0·27956
7, 3, 12*	1·80669	-0·48496	0·32648	0·27960

(b) Circular $(A = 1{\cdot}2732, M = 0, x_o = 0{\cdot}6366\bar{c})$

Solution m, N, q	$-z_\theta$	$-m_\theta$	$-z_{\dot\theta}$	$-m_{\dot\theta}$
11, 2, 4	0·89439	-0·29968	0·76657	0·11286
11, 3, 6	0·89529	-0·29669	0·76335	0·11265
11, 4, 8	0·89514	-0·29690	0·76365	0·11272
11, 4, 8*	0·89514	-0·29693	0·76362	0·11277
Exact	0·8951	-0·2969	0·7632	0·1128

(c) Planform 5 $(A = 4{\cdot}3292, M = 0, x_o = 0{\cdot}7900\bar{c})$

Solution m, N, q	$-z_\theta$	$-m_\theta$	$-z_{\dot\theta}$	$-m_{\dot\theta}$
11, 3, 1	1·91020	-0·55371	0·30887	0·35076
11, 3, 2	1·92893	-0·55708	0·38213	0·35385
11, 3, 4	1·92752	-0·55082	0·39259	0·35057
11, 3, 8	1·92562	-0·54969	0·39059	0·34939
11, 3, 8*	1·92562	-0·55772	0·38256	0·35810
23, 3, 1	1·92993	-0·55972	0·36383	0·35902
23, 3, 2	1·92758	-0·55237	0·37887	0·35367
23, 3, 4	1·92572	-0·55116	0·37740	0·35235
23, 3, 4*	1·92572	-0·55541	0·37315	0·35657

*Derivatives are calculated from coefficients for the wing in reverse flow.

TABLE 44

Oscillatory Pitching Derivatives of Constant-Chord Sweptback Wings ($x_0 = 0{\cdot}5\bar{c}$).

(a) Planform 6 with hyperbolic edges ($A = 4$, $M = 0$)

Solution m, N, q	$-z_\theta$	$-m_\theta$	$-z_{\dot\theta}$	$-m_{\dot\theta}$
15, 2, 1	1·62853	0·43228	1·00874	0·71227
15, 2, 2	1·61727	0·43410	0·99140	0·69625
15, 2, 4	1·61544	0·43197	0·98297	0·69231
7, 2, 8	1·61483	0·43200	0·98490	0·69285
15, 3, 1	1·62939	0·42030	0·99686	0·71094
15, 3, 2	1·62233	0·43210	0·99744	0·70445
15, 3, 4	1·61725	0·43252	0·98850	0·69697
15, 3, 6	1·61649	0·43146	0·98528	0·69507
7, 3,12	1·61601	0·43146	0·98722	0·69560
15, 4, 1	1·61222	0·42063	0·97299	0·69628
15, 4, 6	1·61711	0·43226	0·98774	0·69693
15, 3, 6*	1·61624	0·43107	0·98456	0·69480

(b) Planform 7 with straight edges ($A = 4$, $\Lambda = 45°$, $M = 0$)

Solution m, N, q	$-z_\theta$	$-m_\theta$	$-z_{\dot\theta}$	$-m_{\dot\theta}$
15, 2, 1	1·52150	1·01610	1·48747	1·49118
15, 2, 2	1·48419	1·01050	1·46712	1·46971
15, 2, 4	1·47981	1·00606	1·45586	1·46103
7, 2, 8	1·47672	1·00805	1·49044	1·48626
15, 3, 1	1·52592	1·00329	1·48508	1·48772
15, 3, 2	1·49599	1·01170	1·48114	1·48512
15, 3, 4	1·48267	1·00918	1·46448	1·47065
15, 3, 6	1·48148	1·00701	1·46016	1·46610
7, 3,12	1·47800	1·00873	1·49416	1·49032
15, 4, 1	1·50760	0·99698	1·45801	1·46469
15, 4, 6	1·48215	1·00892	1·46388	1·47084
15, 3, 6*	1·52345	1·00741	1·42000	1·43008

*Derivatives are calculated from solutions for the wing in reverse flow.

TABLE 45

Oscillatory Pitching Derivatives of Arrowhead Planforms 9, 10 *and* 12.

(a) $A = 2\sqrt{2}$, $x_o = 0{\cdot}75\bar{c}$

	Solution m, N, q	$-z_\theta$	$-m_\theta$	$-z_{\dot\theta}$	$-m_{\dot\theta}$
M = 0	15, 3, 1	1·39781	0·51047	1·38736	0·84345
	15, 3, 2	1·36423	0·53215	1·36211	0·84035
	15, 3, 4	1·36372	0·52906	1·36072	0·83838
M = 0·8	15, 3, 1	1·60997	0·62636	1·30562	1·02146
	15, 3, 2	1·56379	0·64859	1·33934	1·01299
	15, 3, 4	1·57009	0·64129	1·36712	1·02418
	15, 4, 1	1·61347	0·60179	1·33355	1·03814
	15, 4, 2	1·57760	0·64342	1·36472	1·03142
	15, 4, 4	1·56806	0·64525	1·36511	1·02457

(b) $A = 1{\cdot}4503$, $M = 0{\cdot}8$, $x_o = 0{\cdot}5848\bar{c}$

Solution m, N, q	$-z_\theta$	$-m_\theta$	$-z_{\dot\theta}$	$-m_{\dot\theta}$
7, 4, 12	1·06349	-0·13242	1·10483	0·37485
11, 4, 8	1·06572	-0·13633	1·08139	0·37328
15, 4, 6	1·06676	-0·13850	1·07022	0·37270

(c) $A = 8$, $M = 0$, $x_o = 0{\cdot}6897\bar{c}$

Solution m, N, q	$-z_\theta$	$-m_\theta$	$-z_{\dot\theta}$	$-m_{\dot\theta}$
15, 3, 1	1·89263	2·78454	2·38965	4·73433
23, 3, 1	1·90210	2·78559	2·43049	4·79468
31, 3, 1	1·91002	2·80310	2·43628	4·80914
41, 3, 1	1·90218	2·80260	2·42707	4·79899
7, 3, 12	1·85124	2·76901	2·50760	4·88624
11, 3, 8	1·84593	2·76724	2·46043	4·83886
15, 3, 6	1·84614	2·76675	2·43925	4·81709
23, 3, 4	1·84894	2·76682	2·41898	4·79385

TABLE 46

Oscillatory Pitching Derivatives of Slender Planforms 13, 14 *and* 15.

(a) Complete delta ($A = 1\cdot5$, $M = 0$, $x_0 = \bar{c}$)

Solution m, N, q	$-z_\theta$	$-m_\theta$	$-z_{\dot\theta}$	$-m_{\dot\theta}$
11, 2, 1	0·90823	0·20572	1·11151	0·50634
11, 2, 8	0·89097	0·19702	1·13159	0·53115
11, 2,12	0·89095	0·19787	1·13083	0·53223
11, 3, 1	0·91445	0·16494	1·15740	0·52310
11, 3, 2	0·89558	0·19830	1·13406	0·53157
11, 3, 4	0·88884	0·19404	1·13392	0·53158
11, 3, 6	0·88865	0·19348	1·13503	0·53229
11, 3, 8	0·88854	0·19340	1·13540	0·53255
11, 3,10	0·88837	0·19338	1·13540	0·53258
11, 3,12	0·88836	0·19342	1·13542	0·53264
11, 4, 1	0·90745	0·15396	1·15608	0·51517
11, 4, 8	0·88855	0·19326	1·13564	0·53198
11, 4,12	0·88847	0·19323	1·13572	0·53226

(b) Complete delta ($A = 0\cdot0001$, $M = 0$, $x_0 = \bar{c}$)

Solution m, N, q	$-z_\theta/A$	$-m_\theta/A$	$-z_{\dot\theta}/A$	$-m_{\dot\theta}/A$
11, 2, 6	0·74656	0·17304	1·19802	0·17907
11, 3, 1	0·77375	0·20393	1·28823	0·71751
11, 3, 2	0·77569	0·26294	1·25991	0·73418
11, 3, 4	0·77259	0·25662	1·26606	0·73820
11, 3, 6	0·77001	0·25651	1·26255	0·73764
11, 4, 6	0·77894	0·24837	1·33515	0·57434
Exact	0·78540	0·26180	1·30900	0·78540

(c) Gothic Planform 15 ($A = 0\cdot0001$, $M = 0$, $x_0 = 0\cdot8333\bar{c}$)

Solution m, N, q	$-z_\theta/A$	$-m_\theta/A$	$-z_{\dot\theta}/A$	$-m_{\dot\theta}/A$
11, 2, 4	0·78574	0·07356	1·13978	0·45052
11, 2, 6	0·78775	0·07923	1·13736	0·45205
11, 3, 1	0·78442	0·05121	1·20586	0·50075
11, 3, 2	0·78553	0·07518	1·19867	0·50970
11, 3, 4	0·78639	0·07409	1·20710	0·51635
11, 3, 6	0·78406	0·07546	1·20301	0 51519
11, 4, 4	0·78621	0·07302	1·22907	0·53584
11, 4, 6	0·78640	0·07525	1·22764	0·53627
Exact	0·78540	0·06545	1·24355	0·54542

TABLE 47

Oscillatory Pitching Derivatives of Curved Planform 17 ($A = 3{\cdot}5564$, $\Lambda = 55°$, $M = 0{\cdot}8$, $x_0 = 0{\cdot}5606\bar{c}$).

Solution m, N, q	$-z_\theta$	$-m_\theta$	$-z_{\dot\theta}$	$-m_{\dot\theta}$
11, 3, 1	1·51259	1·40437	1·53003	2·10147
11, 3, 2	1·40335	1·34883	1·55412	2·05912
11, 3, 4	1·34727	1·31594	1·48847	1·96098
11, 3, 6	1·35542	1·30973	1·49859	1·96079
11, 3, 8	1·35528	1·31211	1·49986	1·96459
15, 3, 6	1·36068	1·31172	1·44211	1·90889
15, 3, 6*	1·38210	1·32350	1·42162	1·89053
23, 3, 1	1·43383	1·35860	1·42167	1·95046
23, 3, 2	1·35934	1·31740	1·39115	1·87678
23, 3, 4	1·36596	1·31231	1·40355	1·88174
23, 3, 4*	1·39588	1·32880	1·37927	1·86115

*m = 11 rounding is used.

TABLE 48

Oscillatory Pitching Derivatives of Arrowhead Planform 11 ($A = 2, M = 0{\cdot}7806, x_0 = 0{\cdot}8080\bar{c}$).

(a) Direct flow

Solution m, N, q	$-z_\theta$	$-m_\theta$	$-z_{\dot\theta}$	$-m_{\dot\theta}$
15, 3, 1	1·28057	0·34638	1·28796	0·77006
15, 3, 2	1·26093	0·35840	1·32819	0·77711
15, 3, 4	1·26452	0·35561	1·34830	0·78473
15, 3, 6	1·26386	0·35614	1·35021	0·78534
15, 3, 8	1·26377	0·35631	1·35106	0·78565
15, 4, 6	1·26503	0·35613	1·35316	0·78794
31, 2, 2*	1·27056	0·34793	1·27354	0·74557
31, 3, 2*	1·27252	0·34770	1·28666	0·76560
15, 3, 6+	1·27502	0·34873	1·28313	0·76765

(b) Reverse flow

Solution m, N, q	$-z_\theta$	$-m_\theta$	$-z_{\dot\theta}$	$-m_{\dot\theta}$
15, 3, 1	1·27968	0·32520	1·29814	0·76297
15, 3, 2	1·28051	0·33272	1·25990	0·75961
15, 3, 4	1·27883	0·33626	1·24700	0·75667
15, 3, 6	1·27932	0·33445	1·24791	0·75703
15, 3, 8	1·27987	0·33327	1·24917	0·75750
15, 4, 6	1·27907	0·33452	1·25153	0·75929
31, 2, 2*	1·27194	0·34836	1·25108	0·74459
31, 3, 2*	1·27328	0·34766	1·26899	0·76055
15, 3, 6+	1·27444	0·34977	1·28002	0·76697

* m = 15 rounding is used with the m = 31 collocation sections.

\+ Rounding from equation (48), based on Ref. 23.

TABLE 49

Solutions for Planforms 13 *and* 16 ($M = 0, \alpha = 1$) *with Double Rounding*

(a) Complete delta ($A = 1{\cdot}5$)

Rounding m, N, q	m = 11 23,3,4	m = 5 11,3,8
y_0	0·78126	0·78058
y_1	0·77352	
y_2	0·75042	0·74973
y_3	0·71249	
y_4	0·66073	0·66026
y_5	0·59646	
y_6	0·52137	0·52122
y_7	0·43751	
y_8	0·34734	0·34700
y_9	0·25393	
y_{10}	0·16078	0·16121
y_{11}	0·07317	
μ_0	-0·10073	-0·08783
μ_1	-0·07509	
μ_2	-0·04936	-0·05035
μ_3	-0·03319	
μ_4	-0·02258	-0·02261
μ_5	-0·01556	
μ_6	-0·01060	-0·01096
μ_7	-0·00761	
μ_8	-0·00661	-0·00601
μ_9	-0·00634	
μ_{10}	-0·00254	-0·00334
μ_{11}	0·00193	
K_0	-0·08229	-0·05883
K_1	-0·05552	
K_2	-0·03065	-0·03436
K_3	-0·01938	
K_4	-0·01226	-0·00961
K_5	-0·00859	
K_6	-0·00287	-0·00609
K_7	-0·00036	
K_8	-0·00132	-0·00141
K_9	-0·01043	
K_{10}	-0·00475	-0·00275
K_{11}	0·01198	
C_L	1·78406	1·78290
$-C_m$	2·15280	2·15922
$\bar{\eta}$	0·41473	0·41482
$x_{ac}/\bar{c}$	1·20669	1·21107

(b) Curved tip ($A = 3{\cdot}8993$, $\Lambda = 60°$)

Rounding m, N, q	m = 7 15,4,8	m = 15 31,3,2
y_0	0·31041	0·29224
y_1	0·33117	0·32256
y_2	0·34537	0·34131
y_3	0·34528	0·34149
y_4	0·32062	0·31803
y_5	0·27214	0·26936
y_6	0·19851	0·19818
y_7	0·10585	0·10622
μ_0	-0·02895	-0·03535
μ_1	-0·01068	-0·00874
μ_2	-0·00102	-0·00315
μ_3	0·00168	0·00096
μ_4	0·00399	0·00230
μ_5	0·00336	0·00210
μ_6	0·00329	0·00011
μ_7	0·00078	0·00428
K_0	0·01900	0·01178
K_1	-0·01424	-0·01296
K_2	-0·00553	-0·00786
K_3	-0·00363	-0·00584
K_4	-0·00082	-0·00429
K_5	-0·00183	-0·00492
K_6	-0·00481	-0·00981
K_7	-0·00539	-0·01105
λ_0	-0·00941	
λ_1	0·00081	
λ_2	-0·00425	
λ_3	-0·00055	
λ_4	-0·00146	
λ_5	0·00092	
λ_6	-0·00244	
λ_7	-0·00179	
C_L	2·38982	2·35002
$-C_m$	4·52205	4·46051
$\bar{\eta}$	0·46547	0·46843
$x_{ac}/\bar{c}$	1·89222	1·89807

TABLE 50

Effect of Rounding on the Aerodynamic Loading of Planforms 7, 9, 13 *and* 16 ($M = 0, \alpha = 1$).

a) Constant-chord ($A = 4$, $\Lambda = 45°$)

Rounding m, N, q η	m = 15 31,3,2	m = 7 15,4,8
	Values of C_{LL}	
0	3·0460	3·1321
0·1951	3·2518	3·2815
0·3827	3·3755	3·3873
0·5556	3·3607	3·3709
0·7071	3·1567	3·1623
0·9239	1·9433	1·9483
η	Values of X_{ac}	
0	0·4034	0·4468
0·1951	0·2701	0·2739
0·3827	0·2524	0·2508
0·5556	0·2410	0·2410
0·7071	0·2206	0·2197
0·9239	0·1331	0·1331
C_L	3·0042	3·0222
$\bar{\eta}$	0·4653	0·4640
$x_{ac}/\bar{c}$	1·1748	1·1766

(b) Arrowhead wing ($A = 2\sqrt{2}$)

Rounding m, N, q η	m = 15 31,3,2	m = 7 15,4,8
	Values of C_{LL}	
0	2·1833	2·1980
0·1951	2·1934	2·1966
0·3827	2·1200	2·1209
0·5556	1·9638	1·9650
0·7071	1·7323	1·7327
0·9239	1·0081	1·0091
η	Values of X_{ac}	
0	0·3878	0·4062
0·1951	0·2925	0·2951
0·3827	0·2653	0·2652
0·5556	0·2517	0·2518
0·7071	0·2364	0·2356
0·9239	0·1552	0·1554
C_L	2·7499	2·7533
$\bar{\eta}$	0·4380	0·4378
$x_{ac}/\bar{c}$	1·1320	1·1354

(c) Complete delta ($A = 1·5$)

Rounding m, N, q η	m = 11 23,3,4	m = 5 11,3,8
	Values of C_{LL}	
0	1·1719	1·1709
0·2588	1·1256	1·1246
0·5000	0·9911	0·9904
0·7071	0·7821	0·7818
0·8660	0·5210	0·5205
0·9659	0·2412	0·2418
η	Values of X_{ac}	
0	0·4057	0·4156
0·2588	0·3158	0·3172
0·5000	0·2842	0·2842
0·7071	0·2703	0·2710
0·8660	0·2690	0·2673
0·9659	0·2658	0·2707
C_L	1·7841	1·7829
$\bar{\eta}$	0·4147	0·4148
$x_{ac}/\bar{c}$	1·2067	1·2111

(d) Curved tip ($A = 3·8993$, $\Lambda = 60°$)

Rounding m, N, q η	m = 15 31,3,2	m = 7 15,4,8
	Values of C_{LL}	
0	2·1334	2·2660
0·1951	2·3547	2·4175
0·3827	2·4915	2·5212
0·5556	2·4929	2·5205
0·7071	2·3216	2·3406
0·9239	1·4467	1·4492
η	Values of X_{ac}	
0	0·4737	0·5449
0·1951	0·2771	0·2851
0·3827	0·2592	0·2530
0·5556	0.2472	0·2451
0·7071	0·2428	0·2376
0·9239	0·2494	0·2334
C_L	2·3500	2·3898
$\bar{\eta}$	0·4684	0·4655
$x_{ac}/\bar{c}$	1·8981	1·8922

TABLE 51

Constant-Chord Wing ($A = 4, \Lambda = 45°, M = 0$) with Double Rounding in Oscillatory Motion.

(a) Coefficients in direct flow

Rounding m, N, q	m = 7 15,3,6	m = 11 23,3,4	m = 15 31,3,2
I_{L1}	3·02152	3·00800	3·00424
I_{L2}	4·78363	4·74831	4·74408
I_{L3}	-0·32363	-0·33111	-0·33374
I_{L4}	8·51511	8·45181	8·45275
I_{L5}	-0·46302	-0·45721	-0·45477
$-I_{m1}$	3·55438	3·53227	3·52927
$-I_{m2}$	6·43946	6·39549	6·39485
$-I_{m3}$	-0·24771	-0·25582	-0·25785
$-I_{m4}$	12·72098	12·64651	12·65811
$-I_{m5}$	-0·05144	-0·04078	-0·03547
$-I^*_{m1}$	5·06766	5·04313	5·04386
$-I^*_{m2}$	10·03470	9·98231	9·98954

(b) Coefficients from reverse flow
(m, N, q) = (31,3,2) with m = 15 rounding

Reversed wing	
$\bar{I}_{L1}$	3·01224
$\bar{I}_{L2}$	-0·50932
$\bar{I}_{L3}$	-0·35382
$\bar{I}_{L4}$	0·99704
$\bar{I}_{L5}$	-0·07477
$-\bar{I}_{m1}$	-1·73151
$-\bar{I}_{m2}$	1·11936
$-\bar{I}_{m3}$	0·12424
$-\bar{I}_{m4}$	-0·94930
$-\bar{I}_{m5}$	0·34458
$-\bar{I}^*_{m1}$	1·95710
$-\bar{I}^*_{m2}$	-1·41991

Reverse flow+	
I_{L1}	3·01224
I_{L2}	4·74375
I_{L3}	-0·35382
I_{L4}	8·43236
I_{L5}	-0·47806
$-I_{m1}$	3·52156
$-I_{m2}$	6·37243
$-I_{m3}$	-0·27905
$-I_{m4}$	12·60031
$-I_{m5}$	-0·05871
$-I^*_{m1}$	5·02792
$-I^*_{m2}$	9·94745

+The coefficients are evaluated from those for the reversed wing by equations (33) and (34).

Constant-Chord Wing ($A = 4, \Lambda = 45°, M = 0$) *with Double Rounding in Oscillatory Motion.*

(c) Pitching derivatives ($x_0 = 0 \cdot 5\bar{c}$)

	Direct flow			Reverse flow
m, N, q	15,3,6	23,3,4	31,3,2	31,3,2
$-z_\theta$	1·51076	1·50400	1·50212	1·50612
$-m_\theta$	1·02181	1·01414	1·01357	1·00772
$-z_{\dot\theta}$	1·47462	1·45660	1·45411	1·44190
$-m_{\dot\theta}$	1·46997	1·45847	1·45913	1·44535

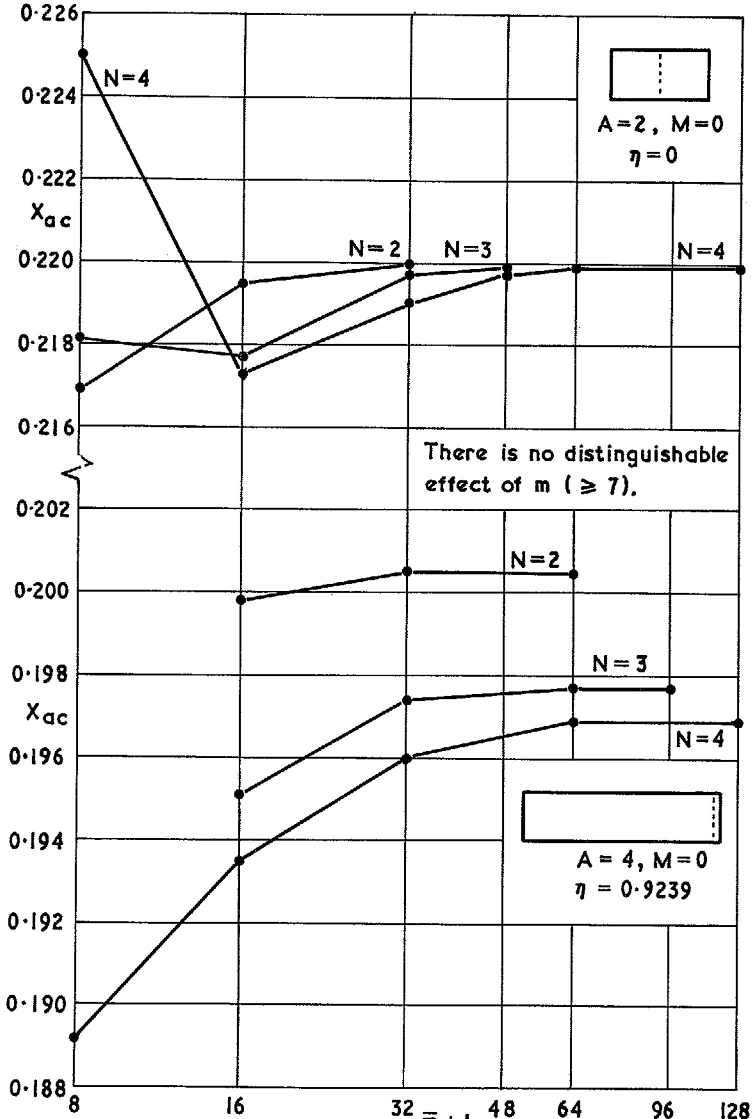

FIG. 1. Convergence of local aerodynamic centres on rectangular wings with respect to $\overline{m}$ and N.

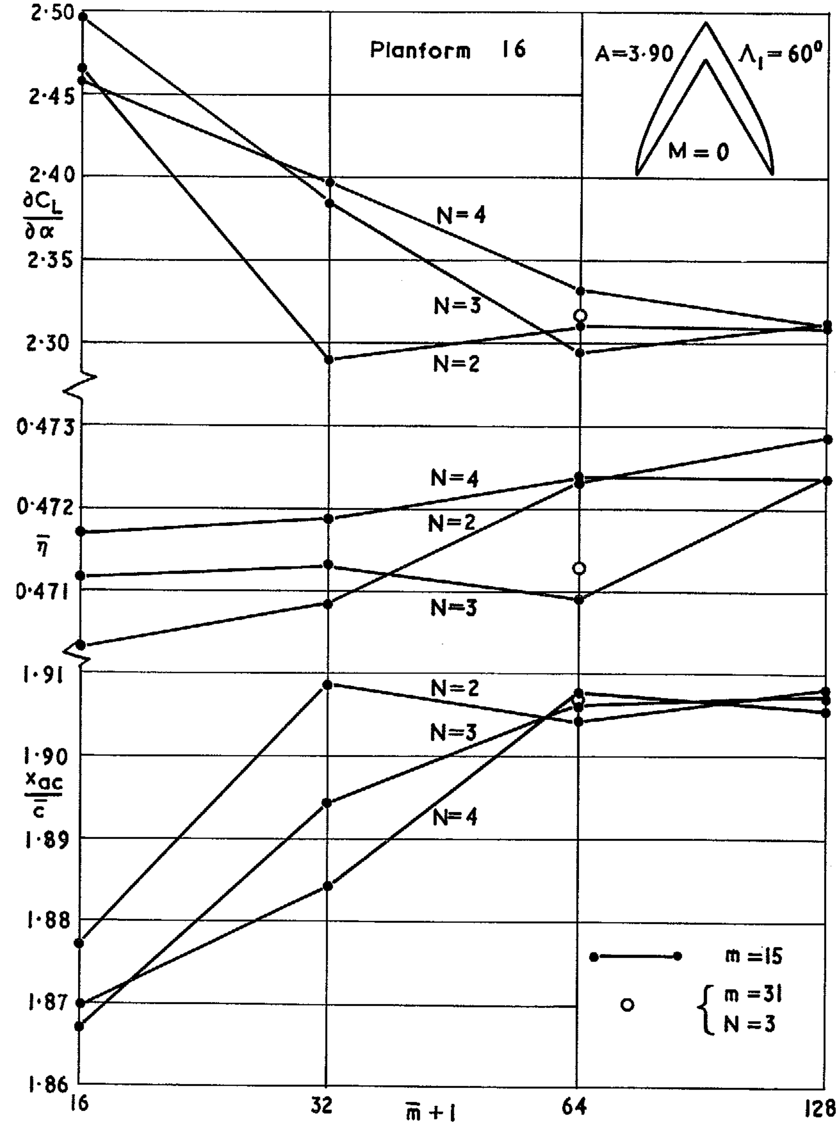

FIG. 2. Convergence of lift slope and centres of lift on a curved-tip wing with respect to $\overline{m}$ and N.

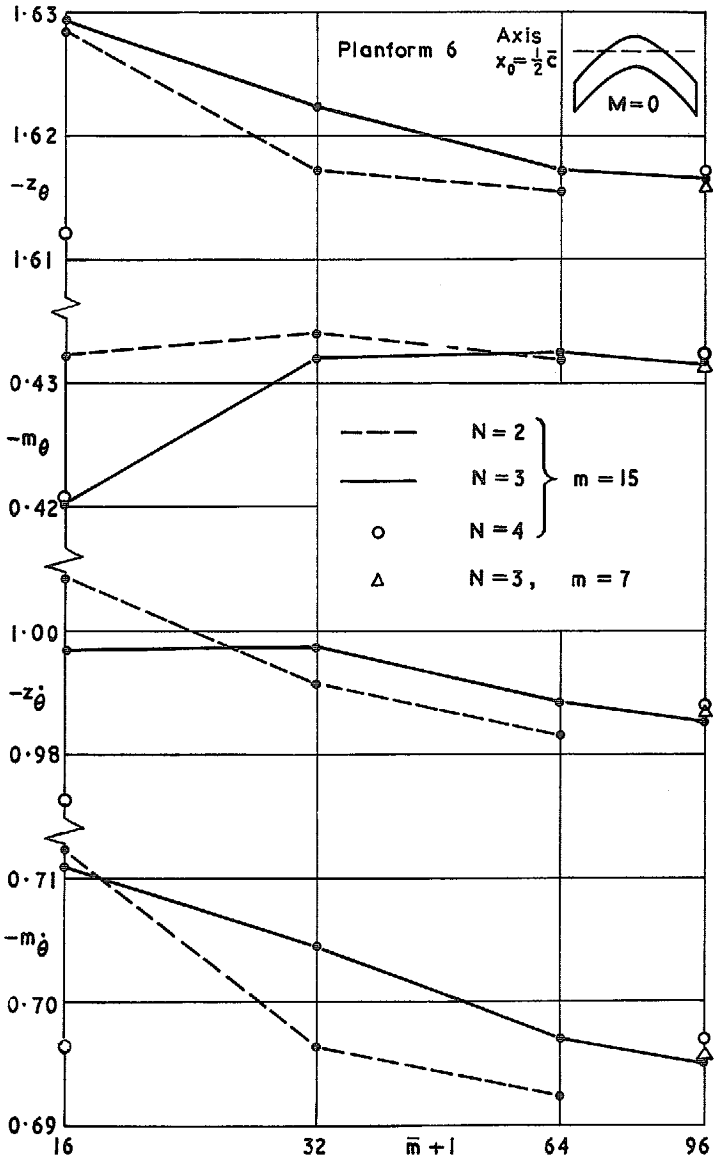

FIG. 3. Convergence of pitching derivatives for a constant-chord wing with hyperbolic leading edge.

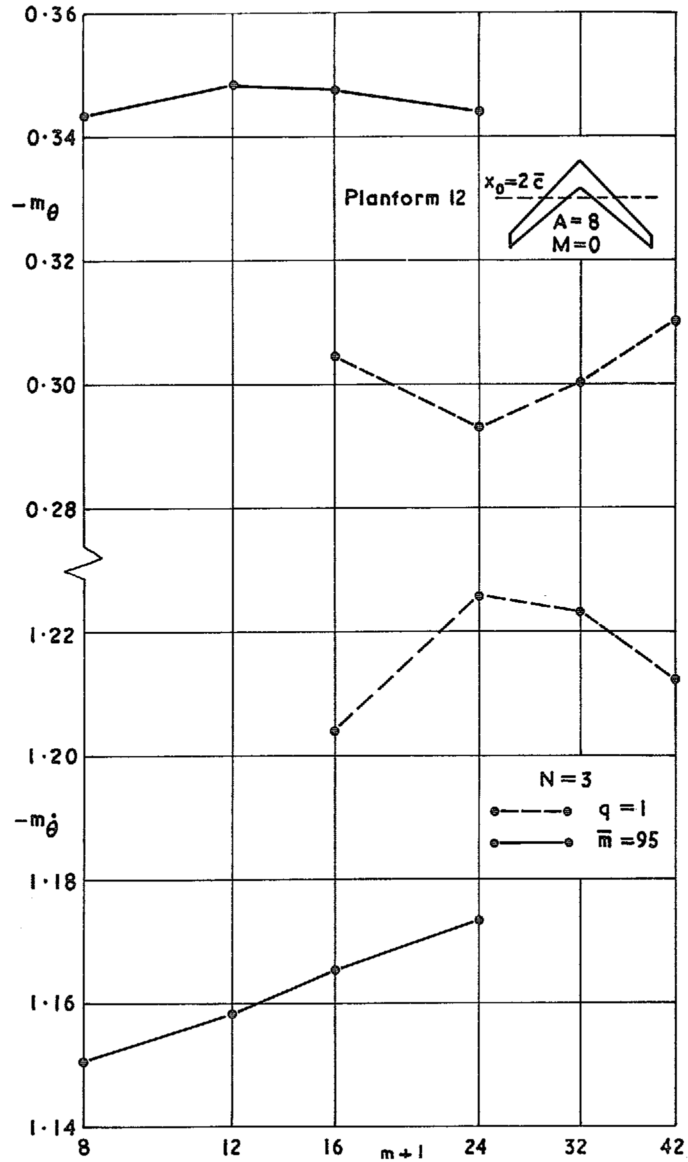

FIG. 4. Convergence of pitching stiffness and damping with respect to m for a sweepback wing of high aspect ratio.

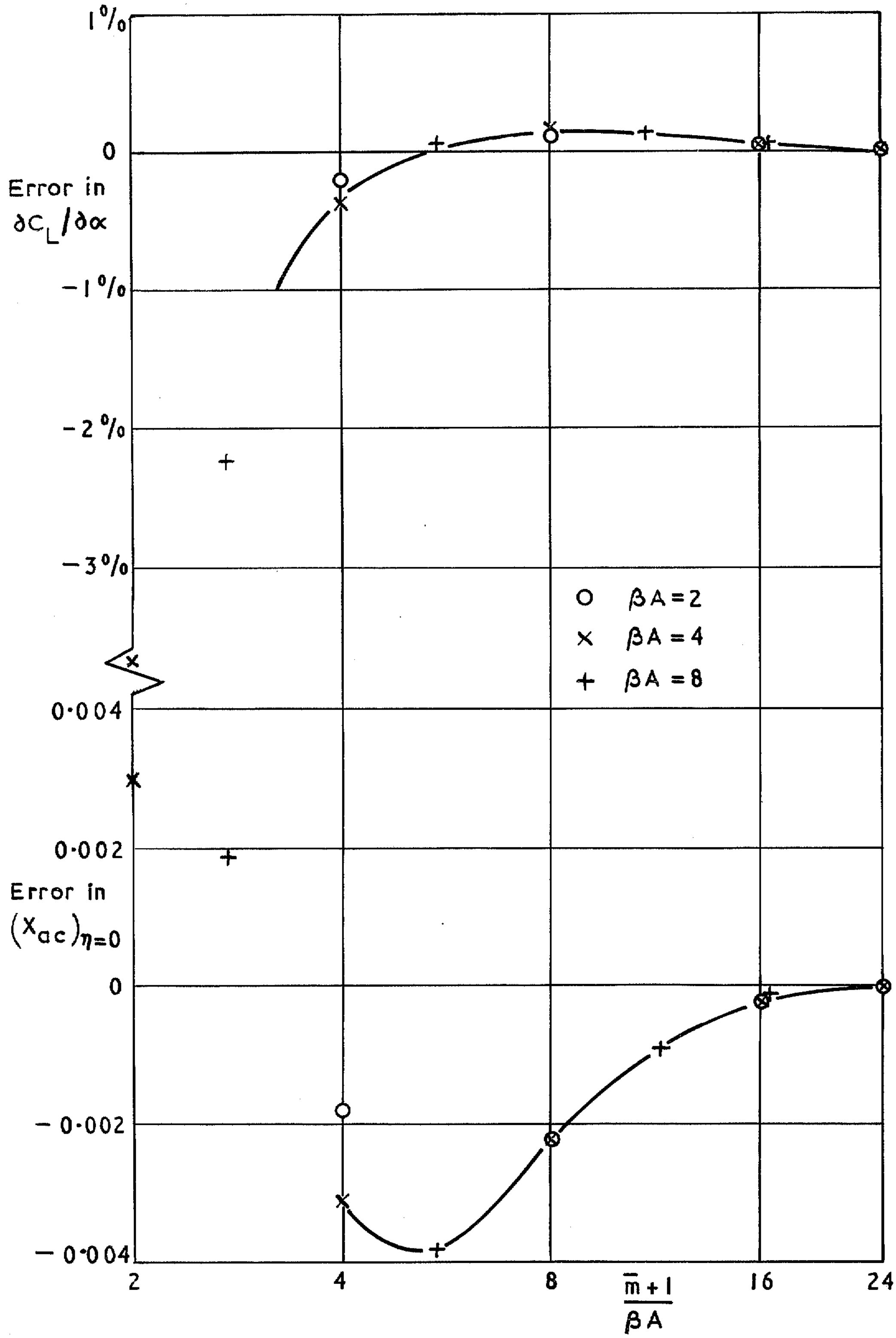

FIG. 5. Correlation of convergence with respect to $\bar{m}$ for rectangular wings in steady flow ($N = 3$).

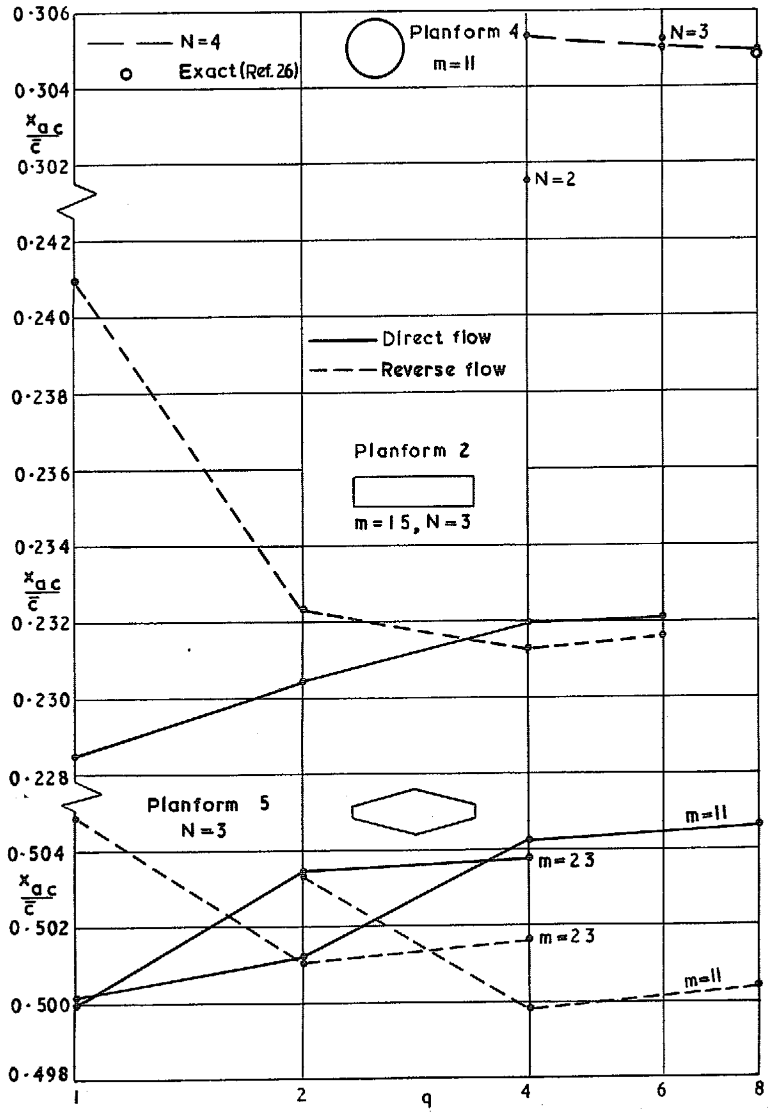

FIG. 6. Convergence of aerodynamic centres of wings with streamwise symmetry from direct and reverse flow ($M = 0$).

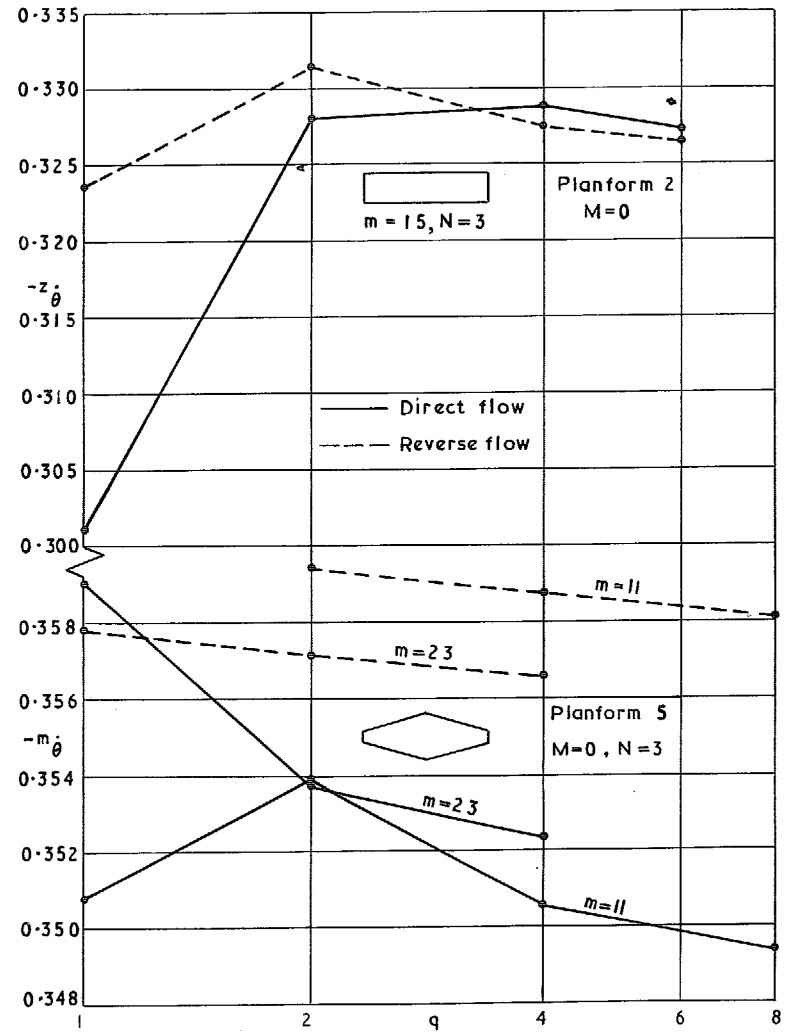

FIG. 7. Convergence of pitching damping derivatives about axis of streamwise symmetry from direct and reverse flow.

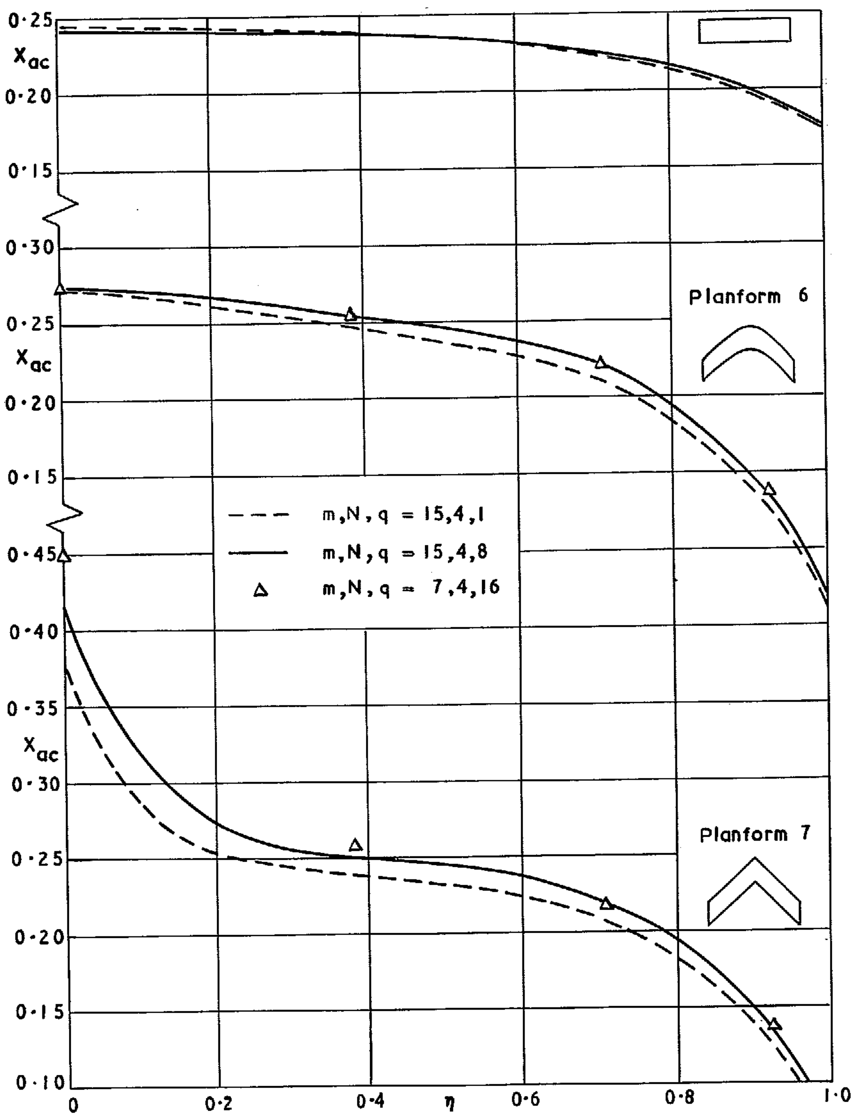

FIG. 8. Effect of m and q on spanwise distributions of X_{ac} for three constant-chord wings of aspect ratio 4 ($M = 0$).

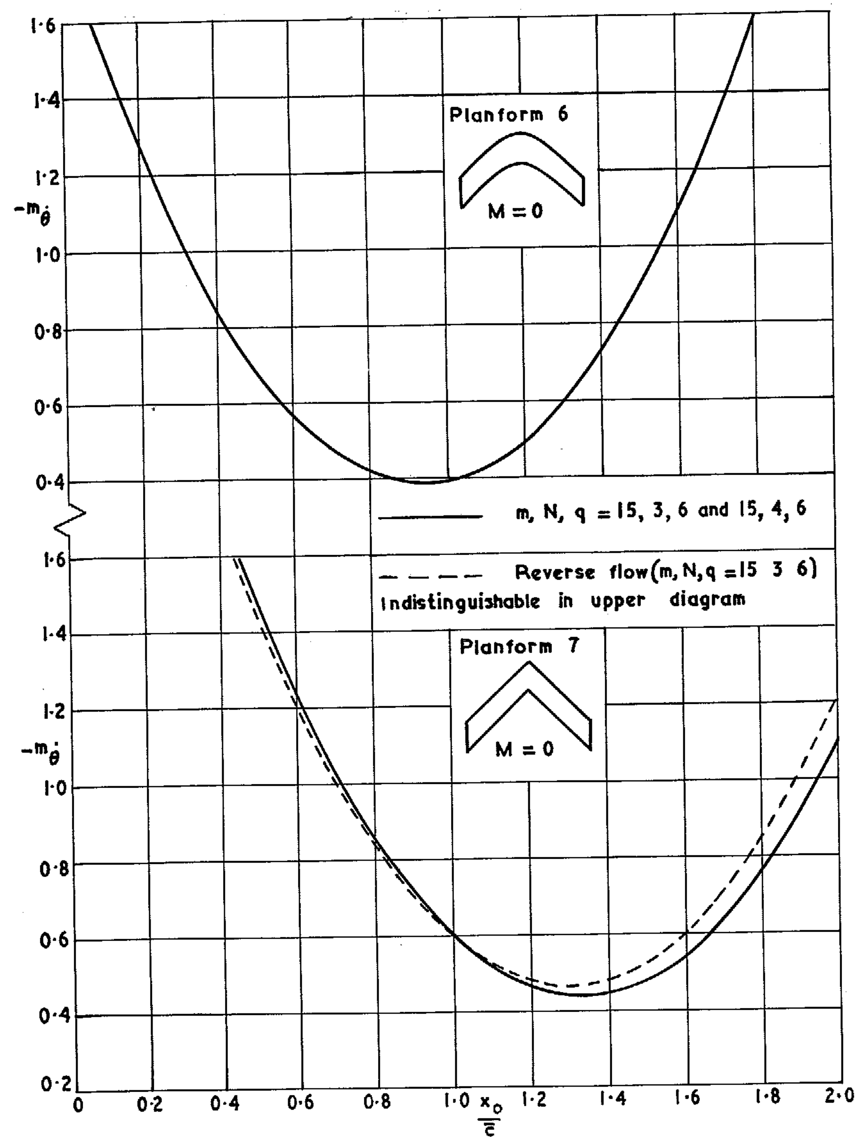

FIG. 9. Pitching damping against axis position for sweptback wings of constant chord with and without central kink.

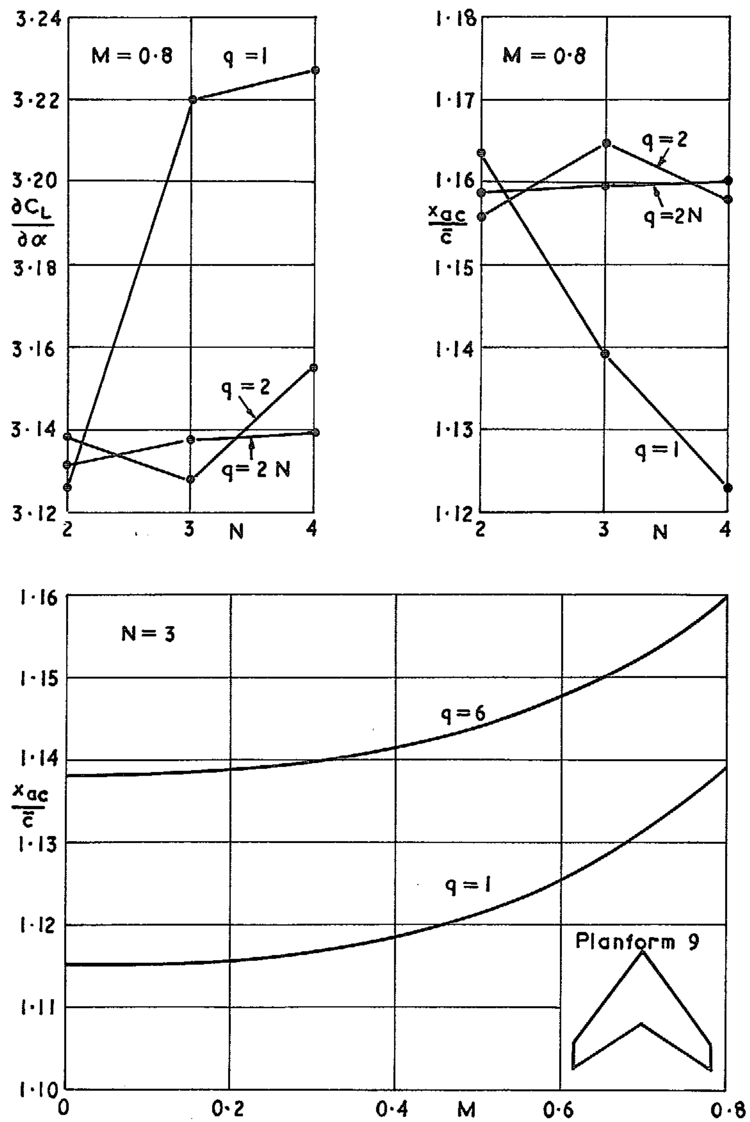

FIG. 10. Effect of q on lift slope and aerodynamic centre of an arrowhead wing in compressible flow ($m = 15$).

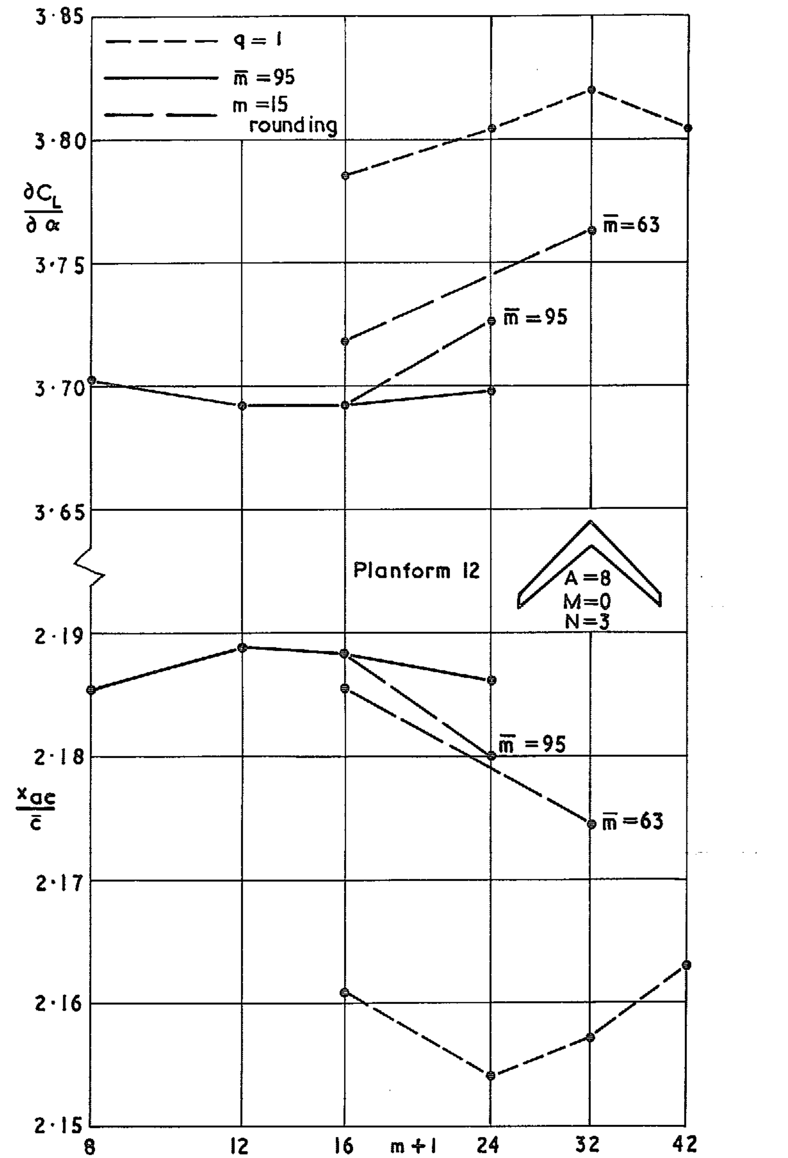

FIG. 11. Convergence of lift slope and aerodynamic centre with respect to m for a sweptback wing of high aspect ratio.

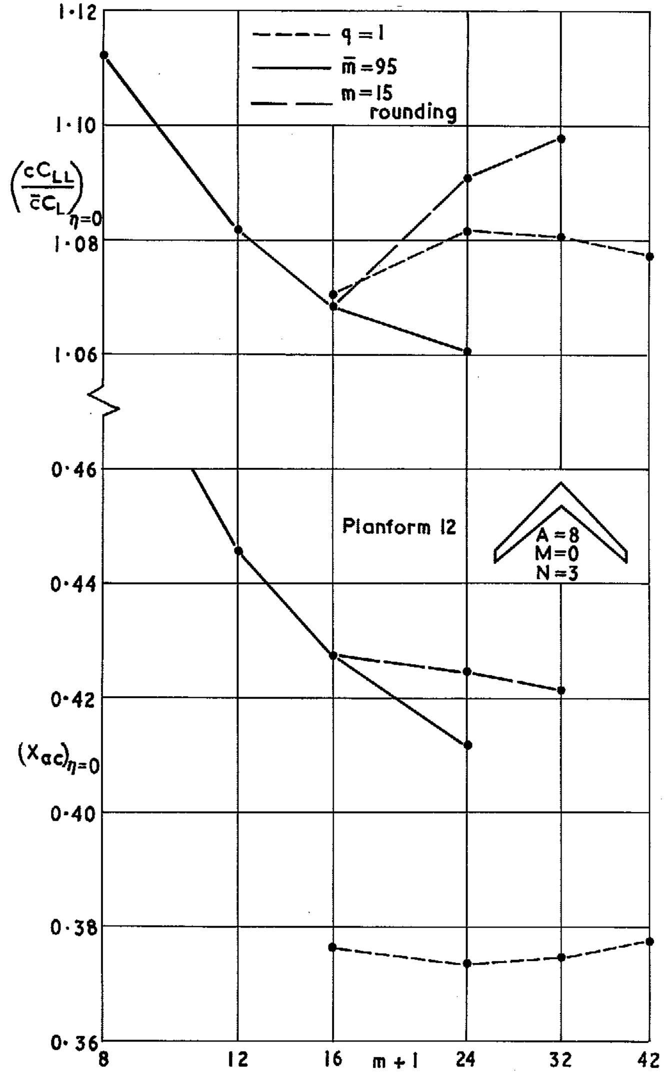

FIG. 12. Convergence of local lift and X_{ac} at centre section of a sweptback wing of high aspect ratio.

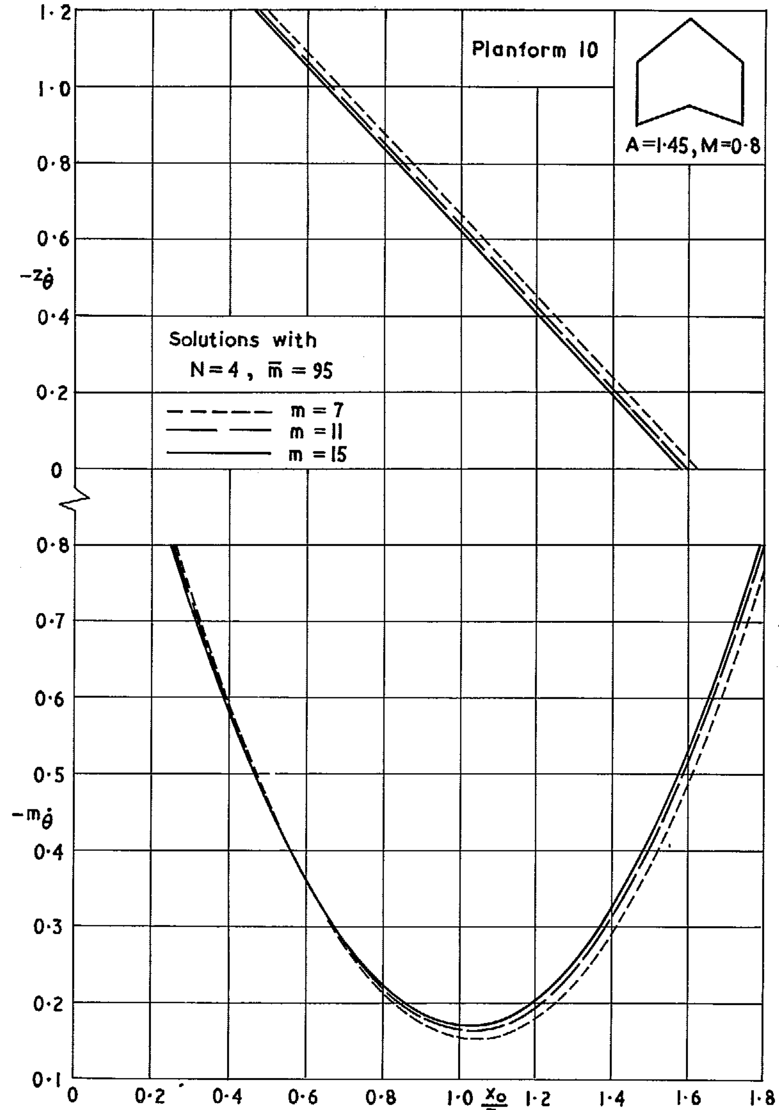

FIG. 13. Effect of m on damping derivatives against axis position for a sweptback wing of low aspect ratio at $M = 0{\cdot}8$.

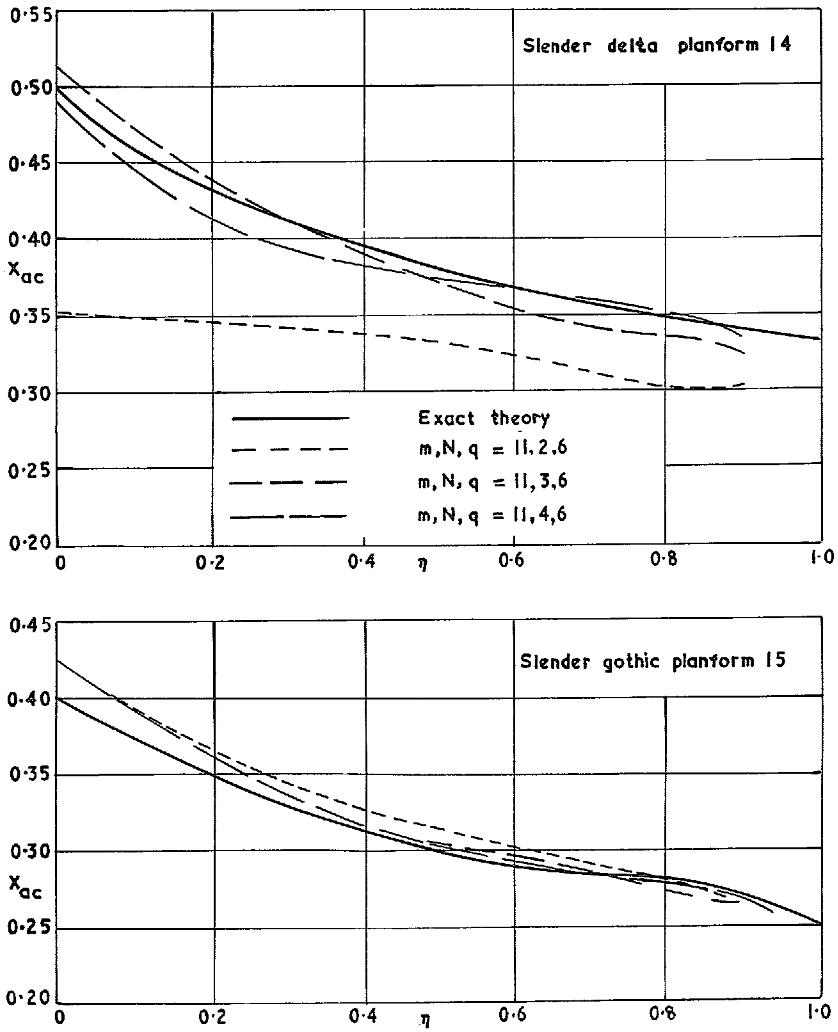

FIG. 14. Effect of N on spanwise distributions of X_{ac} on slender delta and gothic wings ($A = 0{\cdot}0001$).

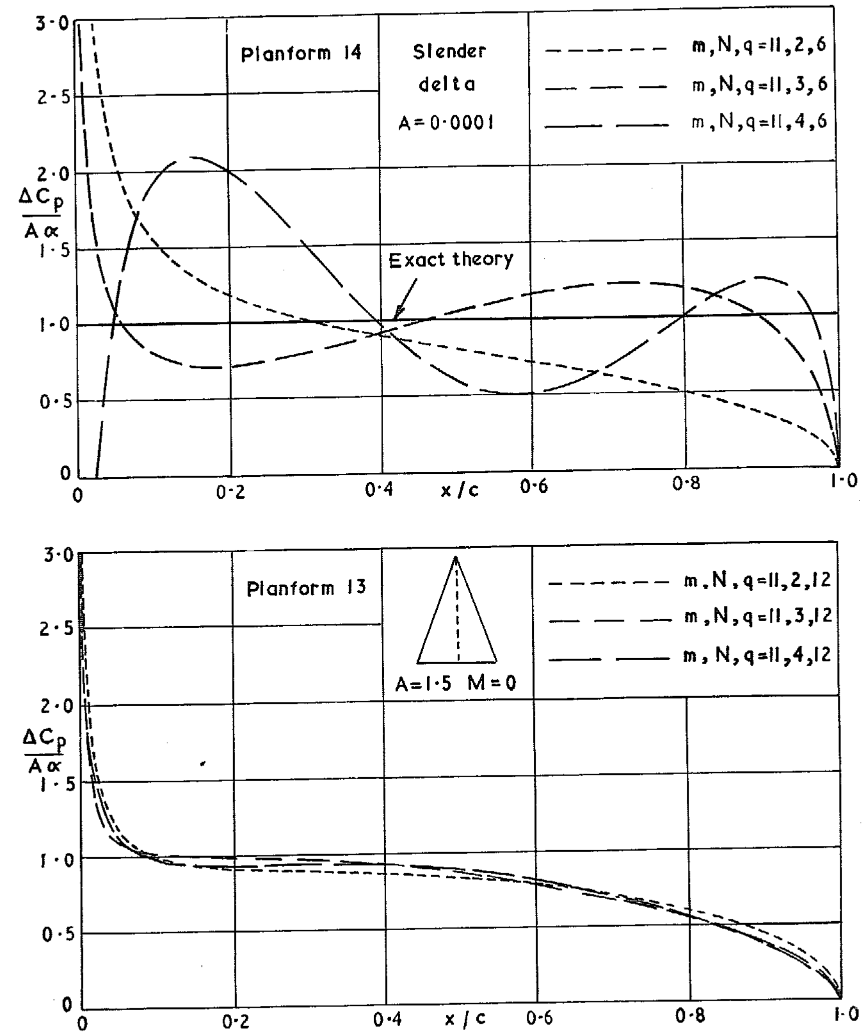

FIG. 15. Effect of N on central chordwise loadings of delta wings of aspect ratios 0·0001 and 1·5.

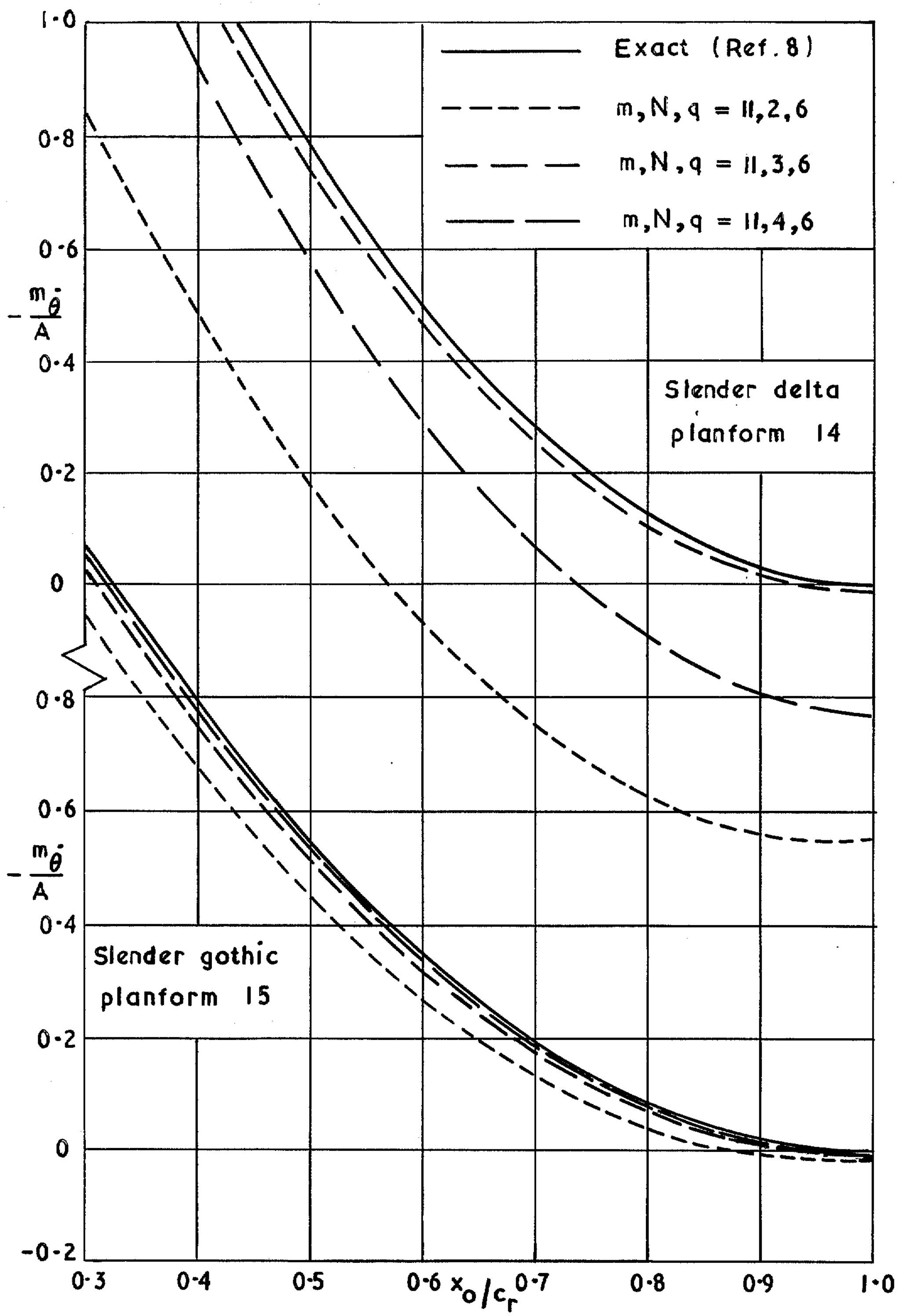

FIG. 16. Effect of N on pitching damping against axis position for slender delta and gothic wings ($A = 0{\cdot}0001$).

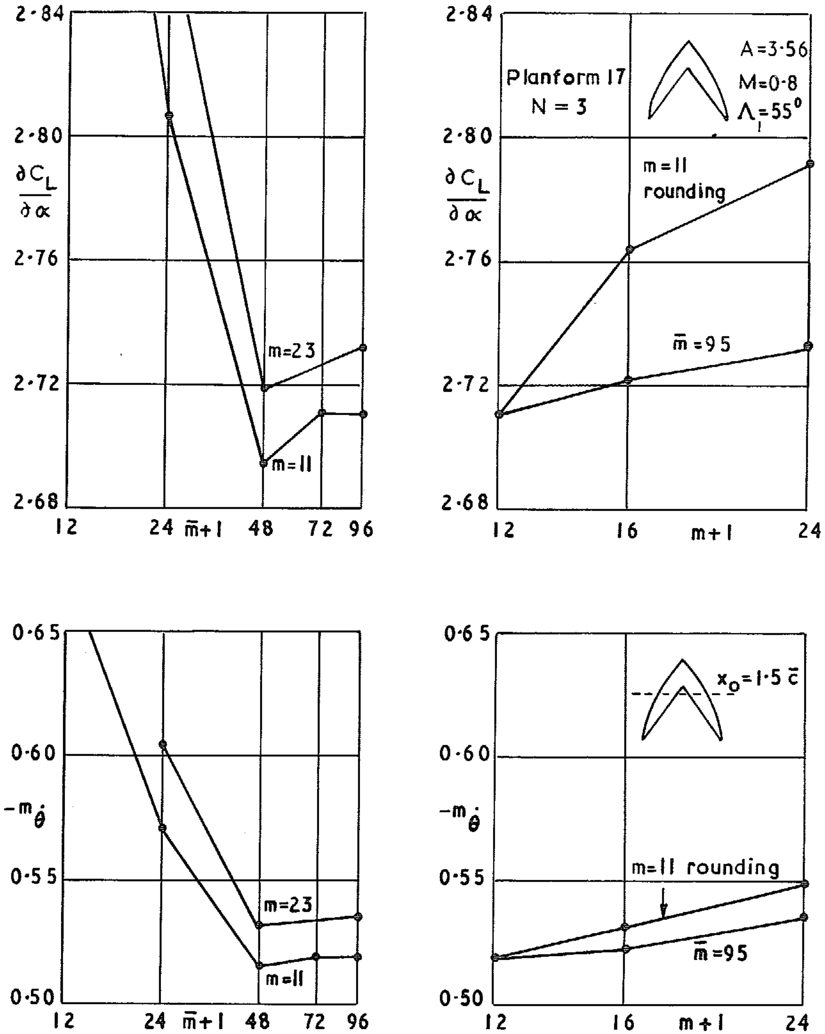

FIG. 17. Convergence of lift slope and pitching damping on a curved-tipped wing at $M = 0{\cdot}8$ with respect to $\overline{m}$ and m.

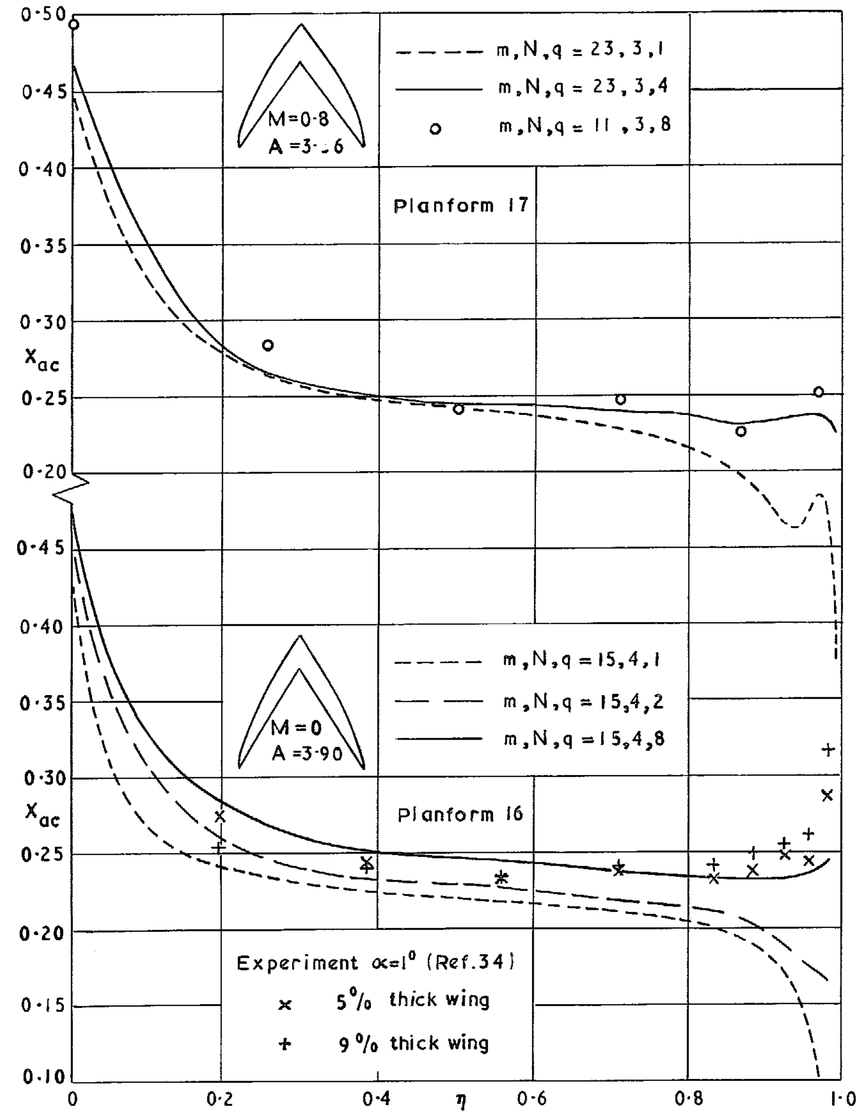

FIG. 18. Effect of q on spanwise distributions of X_{ac} for two curved-tipped wings and comparison with experiment.

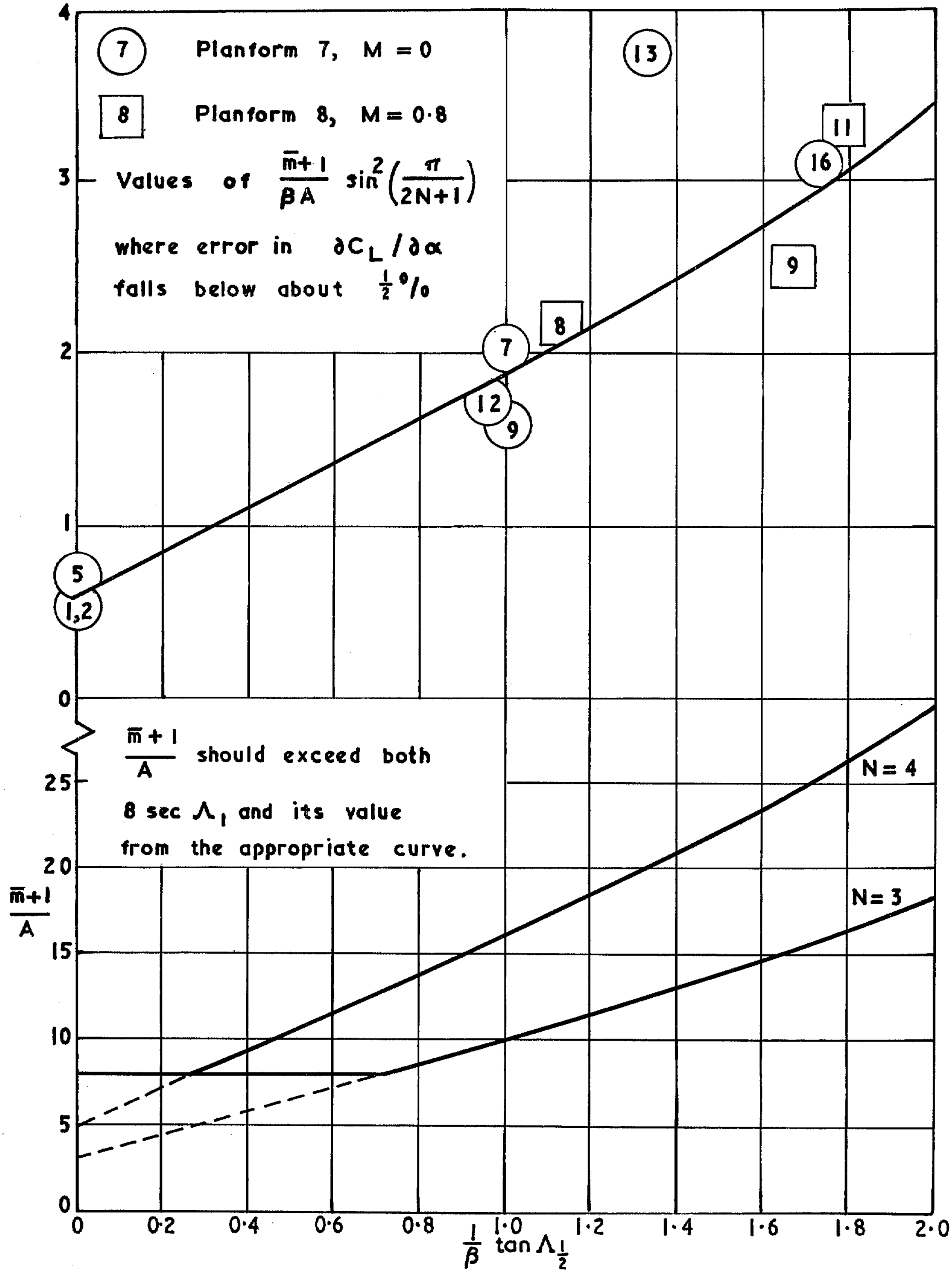

FIG. 19. Approximate criterion for selecting $\bar{m}$ for a given planform, Mach number and number of chordwise terms.

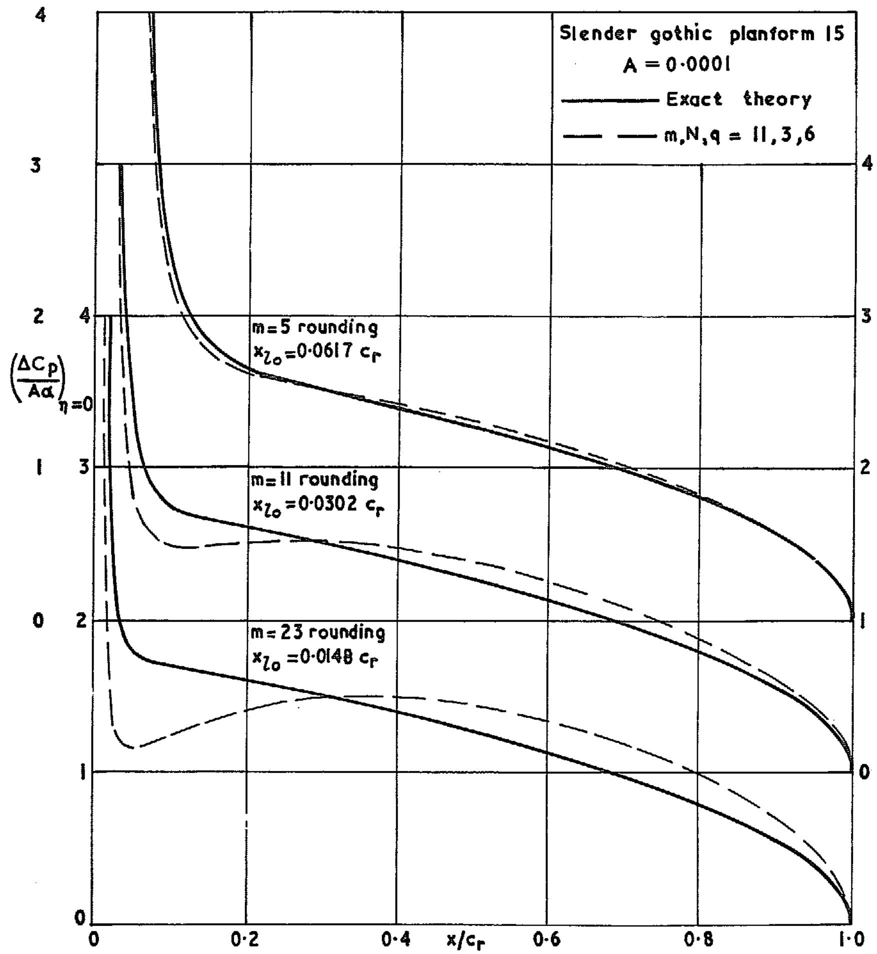

FIG. 20. Comparisons with exact theory of central chordwise loadings of a slender gothic wing with various amounts of rounding.

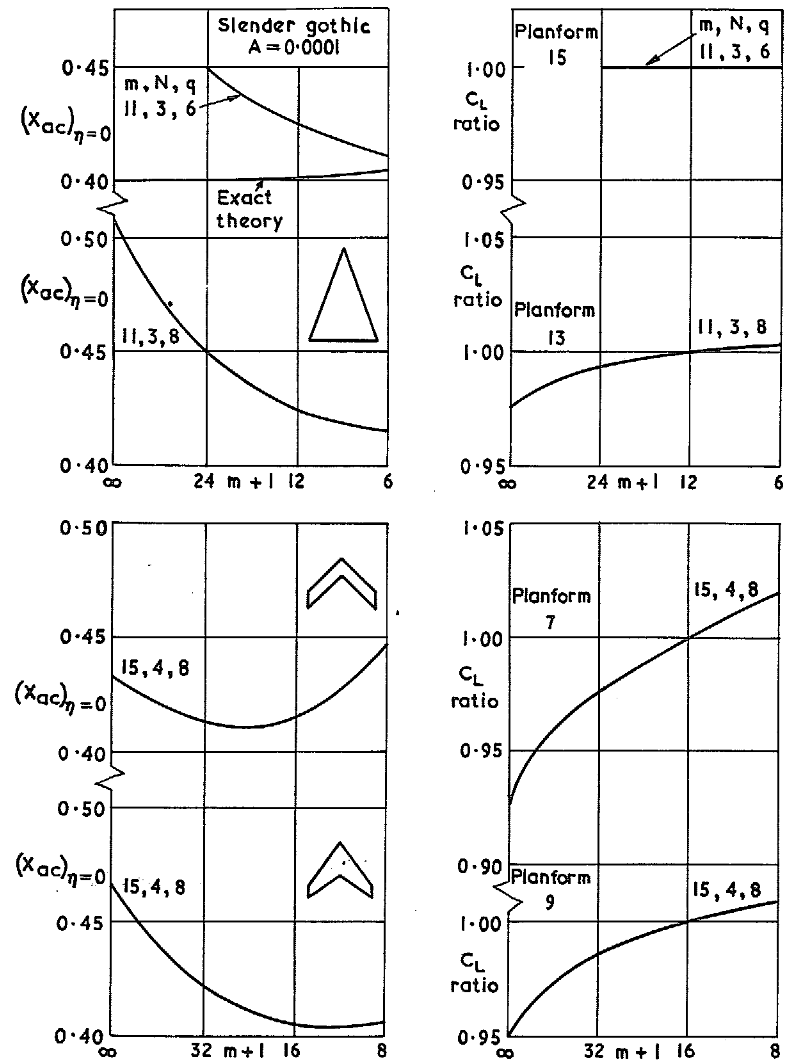

FIG. 21. Calculated effect of m as a rounding parameter on central X_{ac} and total lift of four wings ($M = 0$).

Printed in Wales for Her Majesty's Stationery Office by Allens Printers (Wales) Limited
Dd. 146916 K.5

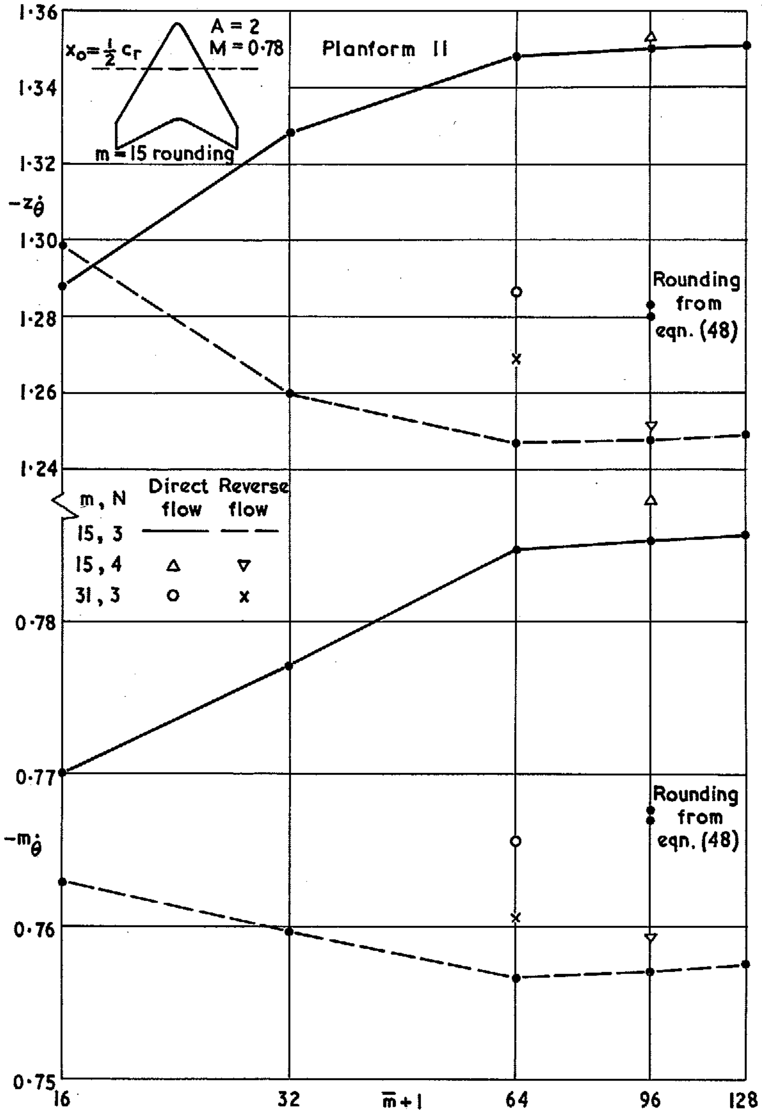

FIG. 22. Convergence of pitching damping derivatives of an arrowhead wing with fixed rounding from direct and reverse flow.

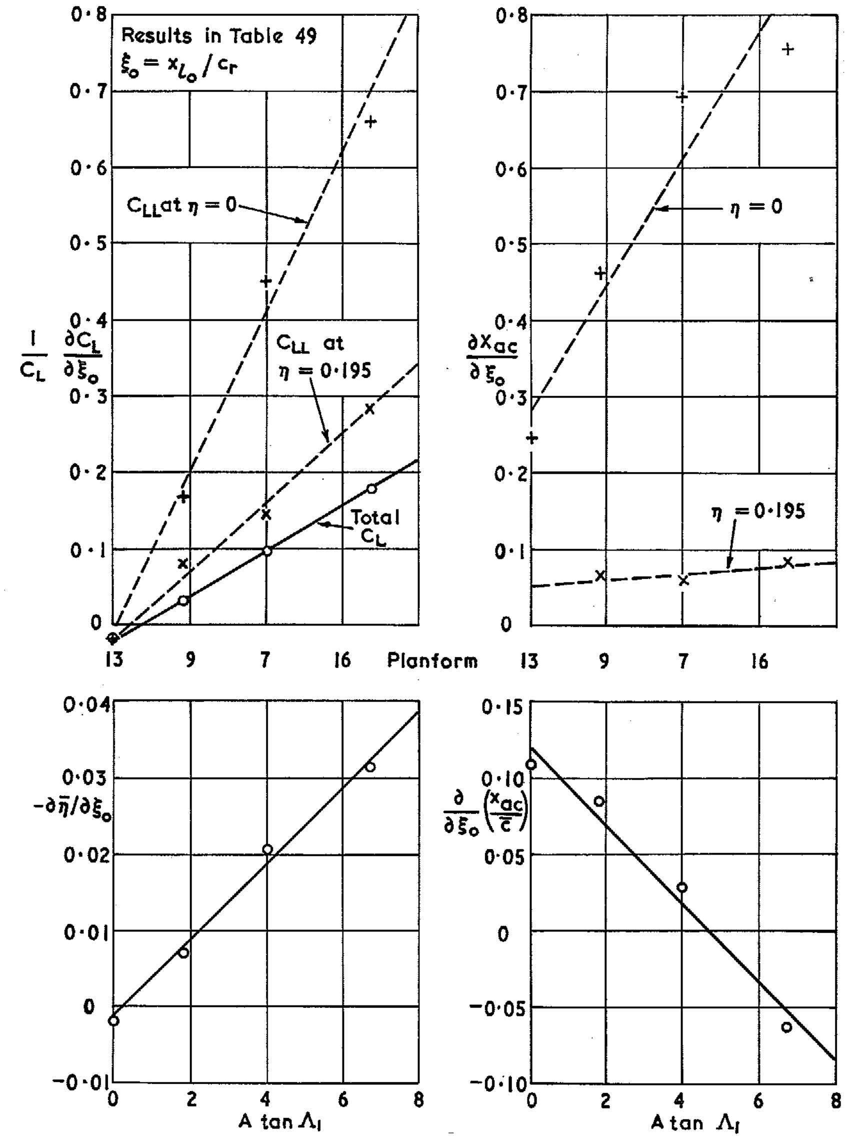

FIG. 23. Approximate effect of rounding on total and locals loads from solutions for sweptback wings with twice the standing rounding.

R. & M. No. 3634

Published by
HER MAJESTY'S STATIONERY OFFICE

To be purchased from
49 High Holborn, London WC1
13a Castle Street, Edinburgh EH2 3AR
109 St Mary Street, Cardiff CF1 1JW
Brazennose Street, Manchester M60 8AS
50 Fairfax Street, Bristol BS1 3DE
258 Broad Street, Birmingham 1
7 Linenhall Street, Belfast BT2 8AY
or through any bookseller

R. & M. No. 3634
SBN 11 470334 5